WORLD METEOROLOGICAL ORGANIZATION

MESOSCALE FORECASTING AND ITS APPLICATIONS

Lectures presented at the fortieth session

of the WMO Executive Council

WMO - No. 712

Secretariat of the World Meteorological Organization - Geneva - Switzerland

WORLD METEOROLOGICAL ORGANIZATION

MESOSCALE FORECASTING AND ITS APPLICATIONS

Lectures presented at the fortieth session

of the WMO Executive Council

WMO - No. 712

Secretariat of the World Meteorological Organization - Geneva - Switzerland
1989

ISBN 92 - 63 - 10712 - 8

NOTE

The designations employed and the presentation of material in this publication do not imply the expression of any opinion whatsoever on the part of the Secretariat of the World Meteorological Organization concerning the legal status of any country, territory, city or area, or of its authorities, or concerning the delimitation of its frontiers or boundaries.

CONTENTS

F O R E W O R D

The subject selected for the scientific lectures presented during the fortieth session of the Executive Council was "Mesoscale forecasting and its applications". This topic is clearly one of those in the forefront of research in the most advanced national Meteorologial Services today. New observation techniques permit more detailed weather analyses, supercomputers allow the running of fine-mesh weather-prediction models, and new telecommunication technology permits the prompt transmission of detailed ultra-short-range weather forecasts to the general public and to specialized users. These are the reasons that make mesoscale forecasting a timely issue.

The topic was addressed by five distinguished scientists who presented the following lectures:

- Mr K.A. Browning (United Kingdom) - The data base and physical basis of mesoscale forecasting
- Ms M.A.F. Silva Dias (Brazil) - Mesoscale weather systems - South American phenomena
- Mr Zou Jingmeng (China) - The monitoring and prediction of rainstorms and severe convective weather systems in China
- Mr N.F. Veltishchev (USSR) Development of mesoscale models for prediction of meteorological elements (in Russian)
- Mr M. Jarraud (France) - Mesoscale forecasting applications (in French)

All five lectures were well received by the Executive Council and are reproduced in this publication to enable all Members of WMO to benefit from them.

I would like to take this opportunity to place on record my appreciation to the lecturers for the time and effort they devoted to this important topic.

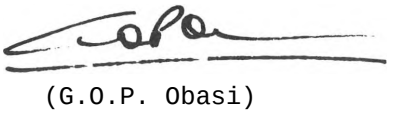

(G.O.P. Obasi)
Secretary-General

THE DATA BASE AND PHYSICAL BASIS OF MESOSCALE FORECASTING

by
K.A. Browning

Meteorological Office, Bracknell, United Kingdom

INTRODUCTION

There has been good progress in weather forecasting in recent years: for example, three-day forecasts are now as good as two-day ones were about five years ago (Flood, 1985). However, one often hears it said that the two-day forecasts seem better than those for the first 24 hours. This arises from the extra level of detail expected during the first 24 hours and from our current limited success in providing it. To provide more detailed forecasts it is neccesary to observe and model phenomena on the mesoscale. These ingredients are now becoming available. In this paper I shall first discuss the available mesoscale data base before going on to consider various approaches to mesoscale forecasting.

THE MESOSCALE DATA BASE

Satellite data

Satellites, together with radars, are the most important source of mesoscale observations. Data are available from both polar-orbiting and geostationary satellites. The high spatial resolution of the imagery from polar-orbiters, together with the availability of special channels, enables the polar-orbiters to be used to identify and classify individual cloud features. Their value for mesoscale forecasting is limited, however, because of the long interval between successive views of the same scene. A notable exception is over polar regions where successive orbits overlap. In contrast, geostationary satellites are able to obtain soundings and cloud images in quick succession over a given area. This ability to provide frequent, uniformly calibrated data sets from a single sensor over a broad range of meteorological scales from the synoptic scale down to the cloud scale gives them a central role in mesoscale forecasting.

Cloud imagery

Satellite imagery enables the forecaster to identify (a) the extent of cloud, (b) the height of cloud tops, (c) the movement of cloud, (d) the type of cloud (e.g. convective versus stratiform), and (e) the existence of characteristic patterns indicative of particular phenomena. The cloud patterns observed in a satellite image and in animated sequences of images represent the integrated effect of ongoing dynamic and thermodynamic processes in the atmosphere. When that information is combined with radar and conventional *in situ* observations and interpreted in the light of conceptual models, many of the important processes in the mesoscale weather situation may be better analysed and understood. This understanding is a prerequisite of mesoscale forecasting.

The spatial resolution of satellite imagery is often very good - it is, for instance, one kilometre at the subsatellite point for the visible

imagery from GOES satellites - and permits the detection of small Cumulus clouds within the boundary layer. Such Cumulus often form along (or predominantly to one side of) convergence lines. These are important as zones of vertical air motion associated with the boundaries between masses of air with contrasting temperature caused by the air having previously been in contact with different underlying surfaces (land/water, dry/wet and, unshaded/ cloud-covered land). Similar cloud lines, referred to as arc clouds, also occur in association with convergence lines at the boundary of some thunderstorm outflows. Purdom (1982) has shown that convergence lines and arc clouds are favoured sites for outbreaks of new storms, especially when two such features intersect.

Another reason for wishing to detect small Cumulus is that they serve as tracers of the detailed flow in the boundary layer (Fujita et al. , 1975; Hasler et al., 1976). Given enough Cumulus and not too much high cloud masking them, they are useful for determining local winds and depicting the mesoscale areas of convergence where thunderstorms may develop (Peslen, 1980). Negri and Vonder Haar (1980) have extended this approach by combining such fields with surface humidity information to give patterns of moisture convergence. Coarse-resolution cloud-track winds are an established source of data for synoptic-scale forecasting, especially in data-sparse tropical areas. However, for forecasting mesoscale fields, high-resolution imagery at five-minute intervals is required, and such data are not yet routinely available.

Digitally enhanced infra-red imagery is useful for identifying cold convective cloud tops. Scofield and Oliver (1977) have developed an operational scheme for estimating convective rainfall amounts from the location and temperature of Cumulonimbus tops, taking into account other factors such as the rate of expansion of the Cumulonimbus anvils, the merging of individual Cumulonimbus and cloud lines. The shape of the cloud tops can also be informative.

Liljas (1982) has devised a scheme for combining two and sometimes three channels to classify cloud type and to separate the cloud clearly from the background. He employs a display system which uses colours to distinguish between land and sea and low, medium and high cloud. Images formed by combining infra-red and visible channels have also been shown by Lovejoy and Austin (1979) to be superior to either alone for mapping the areal extent to surface precipitation. This is because, although precipitation clouds are often identifiable in the infra-red from their cold high tops, the visible channel shows where the clouds are also thick, thereby enabling regions of non-precipitating Cirrus, for example, to be ignored.

During the daytime a combination of visible and infra-red imagery enables fog to be distinguished from other forms of cloud (Liljas, 1982). For mapping night-time fog, Eyre et al. (1984) have shown that a combination of infra-red (11 μm) and near infra-red (3.7 μm) imagery is useful. Infra-red imagery alone cannot always discriminate the fog tops from the ground because both may be at a similar temperature. However, the emissivity of the fog droplets (but not the underlying surface) is different in the two channels so that a comparison of the channels enables the fog to be discriminated. At present, the 3.7 pm channel is available only on polar-orbiting satellites but, because of the value for forecasting purposes of having time sequences of fog imagery, there is a case for such a channel being included in the next generation of geostationary satellites.

Products derived from multispectral imagery are potentially valuable for initializing mesoscale NWP models. Saunders (1988) describes a procedure whereby the AVHRR channels on the polar-orbiting satellites can be analysed on a 1/5° x 1/5° latitude-longitude grid to provide a model input of fractional cloud cover, cloud-top height and, in cloud-free regions, also surface skin temperature and surface albedo. Mesoscale models in Europe will, of course, be better served by the more frequent data that will be obtained when similar multichannel radiometers are flown on board the next generation of METEOSAT satellites.

Other kinds of imagery

The 6.7 μm-channel water-vapour imagery available from some geostationary satellites gives an indication of the humidity in the upper troposphere. Water-vapour inhomogeneities can be tracked in the imagery to give wind estimates (Mosher and Stewart, 1981) but the resolution is too coarse for detailed mesoscale applications. The main use of water-vapour imagery in mesoscale forecasting is for observing the location and evolution of upper-air circulation systems (Gurka, 1987). For example, intrusions of dry air downwards from the stratosphere show up as clear signatures. Such dry intrusions are important in mesoscale forecasting because they lead to potential instability and outbreaks of convection, and because they are characterized by high-potential vorticity which gives rise to cyclogenesis when they overrun a zone of low-level baroclinicity (Hoskins et al., 1985).

Satellite-borne microwave radiometers operating in the absorption mode provide a semi-quantitative indication of precipitation distribution over sea areas (Katsaros and Lewis, 1986). Microwave radiometers operating in the scattering mode also provide a qualitative indication of precipitation over the land. At present these microwave channels are available only on polar-orbiting satellites and their role in mesoscale forecasting is in helping to calibrate the more frequently available cloud imagery from geostationary satellites

Satellite soundings

The TOVS temperature soundings available globally from NOAA polar orbiters are leading to improvements in the definition of synoptic-scale systems, especially in data-sparse regions (e.g. Kelly et al. , 1982). However, the limited accuracy and vertical and temporal resolution of TOVS data restrict their utility for routinely representing smaller mesoscale features in NWP models. Most of the promise - where TOVS and its planned successor Advanced TOVS are concerned - is in the direct assimilation of raw radiance data into large-scale numerical weather prediction models (Eyre, 1988), which will improve the mesoscale forecasts in so far as their initialization depends on accurate synoptic-scale background fields. For a more direct impact on mesoscale forecasting, however, the sounders need to be on a geostationary platform. The so-called VAS (VISSR atmospheric sounder) on the geostationary satellite GOES produces hourly a number of products that are useful in mesoscale forecasting, especially for thunderstorm prediction (Chesters et al., 1986). Several products are already being provided in real-time for operational use by the US National Severe Storm Forecast Center. Two of them, total precipitable water vapour and a thermodynamic stability index, can be provided as images with 7 km resolution. The infra-red VAS soundings are useful in areas such as the USA, where thunderstorms often develop from a previously cloud-free or partially cloudy

environment. In Europe, where extensive cloud is a problem for infra-red sounding, the possibility of using a microwave sounder in geostationary orbit is being considered; it will, however, be difficult to achieve adequate spatial resolution by this means.

Radar data

Since the 1950s, radar has played a central role in mesoscale research. The reflectivity of the radar echo from various atmospheric targets, the shape and evolution of the echo, the associated Doppler velocity and the polarization characteristics, all provide information about the targets themselves and about the convection and mesoscale air motions affecting them. Most of the echoes seen with present-day S-band and C-band weather radars are from precipitation but useful information about the motion and organization of the atmosphere can also be obtained in the clear (and cloudy) air from echoes from refractive index inhomogeneities and even insects. The richness of the radar information often leads to sophisticated interpretation which, though invaluable for research, has tended to impede its exploitation in forecasting. Progress in forecasting applications depends on finding simple ways of presenting basic radar information because the radar data, although important, is but one strand among many. Practical forecasting applications are based on two primary attributes of the radar echo: the magnitude and pattern of (a) radar reflectivity and (b) Doppler velocity gradients. The increasingly effective use of radar in mesoscale forecasting over the past two decades owes much to the development of digital data processing, communication, and display techniques capable of providing forecasters with clear displays of these primary attributes.

Radar reflectivity

Vertical sections and multiple upper-level plan sections are of interest in some situations but generally the most useful way of displaying radar reflectivity fields for forecasting purposes is as a single plan section. In the case of severe convective storms it may be helpful to show the plan distribution of vertically integrated reflectivity or perhaps maximum reflectivity but for general purposes it is best to display the plan distribution of echo as close to the surface as the radar can scan. The sensitivity of most weather radars limits them to detecting only precipitation. The magnitude of the equivalent reflectivity factor Z_e is a measure of the rainfall intensity (Brandes and Wilson, 1982) or, if Z_e > 60 dBZ, of the existence of hail. The pattern of reflectivity from a single radar provides information on the atmospheric organization both on the meso- and convective scales.

Present-day research radars, and also the operational NEXRAD radars - many of which are to be established by the USA over the next few years - are sufficiently sensitive to detect not only precipitation but also clear-air echoes such as those associated with thunderstorm gust fronts and boundary-layer convergence lines. Wilson and Schreiber (1986) have demonstrated a close link between such lines as detected by radar and the subsequent development of convective storms along them.

Radar coverage and networks of radars

A well-sited radar provides good coverage out to 200 km for deep thunderstorms, with useful but less quantitative coverage to 400 km as the

radar beam broadens and rises above the surface. Convergence lines, on the other hand, may be too shallow or have too weak a reflectivity to be detectable beyond a few tens of kilometres except when they are particularly intense. The coverage of radars is rather limited also for frontal precipitation, notably when the precipitation is shallow or the melting level low. Experience in the United Kingdom has shown that the performance of radar in frontal precipitation degrades significantly beyond 75 km. The range degradation is insidious and can be misleading both quantitatively and qualitatively.

For mesoscale forecasting purposes, it is important to achieve uniformly good-quality observations over large portions of synoptic-scale precipitation systems and to obtain such observations over considerable distances upwind of the forecast area. This calls for the use of networks of radars. Ligda (1957) demonstrated the usefulness of composite precipitation maps by manually combining the data from different radars in the form of series of montages. Nowadays, integrated weather-radar networks have been established in several countries (see Browning and Collier, 1982; Gilet, 1984) and even across whole groups of countries (Roesli et al. , 1987). The radar data are automatically transmitted to a central location where a composite display is generated for onward transmission to forecasters, in some cases within minutes of data time. An important facet of the forecaster's display is the ability to replay sequences of such pictures so as to depict the movement and development of rainbands and other mesoscale features.

A typical resolution for weather radar data is one kilometre and five minutes. The operational compromise arrived at in the design of the United Kingdom weather radar network, however, is 5 km and 15 minutes - at least for the remote composite displays - which is found to be adequate for the purpose of mapping and tracking most precipitation systems there. Nevertheless, the spatial resolution of 5 km would not be good enough in areas where severe convection is common because it would not resolve important details of individual convective storm cells and convergence lines. A similar reservation applies to the use of radar network data to track small, short-lived showers. Bond et al. (1981) have shown that, in a few specific but important weather situations, radar observations of very small fast-moving showers can give a useful indication of the presence of strong surface-wind gusts. An objective echo-tracking procedure was found to be capable of determining the speed of travel of the showers, but only if the radar data were available every five minutes.

Doppler velocity

Increasing numbers of weather radars nowadays are capable of measuring line-of-sight velocity from the Doppler shift. Several methods have been evolved for making use of the resulting information. One method is to combine the velocity components measured by two or more spaced Doppler radars (Lhermitte, 1970) but the use of multiple radars scanning a common volume is too elaborate and costly for most forecasting applications. In another method, a single Doppler radar makes a series of conical scans at different elevation angles from which it is possible to derive the mean wind velocity, divergence and deformation within a set of vertically stacked circles centred on the radar (Browning and Wexler, 1968). This approach produces only a single spatially averaged vertical profile at any given time and ignores important small-scale structures within the windfield.

A more useful approach in practice is for the line-of-sight component of velocity measured during a low-elevation azimuth scan to be displayed in colour on a PPI (plan position indicator) screen. The resulting display reveals various mesoscale and convective features, such as the wind shift line at a cold front, the divergence pattern accompanying a microburst and the large azimuthal shear in the radial wind associated with a mesocyclone and tornado vortex (Wilson and Roesli, 1985). However, these displays require close scrutiny and judgement to identify significant features. Algorithms have been developed to enable key signatures of the Doppler velocity and reflectivity patterns to be identified automatically. They will be used in the detection of hazardous weather when the new NEXRAD radars come into service. Algorithms are also being developed in Europe under the aegis of the COST-73 project. A critical task is to achieve a high probability of detection and a low false-alarm rate and one that has been achieved in the case of detecting mesocyclones in severe local storms (Zrnic el al., 1985). Nevertheless, the difficulties of using Doppler data operationally should not be underestimated and, in regions where tornadoes and other severe wind hazards are uncommon, careful thought must be given regarding their cost-effectiveness.

A possible future method for obtaining more from Doppler radar data has been proposed by Wolfsberg (1987), whereby a time series of volume scans from a single Doppler radar is analysed to determine the complete 3-D fields of both wind and temperature. This ambitious approach, referred to as "single Doppler velocity retrieval", makes use of the equations of fluid dynamics by seeking an initial state for the unknown variables which produces the best forecast of the observed velocity components. The method is computationally extravagant and at this stage it is not clear whether it will be sufficiently resistant to observational and model errors to yield useful results in practice.

Wind profilers

In his forward-looking paper on ground-based remote sensors for nowcasting, Little (1982) foresaw that the optimal upper-air profiling system of the future would be based on some combination of satellite sounders and an array of ground-based profilers. He envisaged each profiler as consisting of a multichannel microwave radiometer measuring vertical profiles of temperature and humidity plus a near-zenith-pointing VHF Doppler radar detecting backscatter from refractive index inhomogeneities and providing vertical profiles of wind. Only limited progress has been made towards establishing ground-based radiometers for this purpose, largely because of the poor vertical resolution achieved, but Little's aspirations are beginning to be realized where wind profilers are concerned. Following the evaluation of a small network of VHF wind profilers (Augustine and Zipser, 1987), a much larger mesoscale network of 30 wind profilers is being established in central USA during the late 1980s (Chadwick and Hassel, 1987). The new network will operate at UHF (~400 MHz) rather than VHF (~50 MHz), thereby going some way towards overcoming the deficiencies of VHF wind profilers in measuring winds in the boundary layer. The data will be available in all weather conditions except in areas of strong convection, and they will be centrally collected for operational use. The network will be capable of providing detailed and almost continuous time-height wind records of particular value for diagnosing the progression of mesoscale features and for initializing numerical weather prediction models. Frontal-scale thermal structure can be retrieved from the detailed wind measurements by using variational analysis

techniques (Brummer et al. , 1984; Kuo et al. , 1987). Theoretical analysis by Gal-Chen (1988) suggests that the combination of this approach with radiometric measurements is likely to provide better results than either of these methods alone.

Ground-based lightning-location systems

The requirement for a lightning-location system suited to mesoscale forecasting is an accuracy of 10 km or better, with an areal coverage of many hundreds of kilometres across, and a reporting period of 30 minutes or less. This excludes a number of short-range experimental high-precision techniques, and lightning-counter techniques, leaving only a few types of lightning-flash locating networks which detect the radio energy emitted from lightning "atmospherics" or "sferics".

The first network to meet mesoscale requirements was the so-called magnetic direction-finding (MDF) system. Flash fixing errors depend on network geometry, but for a large network of well-sited DF stations, 1-2 km accuracy is achievable near the network centre, and 6-8 km near the outer edges. Stations must be connected in a relatively dense network with separations of 100-200 km or so, depending on detailed requirements. This type of equipment is commercially available (Maier et al., 1983) and existing networks now cover about half the total area of Canada and the USA with concentrated coverage in the western half associated with forest fire-fighting. A smaller pair of networks covers Norway and Sweden south of 64°N.

More recently, the time of arrival (TOA) system has been developed whose outstations time the arrival of a feature within the first 1-5 ps of the sferic waveform (Bent and Lyons, 1984). The differences in arrival times at various outstations enable the flash to be located, although range is limited by the radio horizon to a reception area not much greater than that for the MDF system. A network of four outstations on a 200 km square will give a theoretical location accuracy of 1 km within the square, falling to 6 km at 400 km range. Commercial TOA systems cover portions of the Florida, upper Midwest and west gulf areas of the USA.

The United Kingdom Meteorological Office has recently deployed the arrival time difference (ATD) system for locating flashes (Lee, 1986). This network operates with a bandwidth of around 10 kHz, centred near 10 kHz, and so operates out to long ranges. Like the TOA system it avoids polarization difficulties by obtaining an arrival time difference between waveforms but, rather than attempting to time specific waveform features, outstations report waveforms to a control station where they are correlated to yield an ATD with errors of a few microseconds from the correlogram peak. Because propagation ranges are lengthy, as few as seven outstations in the United Kingdom and the Mediterranean provide cover over a very large area. The lengthy baselines, coupled with an intrinsically precise ATD measurement and the statistical advantage of most outstations contributing to most flashes, should give an RMS accuracy well under 10 km over most of the area from 30° to 70°N, and from 40°W to 40°E. An accuracy of better than 2 km should be achieved over most of the United Kingdom.

Other ground-based data

Other kinds of remote-sensing instrumentation, such as laser-based systems, may be established here and there for special purposes but are

unlikely to be deployed sufficiently abundantly for general-purpose mesoscale forecasting. Networks of Doppler acoustic radars (Sodar) for measuring boundary-layer winds and, perhaps, combined radio-acoustic (RASS) systems for measuring detailed low-level temperature profiles might be contemplated in the future. Surface mesoscale networks of *in situ* sensors do exist which have the capability of measuring a variety of parameters not easily determined by satellite and radar methods. These are used in research studies but are not an economic proposition for widespread use in operational forecasting. Rather, the philosophy in mesoscale forecasting is to use the mesoscale fields derived from satellites and radars as a means of making better use of the sparsely distributed sensors from existing manned and automatic weather stations. Thus, for example, the location of a sharp surface cold front as identified in satellite or radar pictures can be used to map the position of a temperature gradient whose magnitude is best determined quantitatively from the *in situ* measurements.

MESOSCALE FORECASTING METHODS

A number of authors (Browning, 1980; Doswell, 1986; Austin *et al*. , 1987) have presented diagrams such as the figure below indicating the relative importance of various inputs to the forecasting process as a function of forecast lead time. Traditional forecasts are represented by the curve labelled "large-scale models". These traditional forecasts are general in nature and, although they can be tailored for specific locations and parameters using either subjective interpretation or model output statistics (Glahn and Lowry, 1972), such forecasts are most appropriate for the period beyond the first 12 hours. The mesoscale forecasting which is the subject of this paper is concerned with the period from 0 to 12 hours, using linear extrapolation, mesoscale models, climatology and what is referred to in the figure below as "knowledge of meteorology", i.e. the application of conceptual models, etc.

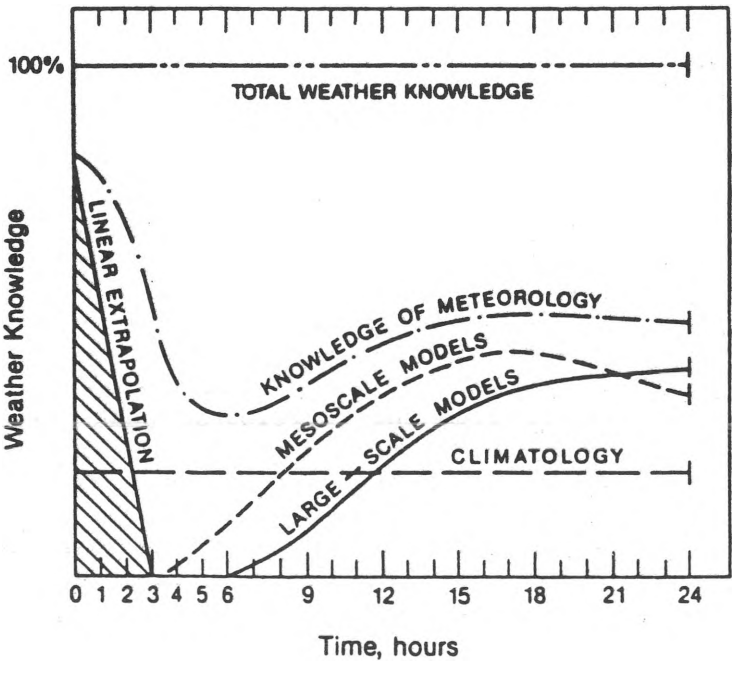

Contribution to the "weather knowledge" at different forecast lead times achievable from a variety of forecasting approaches (from Doswell, 1986)

Linear extrapolation

The growth of so-called nowcasting over the last decade has been stimulated by the ability of remote-sensing techniques to detect and track the individual mesoscale phenomena of interest. Many of the developments in this area relate to the extrapolation of sequential estimates of rainfall from satellite and radar data. There are several approaches. One approach, suited to situations with isolated storm cells, is to extrapolate a linear least-squares fit through successive positions of the centroid of the storm cell (e.g. Wilk and Gray, 1970). Clustering techniques can be used to deal with more complex and evolving patterns (Blackmer et al. , 1973). A simpler, more robust, and for many purposes more effective approach, is to extrapolate using motions estimated by a cross-correlation technique either in an overall sense (Austin and Bellon, 1974) or within a number of sub-areas to enable different motions to be applied in different regions (Bellon et al., 1980).

The fact that the extrapolation of weather radar echoes could yield useful very-short-range forecasts of precipitation was apparent from the earliest days of radar. Progress has been impeded, however, by the susceptibility of the forecasts to deficiencies in the data such as ground clutter, bright band effects and the range dependency of echo intensity owing to the beam overshooting precipitation at long range (Browning et al. , 1982). Bellon and Austin (1984) estimate errors in the radar rainfall forecasts of 50 to 60 per cent for forecasts in the 0.5-3 h time domain on a scale of 4 km. The skill of extrapolation forecasts of rainfall patterns derived from radars and satellite falls off dramatically a few hours after data time because of development and decay. Tsonis and Austin (1981) tried using observed trends in rainfall area and intensity to enhance the extrapolation forecasts but were unable to improve the forecasts in this way. A more promising approach may be to apply trends derived from NWP models.

The linear extrapolation approach can be applied to other phenomena besides precipitation, e.g. cloud areas as seen by satellite and thunderstorm areas as detected by lightning-detection systems. Other phenomena, such as microbursts, tornado vortex signatures and wind-shift lines detectable by Doppler radar, are more evanescent and extrapolation may be valid for only minutes or tens of minutes ahead. Because of the severity of the associated weather, however, even this can be valuable, given appropriate means of disseminating the information.

Conceptual models

Conceptual models encapsulating an understanding of the structure, mechanism and life cycle of an observed phenomenon (Browning, 1986) may be used to enhance the extrapolation forecasts in many situations. Thus, it is possible, on the basis of conceptual models, to interpret the satellite imagery or the pattern of radar reflectivity or Doppler velocity in terms of a particular category of mesoscale phenomenon, its detailed structure and the stage in its life cycle. An example is the case just mentioned of a tornado vortex signature detectable by Doppler radar. It is known that as early as 40 minutes before the tornado touches down, the tornado vortex signature may be detected aloft in the middle or upper troposphere (e.g. Donaldson, 1975; Brown et al., 1975), thereby giving the potential for useful advance warning (Kennington and Burgess, 1981).

Zipser (1982) has described the application of a life-cycle model of a mesoscale convective system (MCS) for enhancing the extrapolation of observed MCSs. The model, from Leary and Houze (1979), shows the varying mixture of convective and stratiform precipitation during the evolution of a class of MCS common in both the tropics and mid-latitudes. During the formative stage (to) and the intensifying stage (t_o + 3 h), cells of heavy convective precipitation predominate. During the mature stage (t_o + 6 h), there is a mixture of convective precipitation and lighter, more widespread, stratiform precipitation. During the decaying stage (t_o + 9 h) , light stratiform precipitation predominates. The decaying stage is often characterized by extensive high cloud, prominent in the satellite imagery, and there may also be widespread lightning. Thus, a forecaster may wrongly predict continuing outbreaks of severe weather unless he keeps the life-cycle model in mind.

Rules of thumb

Although objective extrapolation and numerical models are playing an increasing role on the mesoscale, rules of thumb are still needed, the application of which requires an appreciation on the part of the forecaster of the mesoscale behaviour of the atmosphere. Unfortunately, rules of thumb tend not to be intellectually satisfying and so there is not much well-organized literature on the subject.

One area where rules of thumb need to be applied is the difficult area of forecasting thunderstorm outbreaks. McGinley (1986) has summarized some of the key steps the forecaster should take based mainly upon experience in the USA:

(a) Analyse accurately the morning radiosondes in the region of interest to determine the stability and amount of life necessary to break any capping inversion;

(b) Watch the evolution of sea breezes and urban heating which may locally enhance or suppress the capping layer;

(c) Look for evidence of increasing boundary-layer moisture;

(d) Note the formation and distribution of the first convective clouds to determine if there is a forcing mechanism on the mesoscale, evident from either satellite or upper-air data. Also watch outflow boundaries as sources of destabilization;

(e) Be alert to the likely patterns of uplift associated with fronts and jet streaks;

(f) Watch for indications of the establishment of a low-level jet.

The pre-conditions for severe storms are similar to those for ordinary thunderstorms but with two notable additions: a source of dry air above the moist layer, and vertical wind shear. Colquhoun (1987) proposes a decision-tree approach to forecasting thunderstorms and their severity. At each decision point, the forecaster uses a rule of thumb which needs to be appropriately tuned for his particular region.

Mesoscale climatology

Topography plays an important part in generating mesoscale phenomena and in localizing the resulting weather effects in ways that depend on the low-level wind and stability. There is therefore considerable benefit to be gained from the derivation of conditional mesoscale climatologies. Thus, for example, lake-effect snowstorms are prone to occur in specific localities in certain well-known situations (Lavoie, 1972), convective shower lines occur repeatedly in specific regions (Monk, 1987), and even tornadoes occur more frequently in certain areas because of topographical forcing by neighbouring high land for some wind directions (Szoke et al., 1984). The prediction of the mesoscale distribution of orographically enhanced frontal rain by the seeder-feeder mechanism (Bergeron, 1965) is another example of where conditional climatology can be used. Given some background rain to accomplish the seeding and a moist low-level flow to produce feeder cloud, the amount and location of orographic rain is known to be related strongly to the low-level wind velocity (Hill et al. , 1981; Hill, 1983). A further example of the use of mesoscale climatology is in the prediction of the distribution of low Stratus in the United Kindgom for different wind directions (Mansfield, 1987). The Stratus tends to be advected over the United Kindgom from the sea. The forecast problem is then a matter of combining the climatological information with the identification and tracking of the Stratus over the sea by satellite. Other techniques, described next, can be used to refine the forecasts further.

Special-purpose 1-D models

For a reliable site-specific forecast of boundary-layer cloud amount and the occurrence of fog, it is neccessary to go beyond the mere extrapolation of observed cloud areas and mesoscale climatolgoy - an estimate must also be made of the daily cycle of the boundary-layer structure. Because of the importance of representing the turbulent processes, the boundary layer needs to be modelled using many levels in the vertical. This can be done either by means of a nested approach in which extra layers are introduced within a limited-area NWP model or, more simply, by means of an air mass transformation (AMT) model in which a one-dimensional boundary-layer model is applied to trajectories calculated by the NWP model (Reiff, 1987). Radiosondes located upwind of the forecast area may be used to define initial temperature and humidity profiles but, when the wind blows from data-sparse sea areas, it is not easy to obtain the required input data. The use of a simple AMT model has the advantage of not requiring the use of large computer resources; it breaks down, however, when the boundary-layer processes feed back on the mesoscale dynamics as, for example, when a land/sea circulation develops, and so the forecaster must be vigilant for early evidence of such effects in the pattern of clouds seen in satellite imagery.

Mesoscale NWP

Good progress has been made recently in the development of mesoscale NWP models. Some are being used solely for research but one or two are in use semi-operationally. One such is the United Kingdom Meteorological Office mesoscale model, derived from the model first described by Tapp and White (1976), which is a three-dimensional, non-hydrostatic primitive equation model now operating with 16 levels and a horizontal grid of 15 km (Golding, 1987(a)).

In view of the advances in mesoscale observational techniques described above, it would be tempting to imagine that an immediate way forward would be to incorporate the new data as input into a mesoscale model. Unfortunately, it is not as easy as that. A problem where existing mesoscale observations are concerned is that they tend to be of parameters such as cloud, rain and lightning which, though important in themselves, are not easily converted into the dynamically relevant variables, temperature, humidity and wind. Moreover, although networks of wind profiles will provide the wanted input when they come into operation, great care will be needed to ensure that the model and the observations are combined in an optimal way to produce initial conditions that are consistent with both the models and the observations (Gal-Chen, 1988).

Whether or not mesoscale input data are crucial for obtaining useful forecasts from mesoscale models depends on the meteorological situation. When the predominant forcing is by terrain features, such as land/water temperature contrasts, the initial state of the atmosphere need not be specified in great detail; indeed, it may be sufficient to rely solely on a background field from a larger-scale model as initial data. This approach can lead to useful forecasts of sea breezes, especially where there is a well-defined peninsula as in the case of Florida (Pielke, 1974), and of the distribution of boundary-layer convergence and resulting precipitation when a cold airstream encounters land after crossing either a relatively warm lake (Lavoie, 1972) or warm sea (Monk, 1987). In the case of mesoscale phenomena driven by their own internal dynamics, such as mesoscale convective systems and mesoscale frontal rainbands, however, there can be no escaping the need for detailed observations to depict the mesoscale phenomena (or their precursors) within the initial data. It may be that the synoptic-scale forcing represented in the background field will lead to the development of these phenomena in the model but in the absence of mesoscale input data it will not necessarily lead to a reliable mesoscale forecast of precisely when or where the development will occur.

Radar and satellite imagery are the only observational data presently available that can match the resolution of the mesoscale model. Although the imagery depicts variables that are of little direct use in a NWP model, the patterns in the imagery contain valuable information about the processes that produced them. Hence, it is the interpretation (by human analyst or eventually to some extent by expert systems) of the patterns seen in imagery that provides the key to producing the initial mesoscale analyses. This will call for the development over the next decade of a variety of indirect approaches:

- Introducing a more realistic distribution of vertical velocity (e.g. Warner et al. , 1982). Satellite and radar imagery provides an indication of the pattern of vertical motion which can be refined by interpreting the imagery in terms of conceptual models. The vertical velocity in the numercial model can then be adjusted via the field of horizontal divergence. Imbalances between the wind- and rainfields are created, and can be maintained, provided a diabatic heat source is available. This leads on to the next topic;

- Introducing more realistic latent heat effects through improved moisture analysis (e.g. Fiorino and Warner, 1981; Danard, 1985; Ninomiya et al., 1987).A knowledge of the detailed distribution of cloud and precipitation from the satellite and radar imagery,

supplemented by surface observations of cloud base etc., can enable the 3-D distribution of relative humidity and cloud water content to be estimated. If such an analysis yields high humidities in a region where the large-scale forcing implied by the background field is already inclined to generate rising motion, or where rising motion is imposed by the analyst via the divergence field, then the effect of latent heat release is to generate positive feedback, thereby intensifying the vertical motion. Realistic enhancement of the mesoscale circulations can be achieved only if the background field provided by the synoptic-scale model is reasonably accurate. In the event of a mismatch between the vertical velocities produced by the background field and the regions of high humidity implied by the imagery, the effect of any such area of high humidity implanted within the model would quickly decay;

- Adjusting the position of features predicted by the background field (Golding, 1987(b)). It is common for the location of a feature such as a front to be misplaced in the background field by a distance which, although perhaps not large by comparison with the grid length of the synoptic-scale model from which it is derived, may be large enough in a mesoscale model to create mismatches of the kind just described between background vertical velocity and observed relative humidity. In these circumstances it is possible to modify the background field to fit the imagery, perhaps by simply displacing fields by a prescribed amount;

- Introducing the effects of cloud boundaries on the radiation balance (Carpenter, 1982). Cloud cover has a major effect over land in decreasing the temperature of the underlying ground and of the air close to it and so the presence of a well-defined boundary to a cloud sheet can lead to the development of solenoidal circulations, resembling inland sea breezes. In some cases the circulation induced by a cloud edge can lead to the triggering of significant convection. Unfortunately, numerical models do not predict the distribution of cloud cover sufficiently well to reproduce accurately its effect on the radiation balance. This is because the actual cloud cover is influenced by so many small-scale effects not represented in the initial data and model formulation. Thus, the pragmatic way forward is to prescribe the detailed cloud cover in the model on the basis of the satellite imagery. This can be supplemented by information on surface temperature derived from the satellite in the cloud-free areas. In order to determine the effect of the cloud on the forecast for some future time, it may be necessary to define the cloud on the basis of an extrapolation of the present pattern. Clearly, however, such extrapolation forecasts are useful over only rather limited periods.

CONCLUDING REMARKS

The observational and forecasting methods just described are the ingredients of mesoscale forecasts: the problem remains of putting the ingredients together. Images from radars and satellites are key elements of mesoscale forecasting. One of the impediments in past years to successful exploitation, however, has been that the radar and satellite data have been available in different formats and projections, and have been separated

from the conventional line charts and numerical forecast products. The task of the forecaster is to synthesize a total picture of the mesoscale weather situation, for which it is necessary to be able to superimpose and otherwise combine all the products on the same display. This can now be achieved using workstations of the kind pioneered in the USA by the McIDAS team at Madison (Suomi et al. , 1983) and by the PROFS group at Boulder (Reynolds, 1983), and in Europe with the development of the FRONTIERS (Conway and Browning, 1988) and METEOTEL (Pircher, 1987) display systems.

The workstation approach is beginning to be adopted more widely and will put some powerful tools into the hands of the forecaster but, however ergonomic and user-friendly the designers are able to make these workstations, the quality of the forecast will still depend finally on the judgement and skill of the forecaster. Although recent developments with expert systems suggest that these will probably take over some of the easier decisions, it will be the forecaster who will have to select and blend the guidance products and forecasting methods most appropriate to each situation. In particular, it has been emphasised in this paper that "knowledge of meteorology" has to be used extensively to bridge the forecasting gap between the purely objective methods of linear extrapolation and NWP models. The forecaster must therefore have a good grasp of physical/dynamical principles and access to a lexicon of conceptual models and rules of thumb representing the structure and behaviour of mesoscale phenomena. It is unlikely that such phenomena will ever be completely sampled by operational observing networks in the foreseeable future and so there will be a need to use the conceptual models which have been built up from special research studies to make sense of the incomplete data that are available to the forecaster. Until recently, the interpretation of radar and satellite imagery in terms of conceptual models and dynamical principles was a neglected field but there is now a thrust towards better forecasting training in this area, including the compilation of improved imagery-interpretation manuals. One such programme which will bring the research and forecasting communities closer together is described by Bader et al. (1988).

Mesoscale forecasting can be regarded as the last bastion of intuitive meteorology. Its practice will bring with it a cure for what Snellman (1977) has referred to as "meteorological cancer" - a condition in which the forecaster feels unable to improve upon forecasts generated entirely by computer.

REFERENCES

Augustine, J.A. and E.J. Zipser, 1987: The use of wind profilers in a mesoscale experiment. Bull. Amer. Meteor. Soc., 68, 4-17.

Austin, G.L. and A. Bellon, 1974:: The use of digital weather records for short term precipitation forecasting. Quart. Jour. R. Meteor. Soc., 100, 658-664.

Austin, G.L., A. Bellon, P. Dionne and M. Roch, 1987: On the interaction between radar and satellite image nowcasting systems and mesoscale numerical models. Proc. Symp. Mesoscale Analysis and Forecasting, Vancouver, Canada. ESA SP-282, 225-228.

Bader, M.J., K.A. Browning, G.S. Forbes, F.J. Oliver and T.W. Schlatter, 1988: Towards improved subjective interpretation of satellite and radar imagery in weather forecasting: results of a workshop. Bull. Amer. Meteor. Soc. (In press).

Bellon, A. and G.L. Austin, 1984: The accuracy of short term radar rainfall forecasts. Jour. Hydrol., 70, 35-49.

Bellon, A., S. Lovejoy and G.L. Austin, 1980: Combining satellite and radar data for the short-range forecasting of precipitation. Monthly Weather Review, 108, 1554-1566.

Bent, R.B. and W.A. Lyons, 1984: Theoretical evaluations and initial operational experiences of LPATS (lightning position and tracking system) to monitor lightning ground strikes using a time-of-arrival (TOA) technique. Seventh Int. Conf. on Atmospheric Electricity, Albany. Amer. Meteor. Soc., 317-324.

Bergeron, T., 1965: On the low-level redistribution of water caused by orography. Supp. Proc. Conf. on Cloud Phys., Tokyo, 96-100.

Blackmer, R.H. Jr., R.O. Duda and E. Reboh, 1973: Application of pattern recognition techniques to digitized weather radar data. Final Report, Contract 1-36072, Stanford Research Institute.

Bond, J.E., K.A. Browning and C.G. Collier, 1981: Estimates of surface gust speeds using radar observations of showers. Meteor, Mag., 110, 29-40.

Brandes, E.A. and J.W. Wilson, 1982: Measuring storm rainfall by radar and raingauge. In: Thunderstorms: a social, scientific and technological documentary. Vol. 3: Instruments and techniques for thunderstorm observation and analysis. E. Kessler (Ed.), US Dept. of Commerce, 241-277.

Brown, R.A. , D.W. Burgess, J.K. Carter, L.R. Lemon and D. Sirmans, 1975: NSSL dual-Doppler radar measurements in tornadic storms: a preview. Bull. Amer. Meteor. Soc., 56, 524-526.

Browning, K.A., 1980: Local weather forecasting. Proc. R. Soc., London, A371, 179-211.

Browning, K.A., 1986: Conceptual models of precipitation systems. Weather and Forecasting, 1, 23-41.

Browning, K.A. and C.G. Collier, 1982: An integrated radar-satellite nowcasting system in the UK. In: Nowcasting. K.A. Browning (Ed.), Academic Press, 47-61.

Browning, K.A. and R. Wexler, 1968: The determination of kinematic properties of a wind field using Doppler radar. Jour. Appl. Meteor., 7, 105-113.

Browning, K.A., C.G. Collier, P.R. Larke, P. Menmuir, G.A. Monk and R.G. Owens, 1982: On the forecasting of frontal rain using a weather radar network. Monthly Weather Review, 110, 534-552.

Brummer, R., R. Bleck and M.A. Shapiro, 1984: The potential use of atmospheric profilers in short-range prediction. Proc. 2nd International Symp. on Nowcasting, Norrköping, Sweden, ESA SP-208, 209-212.

Carpenter, K.M., 1982: Model forecasts for locally forced mesoscale systems. In: Nowcasting. K.A. Browning (Ed.), Academic Press, 223-234.

Chadwick, N.B. and N. Hassel, 1987: Profiler: the next-generation, surface-based atmospheric sounding system. Preprints 3rd International Conference on Interactive Information and Processing Systems for Meteorology, Oceanography and Hydrology, New Orleans. Amer. Meteor. Soc., Boston, 15-21.

Chesters, D., A. Mostek and D.A. Keyser, 1986: VAS sounding images of atmospheric stability parameters. Weather and Forecasting, 1, 5-22.

Colquhoun, J.R., 1987: A decision tree method of forecasting thunderstorms, severe thunderstorms and tornadoes. Weather and Forecasting, 2, 337-345.

Conway, B.J. and K.A. Browning, 1988: Weather forecasting by interactive analysis of radar and satellite imagery. Phil. Trans. R. Soc. London., A324, 299-315.

Danard, M., 1985: On the use of satellite estimates of precipitation in initial analyses for numerical weather prediction. Atmos-Ocean, 23, 23-42

Donaldson, R.J. Jr., 1975: History of a tornado vortex traced by plan shear indicator. Preprints 16th Radar Meteor. Conf. Amer. Meteor. Soc., Boston, 80-82.

Doswell, C.A. III, 1986: Short-range forecasting. In: Mesoscale meteorology and forecasting. P.S. Ray (Ed.). Amer. Meteor. Soc., Boston, 689-719.

Eyre, J.R., 1988: Inversion of cloudy satellite sounding radiances by non-linear optimal estimation: theory and simulation for TOVS data. Submitted to Quart. Jour. R. Meteor. Soc.

Eyre, J.R., J.L. Brownscombe and R.J. Allam, 1984: Detection of fog at night using AVHRR imagery. Meteor. Mag., 113, 266-271.

Fiorino, M. and T.T. Warner, 1981: Incorporating surface winds and rainfall rates into the initialization of a mesoscale hurricane model. Monthly Weather Review, 109, 1914-1929.

Flood, C.R., 1985: Forecast evaluation. Meteor. Mag., 114, 254-260.

Fujita, T.T., E.W. Pearl and W.E. Shenk, 1975: Satellite-tracked cumulus velocities. Jour. Appl. Meteor., 14, 407-413.

Gal-Chen, T., 1988: A theory for the retrievals of virtual temperature from remote measurements of horizontal winds and thermal radiation. Monthly Weather Review. (In press).

Gilet, M. , 1984: The French weather radar network - a status report. Proc. 2nd International Symp. on Nowcasting, Norrköping, Sweden, ESA SP-208, 417-422.

Glahn, H.R. and D.A. Lowry, 1972: The use of model output statistics (MOS) in objective weather forecasting. Jour. Appl. Meteor., 11, 1203-1211.

Golding, B.W., 1987(a): Short range forecasting over the United Kingdom using a mesoscale forecasting system. In: Short and medium range weather prediction. Ed. Matsumo, Tokyo. Meteor. Soc. Japan, 563-572.

Golding, B.W., 1987(b): Strategies for using mesoscale data in an operational mesoscale model. Proc. Symp. Mesoscale Analysis and Forecasting, Vancouver, Canada, ESA SP-282, 569-578.

Gurka, J.J., 1987: Examples showing how analysis of water vapor imagery suggests modification to numerical model analysis and prediction. In: Satellite and radar imagery interpretation. M. Bader and A. Waters (Eds.). Published by EUMETSAT, Darmstadt Eberstadt, Federal Republic of Germany, 125-141.

Hasler, A.F., W.E. Shenk and W.C. Skillman, 1976: Wind estimates from cloud motions: phase 1 of an in situ aircraft verification experiment. Jour. Appl. Meteor., 15, 10-15

Kennington, L. and D.W. Burgess, 1981: Automatic recognition of mesocyclones from single Doppler radar data. Preprints 22nd Conf. on Radar Meteor., Amer. Meteor. Soc., Boston, 704-706.

Hill, F.F., 1983: The use of average annual rainfall to derive estimates of orographic enhancement of frontal rain over England and Wales for different wind directions. Jour. Climatology, 3, 113-129.

Hill, F.F., K.A. Browning and M.J. Bader, 1981: Radar and raingauge observations of orographic rain over South Wales. Quart. Jour. R. Meteor. Soc., 107, 643-670.

Hoskins, B.J., M.E. McIntyre and A.W. Robertson, 1985: On the use and significance of isentropic potential vorticity maps. Quart. Jour. R. Meteor. Soc., Ill, 877-946.

Katsaros, K.B. and R.M. Lewis 1986: Mesoscale and synoptic scale features of North Pacific weather systems observed with the scanning multichannel microwave radiometer on NIMBUS-7. Jour. Geophys. Res., 91, 2321-2330.

Kelly, G.A.M., B.W. Forgan, P.E. Powers and J.F. LeMarshall, 1982: Mesoscale observations from a polar orbiting satellite vertical sounder. In: Nowcasting. K.A. Browning (Ed.), Academic Press, 107-121.

Kuo, Y-H., D.O. Gill and L. Cheng, 1987: Retrieving temperature and geopotential fields from a network of wind profiler observations. Monthly Weather Review, 115, 3146-3165.

Lavoie, R.L., 1972: A mesoscale numerical model of lake-effect storms. Jour. Atmos. Sci., 29, 1025-1040.

Leary, C.A. and R.A. Houze, Jr., 1979: The structure and evolution of convection in a tropical cloud cluster. Jour. Atmos. Sci., 36, 437-457.

Lee, A.C.L., 1986: An operational system for the remote location of lightning flashes using a VLF arrival time difference technique. Jour. Atmos. Ocean. Tech., 3, 630-642.

Lhermitte, R.M. , 1970: Dual Doppler radar observations of convective storm circulation. Preprints 14th Radar Meteor. Conf., Tucson, Arizona. Amer. Meteor. Soc., Boston, 153-156.

Ligda, M.G.H., 1957: Middle latitude precipitation patterns as observed by radar. Dept. of Oceanography and Meteorology, Texas A. and M. University Tech. Rep.

Liljas, E., 1982: Automated techniques for the analysis of satellite cloud imagery. In: Nowcasting. K.A. Browing (Ed.), Academic Press, 167-176.

Little, C.G., 1982: Ground-based remote sensing for meteorological nowcasting. In: Nowcasting. K.A. Browning (Ed.), Academic Press, 65-85.

Lovejoy, S. and G.L. Austin, 1979: The delineation of rain areas from visible and IR satellite data for GATE and mid-latitudes. Atmos-Ocean, 17, 77-92.

Maier, M.W., R.C. Binford, L.G. Byerley, E.P. Krider, A.E. Pifer and M.A. Uman, 1983: Locating cloud-to-ground lightning with wideband magnetic direction finders. Fifth Symposium Meteorological Observations and Instrumentation, 11-15 April 1983, Toronto, 497-504

Mansfield, D., 1987: Forecasting stratus over the British Isles. Proc. Symp. Mesoscale Analysis and Forecasting, Vancouver, Canada, ESA SP-282, 423-428.

McGinley, J., 1986: Nowcasting mesoscale phenomena. In: Mesoscale meteorology and forecasting. P.S. Ray (Ed.), Amer. Meteor. Soc., Boston, 657-688.

Monk, G.A., 1987: Topographically related convection over the British Isles. In: Satellite and radar imagery interpretation. M. Bader and A. Waters (Eds.). Published by EUMETSAT, Darmstadt, Federal Republic of Germany, 305-324.

Mosher, F.R. and T.R. Stewart, 1981: Characteristics of water vapour tracked winds. NAVENVPREDRSCHFAX contract report CR.81-06, 51 pp.

Negri, A.J. and T.H. Vonder Haar, 1980: Moisture convergence using satellite-derived wind fields: a severe local storm case study. Monthly Weather Review, 108, 1170-1182.

Ninomiya, K., R. Taira, M. Ueno, K. Kurihara and T. Kudo, 1987: Mesoscale very short-range numerical prediction with dynamical initialization including condensation heating. Proc. Symp. Mesoscale Analysis and Forecasting, Vancouver, Canada, ESA SP-282, 611-616.

Peslen, C.A., 1980; Short-interval SMS wind vector determination for a severe local storm area. Monthly Weather Review, 108, 1407-1418.

Pielke, R.A., 1974: A three-dimensional numerical model of the sea breezes over south Florida. Monthly Weather Review, 102, 115-139.

Pircher, V., 1987: Combined use in operational forecasting of animated imagery and NWP fields. In: Satellite and radar imagery interpretation. M. Bader and A. Waters (Eds.). Published by EUMETSAT, Darmstadt Eberstadt, Federal Republic of Germany, 365-383.

Purdom, J.F.W., 1982: Subjective interpretation of geostationary satellite data for nowcasting. In: Nowcasting. K.A. Browning (Ed.), Academic Press, 149-166.

Reiff, J., 1987: Forecasting boundary layer clouds and fog: a review on operational numerical models. Proc. Symp. Mesoscale Analysis and Forecasting, Vancouver, Canada, ESA SP-282, 407-414.

Reynolds, D.W., 1983: Prototype workstation for mesoscale forecasting. Bull. Amer. Meteor. Soc., 64, 264-273.

Roesli, H.P., J. Joss and C.G. Collier, 1987: COST-73 and its application in very-short-range forecasting. Proc. Symp. Mesoscale Analysis and Forecasting, Vancouver, ESA SP-282, 13-18.

Saunders, R.W., 1988: A comparison of satellite retrieved parameters with mesoscale model analyses. Submitted to Quart. Jour. R. Meteor. Soc.

Scofield, R.W. and V.J. Oliver, 1977: A scheme for estimating convective rainfall from satellite imagery. Tech. Memo. NESS 86, NOAA Environmental Laboratories, Boulder, 41 pp.

Snellman, L.W., 1977: Operational forecasting using automated guidance. Bull. Amer. Meteor. Soc., 58, 1036-1044

Suomi, V.E., R. Fox, S.S. Limaye and W.L. Smith, 1983: McIDAS III: a modern interactive data access and analysis system. Jour. Clim. and Appl. Meteor., 22, 766-778.

Szoke, E.J., M.L. Weisman, J.M. Brown, F. Caracena and T.W. Schlatter, 1984: A subsynoptic analysis of the Denver tornadoes of 3 June 1981. Monthly Weather Review, 112, 790-808.

Tapp, M.C. and P.W. White, 1976: A non-hydrostatic mesoscale model. Quart. Jour. R. Meteor. Soc., 102, 277-296.

Tsonis, A.A. and G.L. Austin, 1981: An evaluation of extrapolation techniques for the short-term prediction of rain amounts. Atmos-Ocean, 19, 54-65.

Warner, T.T., T.C. Tarbell and S.W. Wolcott, 1982: An example of the use of satellite cloud and surface rainfall data to initialize a numerical weather prediction model. In: Nowcasting. K.A. Browning (Ed.), Academic Press, 235-247.

Wilk, K.E. and K.C. Gray, 1970: Processing and analysis techniques used with the NSSL weather radar system. Proc. 14th Weather Radar Conf., Amer. Meteor. Soc., Boston, 369-374.

Wilson, J. and H.P. Roesli, 1985: Use of Doppler radar and radar networks in mesoscale analysis and forecasting. ESA Journal, 125-146.

Wilson, J.W. and W.E. Schreiber, 1986: Initiation of convective storms at radar-observed boundary-layer convergence lines. Monthly Weather Review, 114, 2516-2536.

Wolfsberg, D.G., 1987: Retrieval of three-dimensional wind and temperature fields from single-Doppler radar data. Cooperative Inst. for Mesoscale Meteorological Studies Rep. No. 84, Norman, Okla., 91 pp.

Zipser, E.J., 1982: Use of a conceptual model of the life cycle of mesoscale convective systems to improve very-short-range forecasts. In: Nowcasting. K.A. Browning (Ed.), Academic Press, 191-204.

Zrnic, D.S., D.S. Burgess and L.D. Kennington, 1985: Automatic detection of mesocyclonic shear with Doppler radar. Jour. Atmos. Oceanic. Technol., 2, 425-438.

MESOSCALE WEATHER SYSTEMS - SOUTH AMERICAN PHENOMENA

by
M.A.F. Silva Dias

Department of Meteorology
Institute of Astronomy and Geophysics
University of Sao Paulo, Brazil

1. INTRODUCTION

In an attempt to forecast the weather a few hours ahead it is necessary to observe and understand the so-called mesoscale weather systems, which include squall lines, mesoscale convective complexes and subsynoptic-scale vortices, and their interaction with surface inhomogeneities, in particular land/water boundaries and mountain-valley circulations. As was stated by Browning (1986), the forecaster needs to have conceptual models of each type of precipitation system in order to recognize the genesis of a particular type and be able to forecast it. In this sense, each geographical region has its own characteristics (climatological and physical) that need to be taken into account and properly incorporated in a conceptual model.

In South America, in the tropical, subtropical and mid-latitude regions, there are several manifestations of mesoscale systems which merit closer study, since they are responsible - as is usually the case with mesoscale systems - for a significant amount of precipitation. Only the major types of system will be presented here, and only a few features of their environment and structure will be shown. Further details may be found in the references. The objective is to call attention to some of the more important mesoscale systems which occur in South America in the sense that they are often the cause of inadequate weather forecasts.

2. SQUALL LINES

2.1 Tropical latitudes

Squall lines have been observed in tropical South America along the northern and north-eastern coasts propagating inland over the Amazon region or over north-eastern Brazil. Kousky (1980) and Cavalcanti and Kousky (1982) point out that the squall lines start out as a line of convection parallel to the coast, generated by the sea-breeze circulation. Not every line of convection develops into a propagating squall line, however, nor does the line of convection form every single day, while the frequency of occurrence has a strong seasonal variation, as may be seen from Figure 1 (from Cavalcanti and Kousky, 1982). In a six-year period the maximum frequency of occurrence of the line of convection (shown in Figure 1(a)), is in the months of July, August and September. Cohen (1988) shows that those are also the months of higher frequency of squall-line occurrence (Figure 1(b)). In the recent experiment GTE/ABLE IIB, which took place in the months of April and May 1987, it was also noted (Climanalise, April and May 1987) that, while not every line of convection developed into a propagating squall line, there were a few days in succession in which squall lines were observed to form and propagate inland, in which case they could be tracked in satellite images for more than 24 hours. It should be noted that the month of July corresponds to the maximum northward displacement of the ITCZ, which leaves the northern coast

with a synoptic situation characterized by the south-easterly trade winds (as may be seen in Figure 2(b)), upon which is superimposed the sea-breeze circulation. According to Kousky and Molion (1981), the minimum of occurrence of the line of convection in January and February is a result of enhanced compensating subsidence over northern and north-eastern Brazil, itself a result of generalized convection in the Amazon region and throughout central Brazil, associated with the thermal low pressure system (shown in Figure 2(a)).

As an example of squall-line development from a line of convection over the tropical north coast of South America, the case of 5, 6 and 7 May 1987 (shown in Figure 3) may be considered.

Betts et al. (1976) and Miller and Betts (1977) analysed environmental conditions and propagating characteristics associated with squall lines which travelled over Venezuela. Although the authors do not discuss the origin of such systems, it may well be that it is the same as that described above for the sea-breeze circulation. In all cases studied it appears that the existence of a low-level jet around 700 hPa plays an important role in generating propagating disturbances. This is also confirmed by the results of Silva Dias et al. (1984) (linear spectral model). Figure 3 from Ferreira (1988) shows the mean wind profiles in soundings prior to squall-line development (Figure 3(e)) and on days where no squall line was observed to form (Figure 3(f)), in northern Brazil during GTE/ABLE IIB. It should be noted that the low-level jet is deeper and faster prior to the squall-line formation.

2.2 Subtropical and mid-latitudes

In subtropical and mid-latitude South America, frontal systems are often accompanied by precipitation bands similar to the ones described by Houze et al. (1976). A few frontal rainbands may develop into squall lines which propagate faster than the surface cold front and with an orientation parallel to either the surface cold front or to the surface warm front or to upper-tropospheric frontal discontinuities (see Browning, 1986). The frontal systems may reach tropical latitudes in South America, as shown by Kousky (1979) and Oliveira and Nobre (1986 (a) and (b)) and associated squall lines are sometimes seen as far north as 15°S. Calheiros (1976) documented pre-frontal squall lines around 23°S.

The environmental impact of such systems may be observed in the altitude synoptic network, as may be seen in Figure 4 (from Scolar and Silva Dias, 1982), which shows vertical profiles of large-scale vorticity and divergence in the presence of squall lines and fronts. It may be seen that the low-level convergence during the times when squall lines were in the area is larger, on average, than the low-level convergence associated with fronts.

As an example of a pre-frontal squall line, consider the case shown in Figures 5 and 6 which took place from 18 to 19 November 1981 and previously described in Lima and Silva Dias (1986) and Silva Dias (1988). Figure 5(b) shows the successive positions of a squall line which propagated due east during the night of 18 November until the early morning of 19 November. In Figure 5(a) it may be seen that on 18 November at 1517 LT, there was extensive cloudiness associated with a cold front (see Figure 6(g)) in southern Brazil but that there were also a few cloud bands with a north-south orientation similar to that which crossed the State of Sao Paulo during the night and shown in the radar display in Figure 5(b). Figure 6 shows large-scale fields

associated with the squall line: a cold front may be seen to move from the south but remains to the south of the squall trajectory. Figure 7 shows the fields in a mesoscale analysis associated with the squall line and also the radar-observed structure of reflectivity in a few portions of the squall line.

3. MESOSCALE CONVECTIVE COMPLEXES

According to the definition of Maddox (1980), the mesoscale convective complexes (MCCs) also occur in tropical and subtropical South America. Velasco and Fritsh (1987) document their occurrence during the period from May 1981 to May 1983. Figure 8 (from Velasco and Fritsh, 1987) shows the geographic and monthly distribution of the MCCs, and it may be noted that there are two preferred locations in South America: downwind from the Andes mountains in the subtropics and downwind from the Andes in the equatorial easterlies. Figure 9 shows a composite analysis of nine MCCs which occurred in springtime in the subtropical region (from Guedes and Silva Dias, 1985) where it may be seen that a low-level warm and moist flow from the Amazon region feeds the systems which formed over northern Argentina and southern Bolivia and travelled due east over Paraguay, Uruguay and southern Brazil (Figure 9(f)). It may also be noted that an upper-level jet remains to the south of the MCC, as may be seen in Figure 10. As also happens in North America, the mountain-valley circulation imposes a diurnal modulation in the formation of the MCC, as may be seen in Figure 11(a). Paegle et al. (1982) discuss the diurnal modulation in the particular case of South America. This is partly due to the diurnal variation of the low-level jet (seen at 850 hPa) and partly due to surface-enhanced convergence in the evening and at night, the first arising from inertial effects acting on the upper branch of the mountain-valley circulation and the latter from the katabatic flow converging with the synoptic flow at the surface in the valley. The tropical MCCs suffer the type of modulation shown in Figure 11(b). The possible role of the upper-level flow in the formation of the MCC as described by Uccellini and Johnson (1979) and Uccellini (1980) should not be disregarded - even in a barotropic environment - since, as noted by Virji (1982) and Silva Dias et al. (1983), convection over the Amazon region enhances the anticyclonic flow in upper levels, thus generating an environment which may favour the MCC formation off the coasts of Colombia and Equador. Velasco and Fritsh (1987) suggest that the tropical MCCs, which occur more frequently in an El Niño year, also contribute to the intensification of the upper-level anticyclonic flow (the "Bolivian high"), thus affecting the speed of the subtropical jet, which in turn may affect the frequency of occurence of MCCs in the subtropical regions during an El Niño year.

4. COLD-AIR VORTICES - INVERTED-COMMA CLOUDS

The inverted-comma clouds which form behind a cold frontal zone - with scales in the meso-alpha range (in Orlanski's classification, 1975) or in the subsynoptic scale (according to the Japanese nomenclature) - have been known to occur in the southern hemisphere in general (Streten and Troup, 1973; Troup and Streten, 1972). Figure 12(a) shows the axes of vortex formation leading to inverted-comma clouds for the summer and intermediate seasons, while Figure 12(b) from Carleton (1981), shows the winter frequency. It may be seen that the south-eastern region of South America, including southern Brazil, Uruguay and north-eastern Argentina, appear as regions of cyclogenesis. Browning (1986) associates the formation of the comma cloud vortex with the cold conveyor belt, parallel to the surface warm front which, after emerging from the west side of the warm conveyor belt, may descend, turning cyclonicaly (see

Figure 13). Figure 14 shows the case of 14 and 15 April 1979 (Bonatti and Rao, 1987). Figure 15 shows the large-scale fields of wind, temperature and vorticity on 13, 14 and 15 April. It may be seen that the vortex starts out in a warm region, probably because of subsidence warming in the descending cold conveyor belt, apparent at the 850 hPa level and also at 700 hPa (not shown). After the initial stages of formation, the vortex has an evolution similar to that of a frontal zone and may acquire dimensions similar to a regular front, as may be seen in Figure 14.

Satyamurty and Mattos (1987) determined the frontogenetical function for the period 1979 - 1987; Figure 16 shows their results concerning the field of the frontogenetical function for the months of January, April, July and October at 850 hPa. It may be noted that, in summer, a maximum in the frontogenetic function in South America is located at the southern end of Argentina and Chile. In winter, the maximum shifts northward, over northern Chile, and north-west Argentina. Also, the dividing line between frontogenesis and frontolysis has a north-west/south-east orientation which, in winter, crosses the Atlantic coast at about 22°S.

5. CONCLUSION

The systems described in the preceding sections have received some attention from the meteorological community in recent years. In the particular case of South America, there is an enormous task to be carried out in the documentation of the complexities and peculiarities of such systems. The effort to forecast them is still a qualitative one. There is a great need for numerical simulations and field experiments to unravel the essence of these systems and to find new ways of representing them, either as conceptual entities or a numerical solutions. Until then, an effort toward documentation in the form of case-studies should be particularly encouraged.

* * *

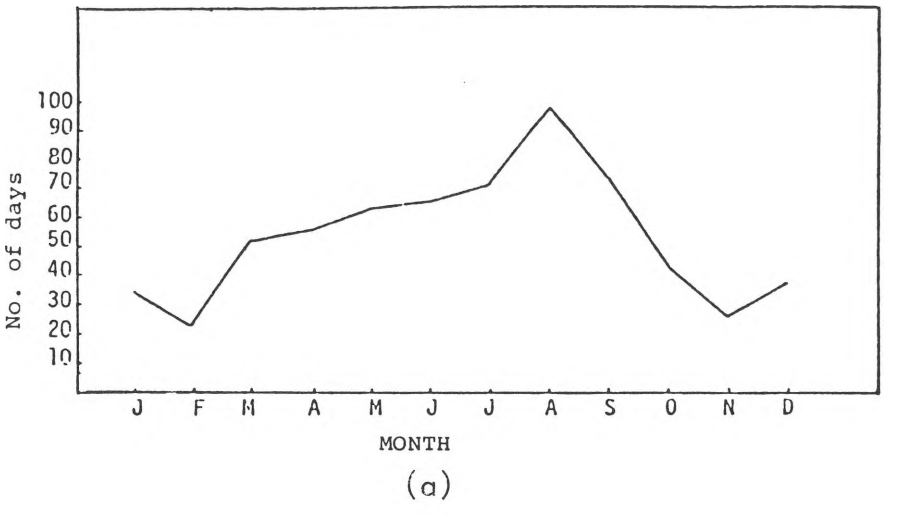

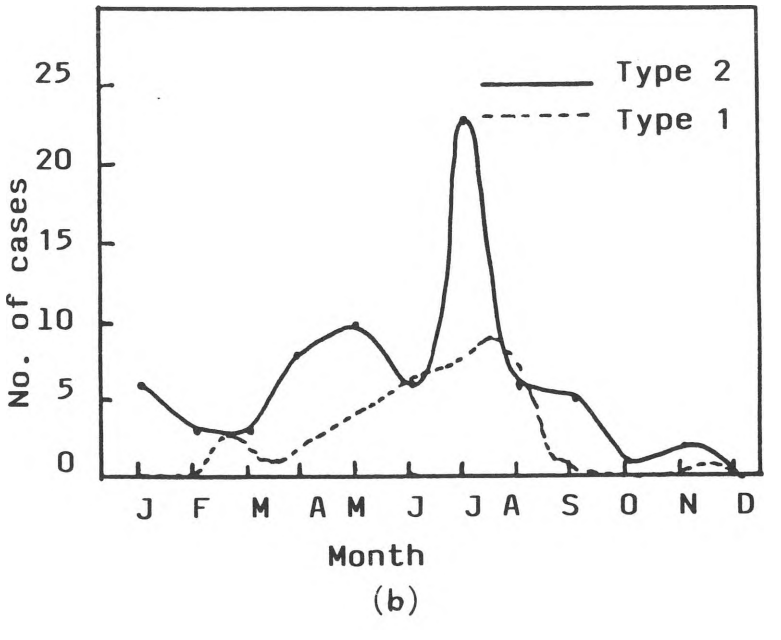

Figure 1 - (a) Monthly frequency of occurrence of a line of convection along the northern coast of Brazil during the period 1975-1989 (from Cavalcanti and Kousky, 1982) ; (b) Monthly frequency of squall-line occurrence in northern Brazil from March 1979 to December 1986. (Type 1 refers to the squall lines which propagate between 170 and 400 km inland and Type 2 refers to squall lines which propagate more than 400 km inland (from Cohen, 1988)

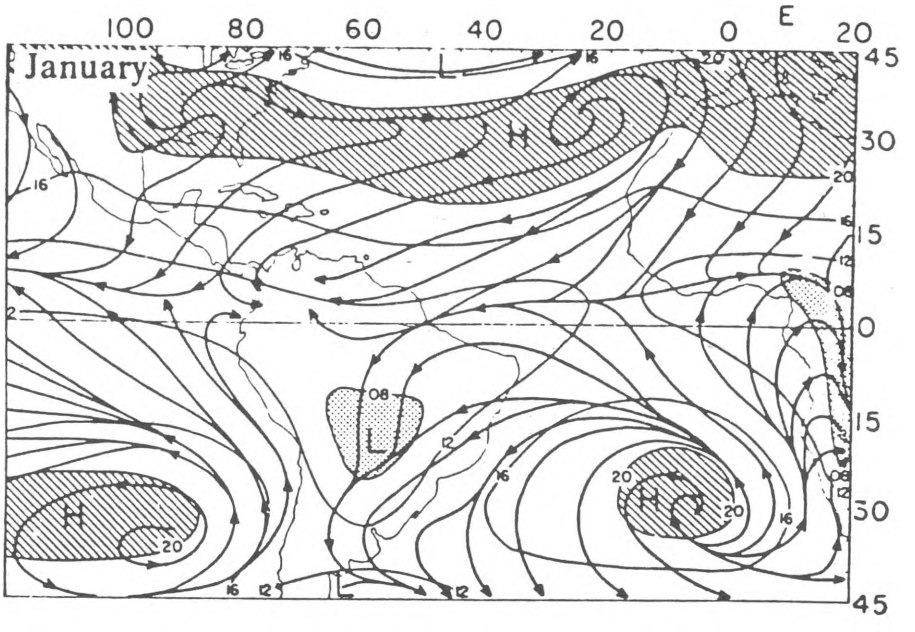

(a)

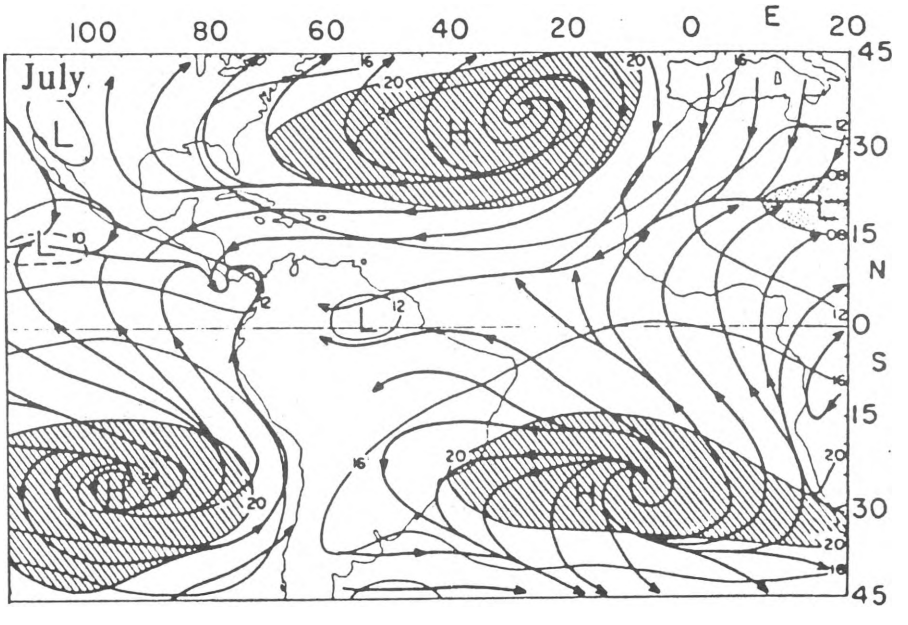

(b)

Figure 2 - Streamlines and pressure field at mean sea-level for (a) January and (b) July (from Riehl, 1979)

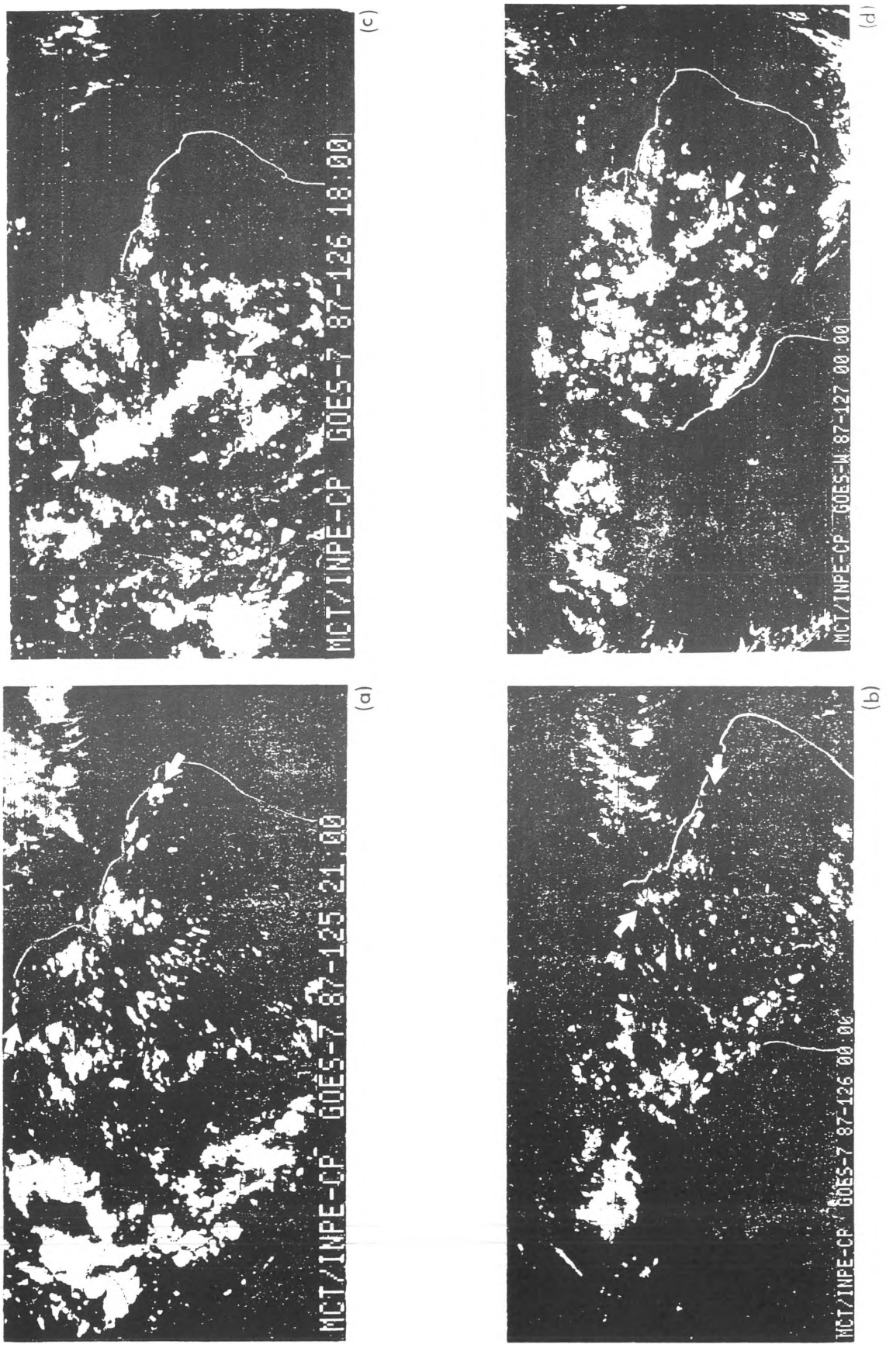

Figure 3 - Infra-red images from GOES-7 on: (a) 5 May 1987 at 2100 GMT; (b) 6 May 1987 at 0000 GMT; (c) 6 May 1987 at 1800 GMT; and (d) 7 May 1987 at 0000 GMT

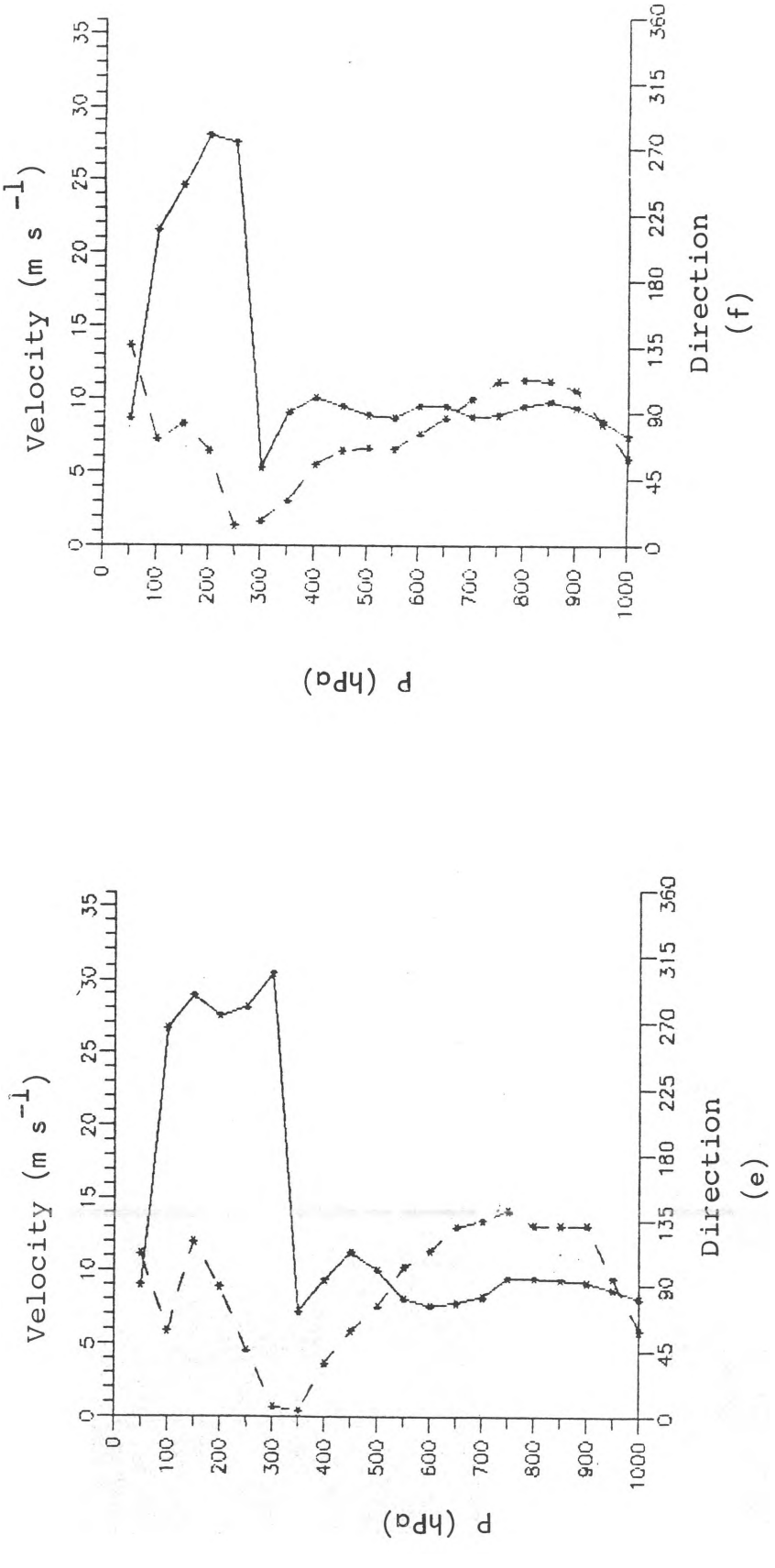

Figure 3 - (e) mean vertical profiles at wind speed (broken line) and direction (cont.) (solid line) for six consecutive days with squall-time development during GTE/ABLE IIB; (f) Same as (e) but for days without squall-line development (from Ferreira, 1988)

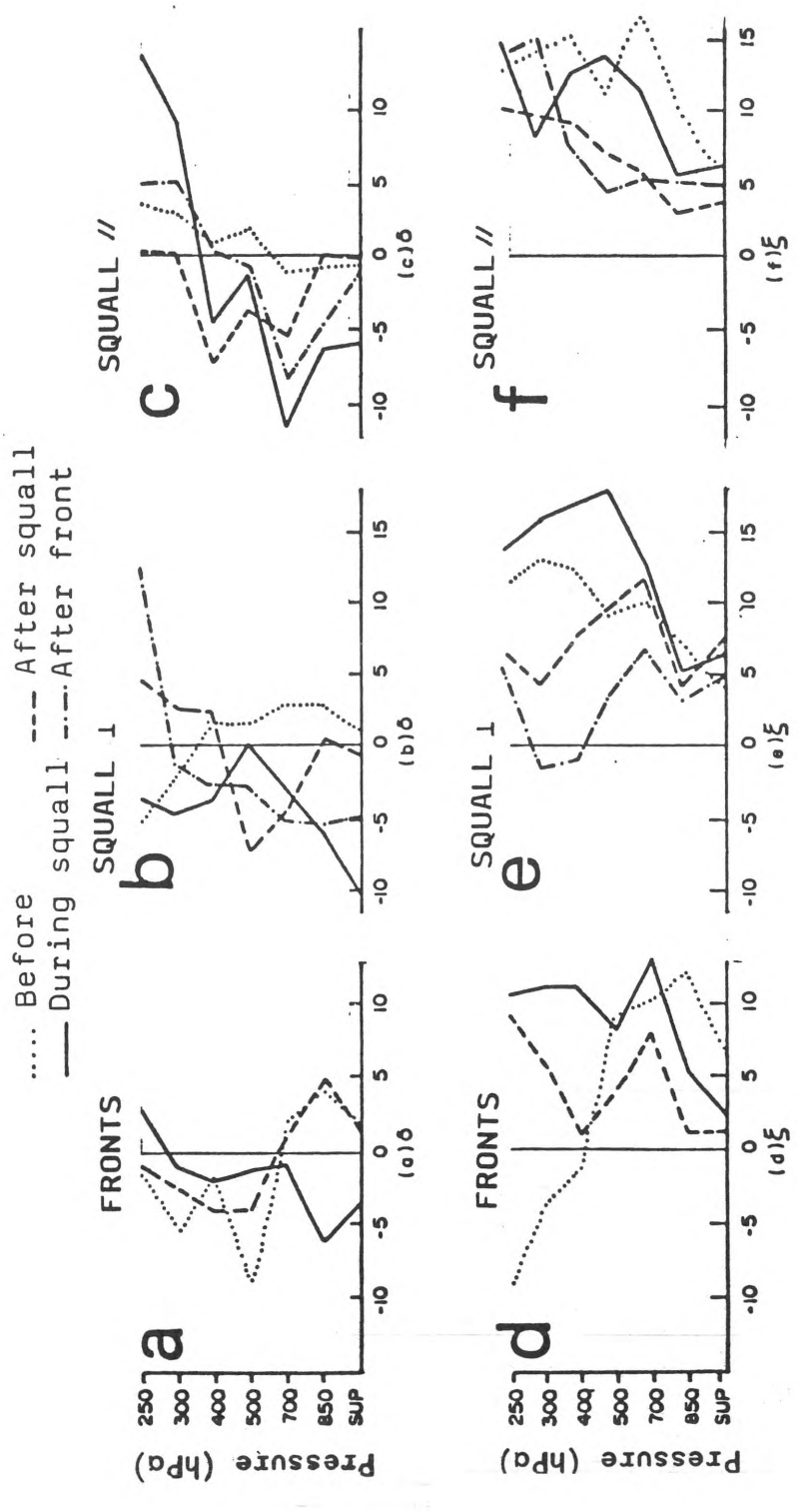

Figure 4 - Mean vertical profiles at divergence (δ) and vorticity (ξ) (in $10^{-6}\ s^{-1}$) for southern Brazil associated with cold fronts (a and d), squall lines perpendicular to the surface cold front (b and e) and squall lines parallel to the surface cold front (c and f) (from Scolar and Silva Dias, 1982)

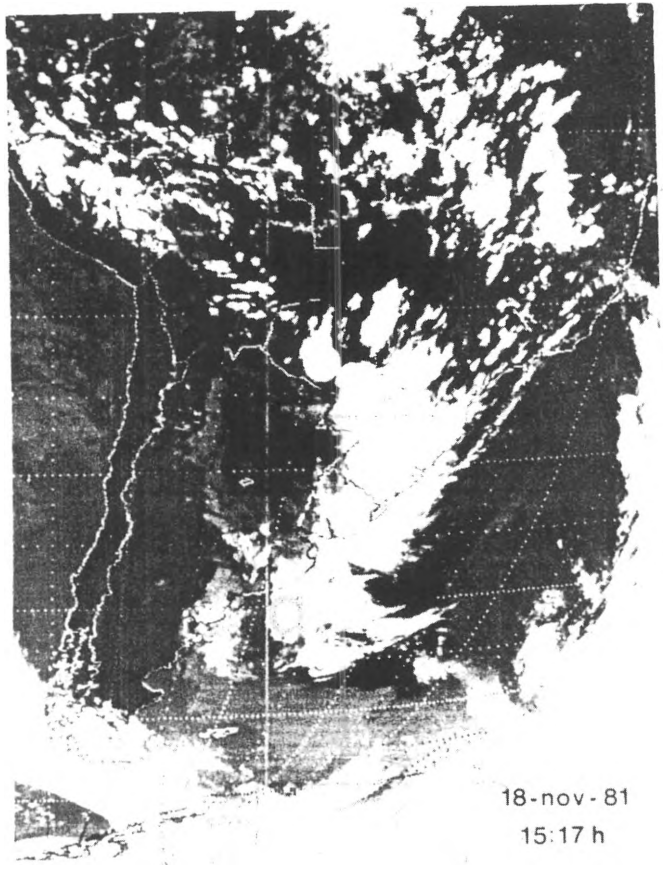

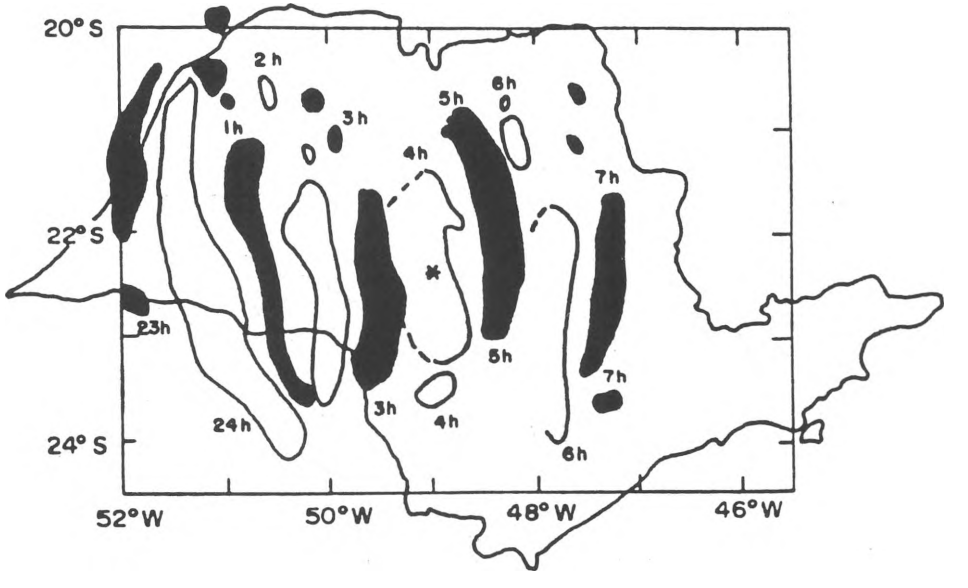

(a) (b)

Figure 5 - (a) Satellite infra-red image from GOES-E at 1517 LT on 18 November 1981; (b) Successive positions of a squall line as detected by the Bauru C-band radar during the night of 18 November and early morning of 19 November 1981. (The times indicated are local times.) (from Lima and Silva Dias, 1986)

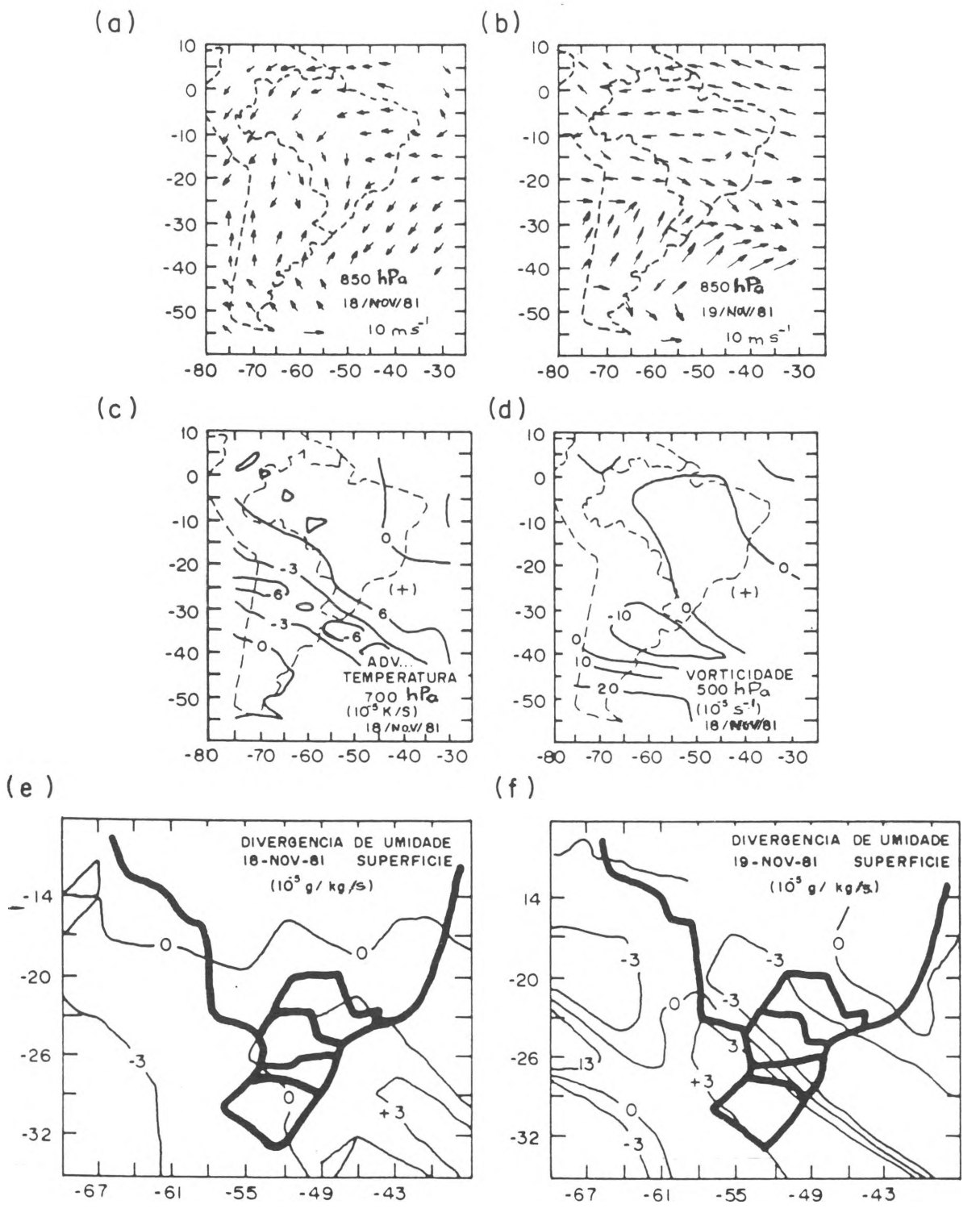

Figure 6 - Synoptic fields at 1200 GMT: (a) and (b) correspond to the windfield on 18 and 19 November 1981, respectively; (c) temperature advection on 18 November at 700 hPa; (d) vorticity at 500 hPa on 18 November; (e) and (f) surface moisture divergence on 18 and 19 November, respectively

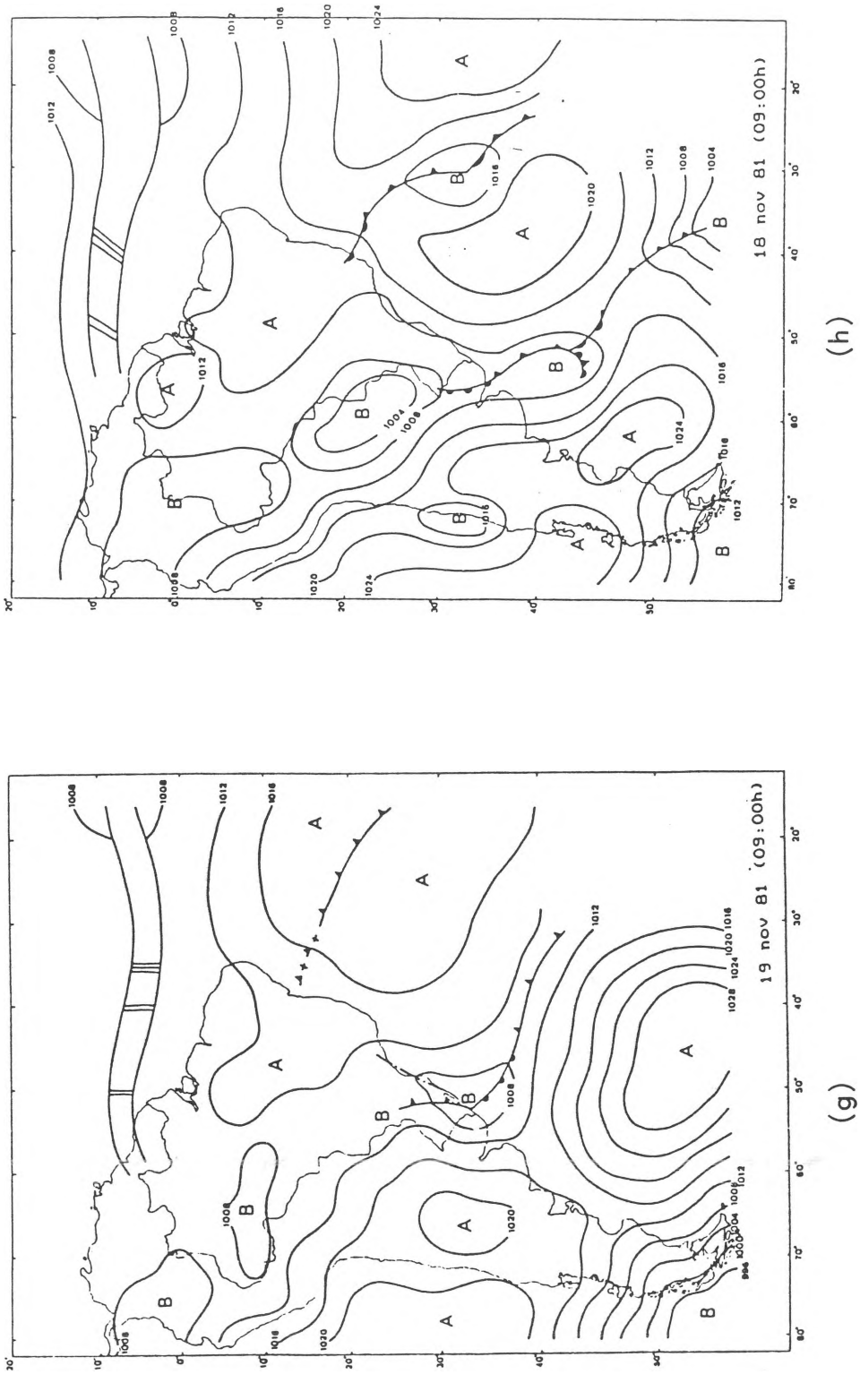

Figure 6 - (g) and (h) sea-level pressure on 18 and 19 November respectively (cont.) (from Silva Dias, 1988 and Lima and Silva Dias, 1986)

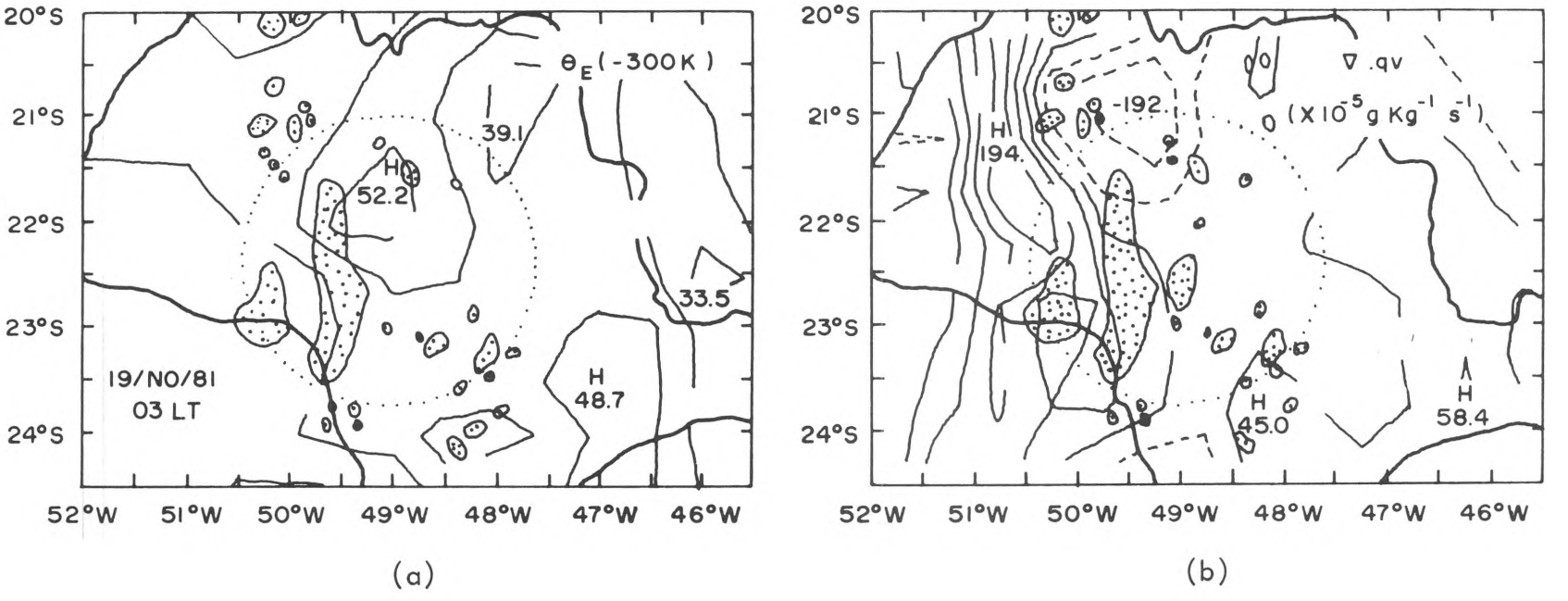

Figure 7 - (a) Equivalent potential temperature at the surface mesoscale analyses on 19 November 1981 at 0300 LT; (b) same for moisture divergence (from Lima and Silva Dias, 1986)

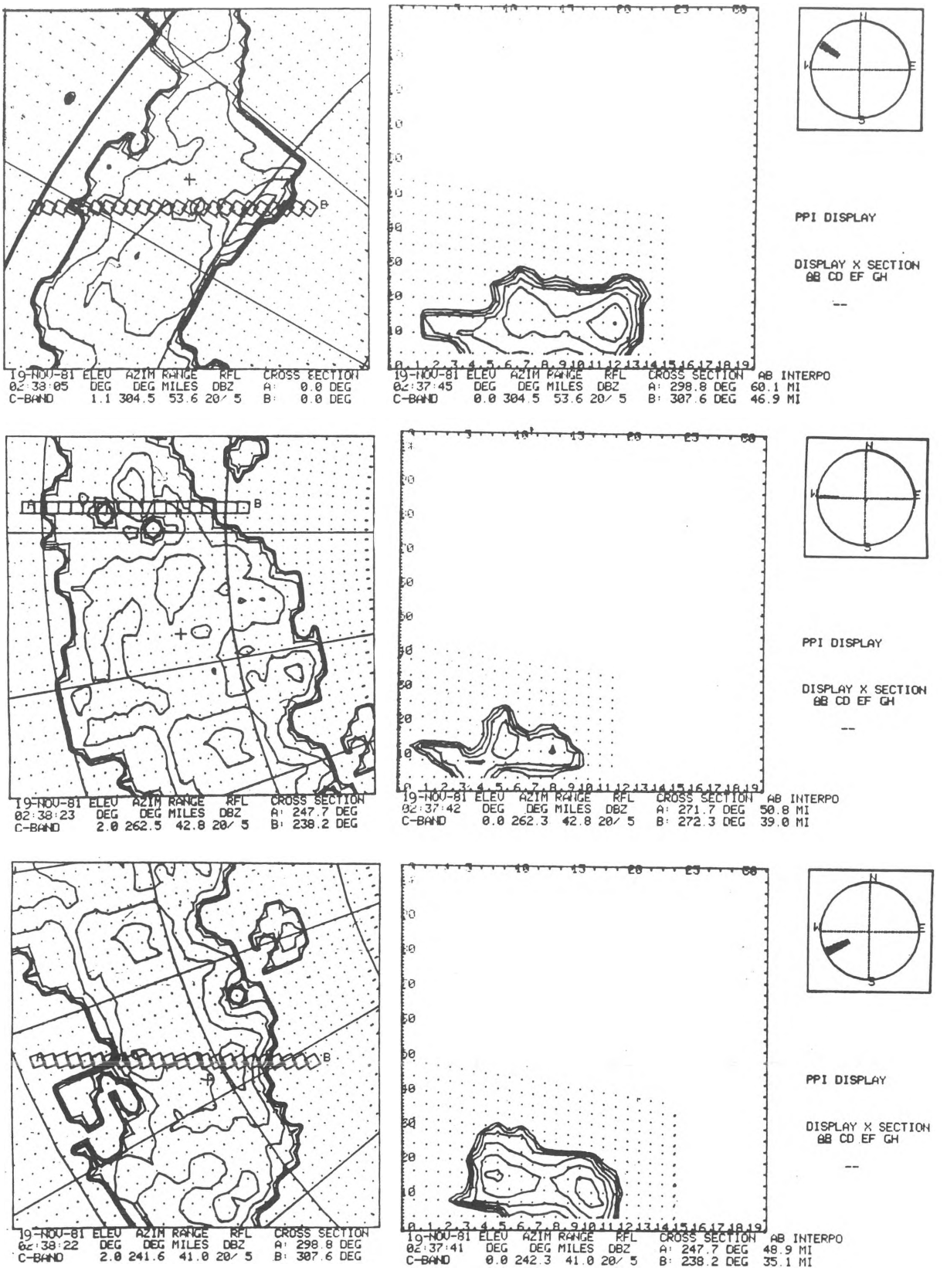

Figure 7(c) - PPI displays and vertical cross-section along the indicated AB lines at 0238 LT from the Bauru C-band radar (source: M.A. Lima)

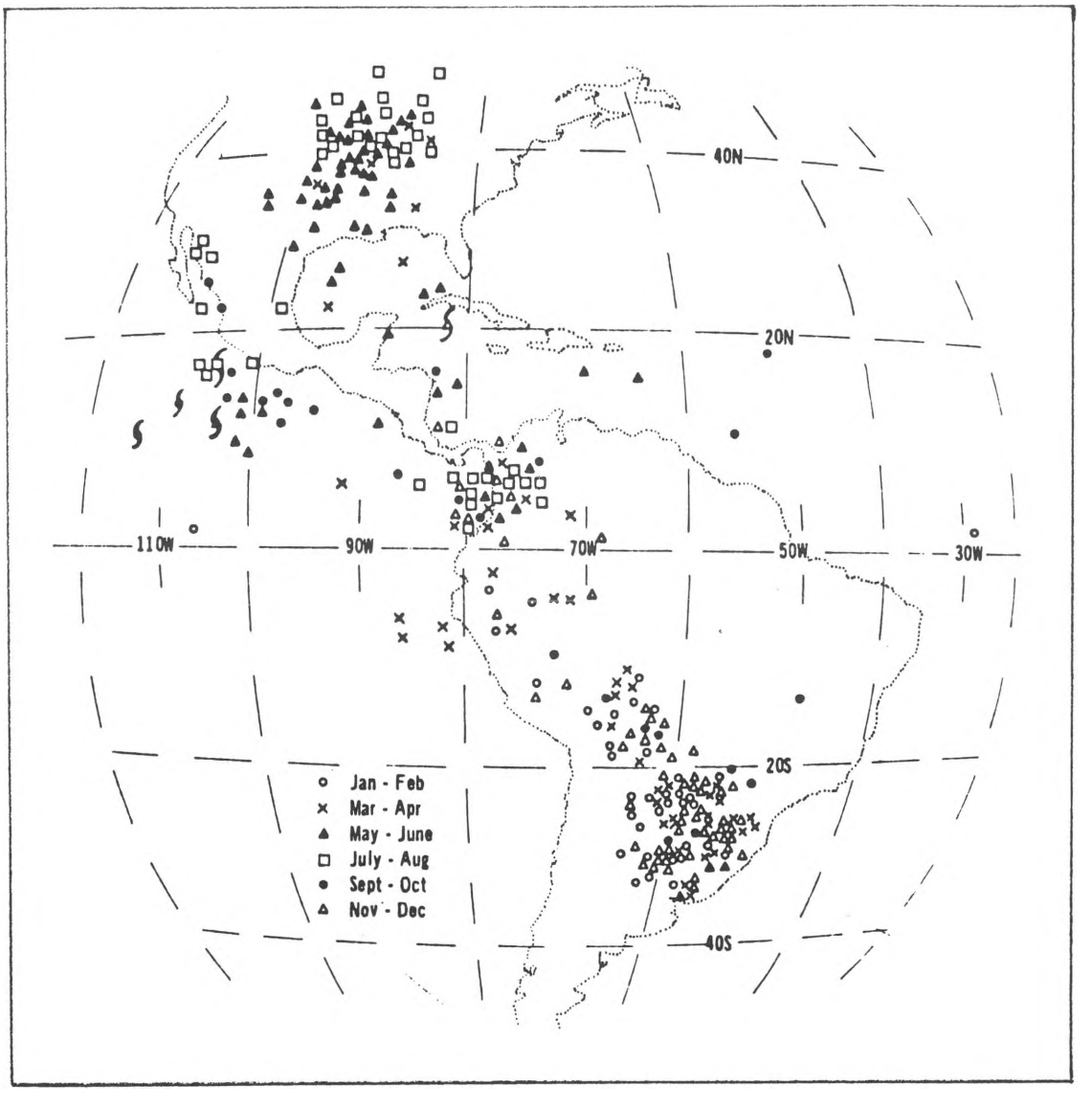

Figure 8 - Geographic and monthly distribution of MCCs in and around the Americas. Locations are for the MCC cold-cloud shield at the time of maximum extent. Hurricane symbols indicate an MCC that developed into a tropical storm. Systems that were first a tropical storm and then an MCC are not shown (from Velasco and Fritsch, 1987)

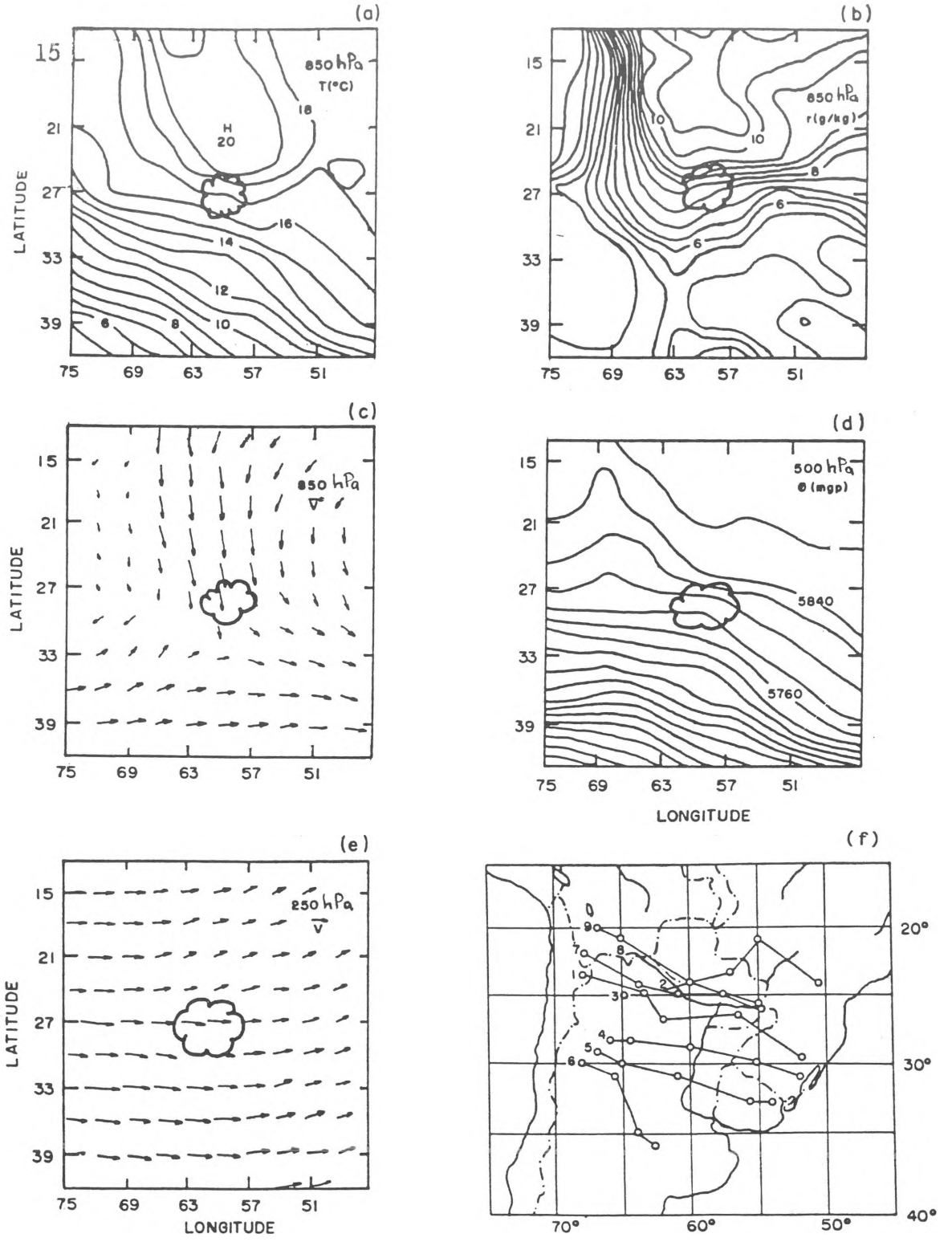

Figure 9 - Composite fields around the MCC (indicated in the centre of the grid of nine springtime MCCs: (a) 850 hPa temperature; (b) 850 hPa water vapour mixing ration; (c) 850 hPa windfield; (d) 500 hPa geopotential; (e) 250 hPa windfield; (f) trajectories (from Guedes and Silva Dias, 1985)

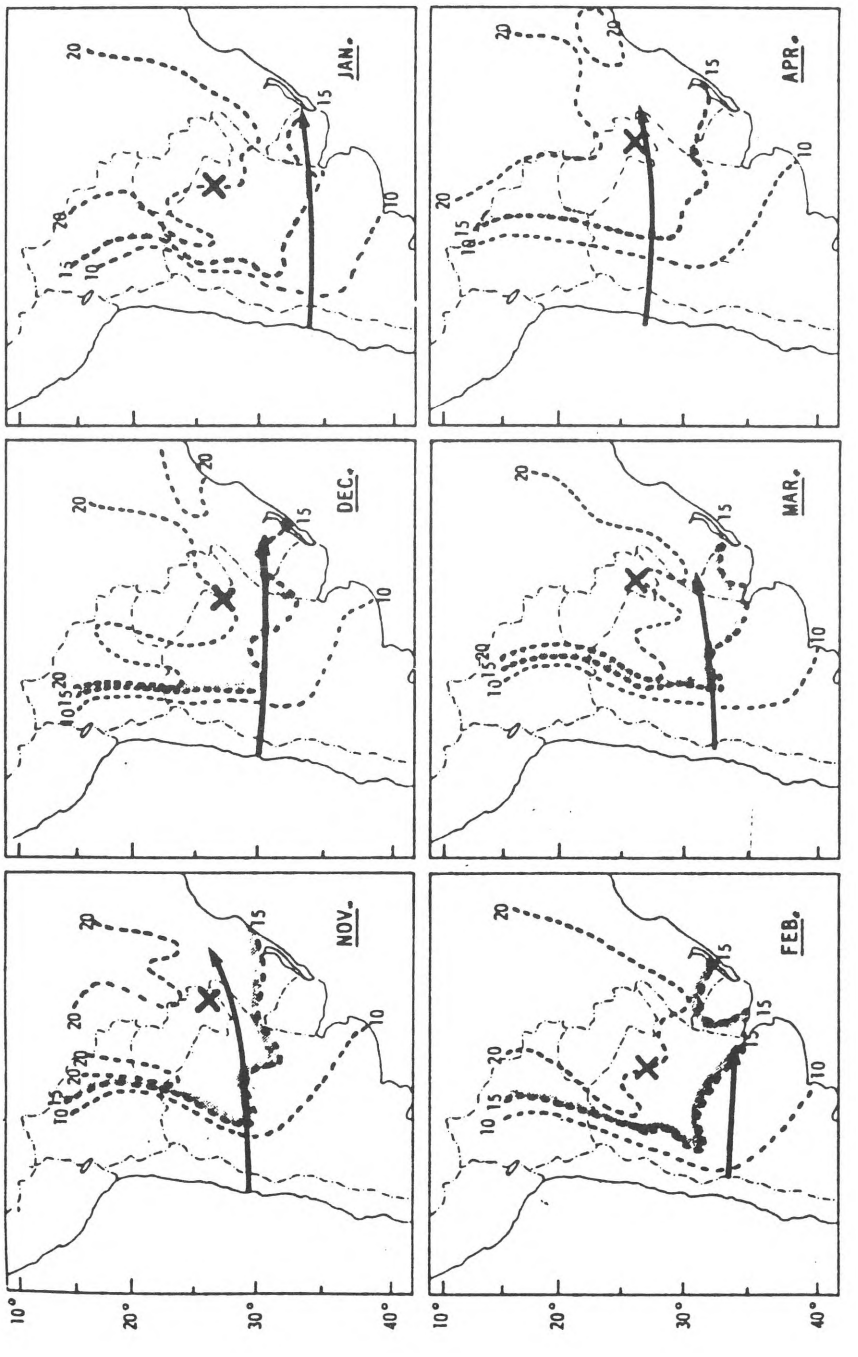

Figure 10 - Monthly evolution at the location of the subtropical jet (arrows), surface isodrosotherms in degrees Celsius (broken lines) and the centroid of MCC activity (cross) in mid-latitude South America (from Velasco and Fritsch, 1987)

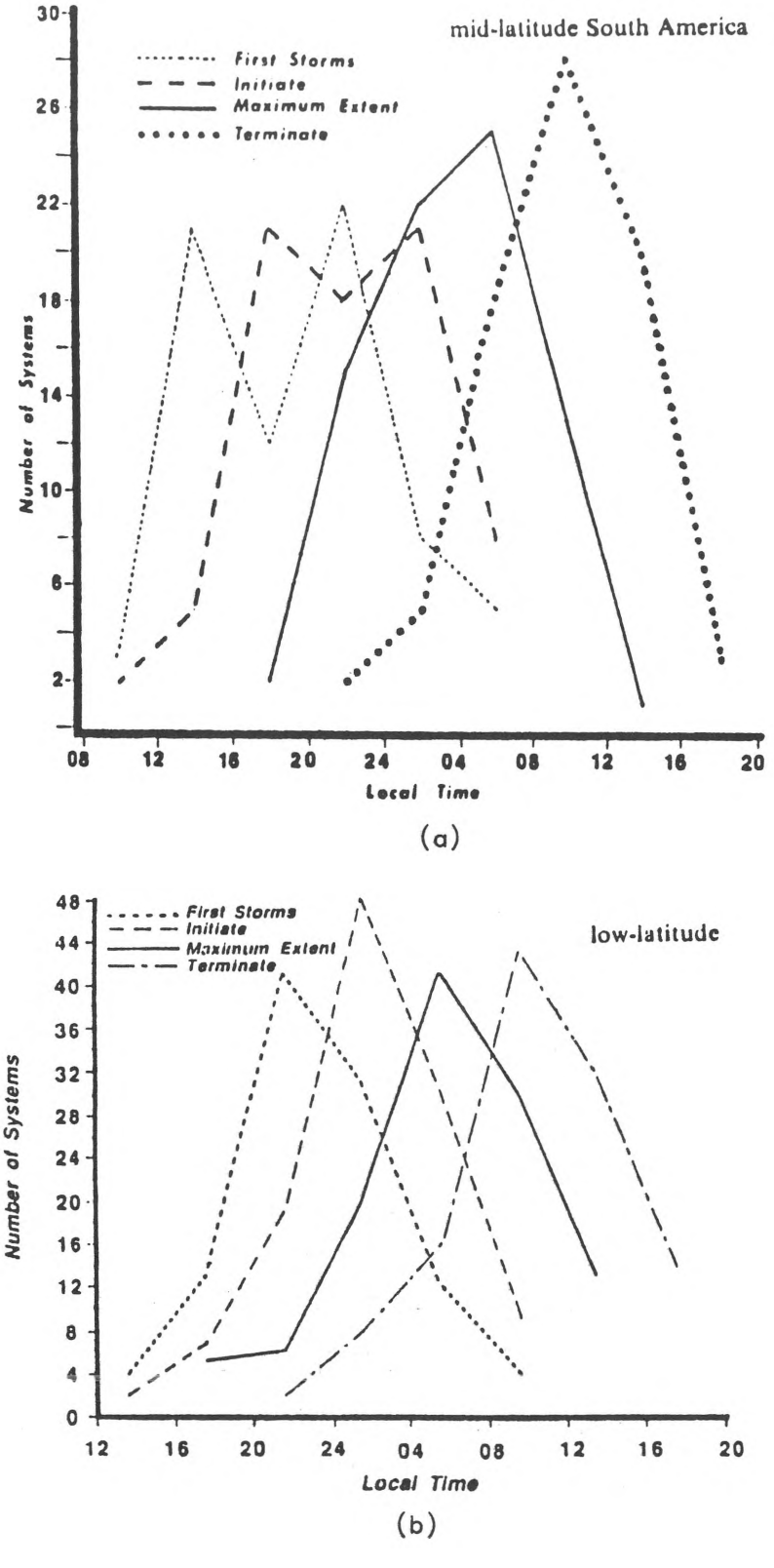

Figure 11 - Life cycle of MCC over (a) mid-latitude South America from 1981 - 1982 and 1981 - 1983 warm seasons; and (b) low-latitude South America (May 1981 - April 1983) (from Velasco and Fritsch, 1987)

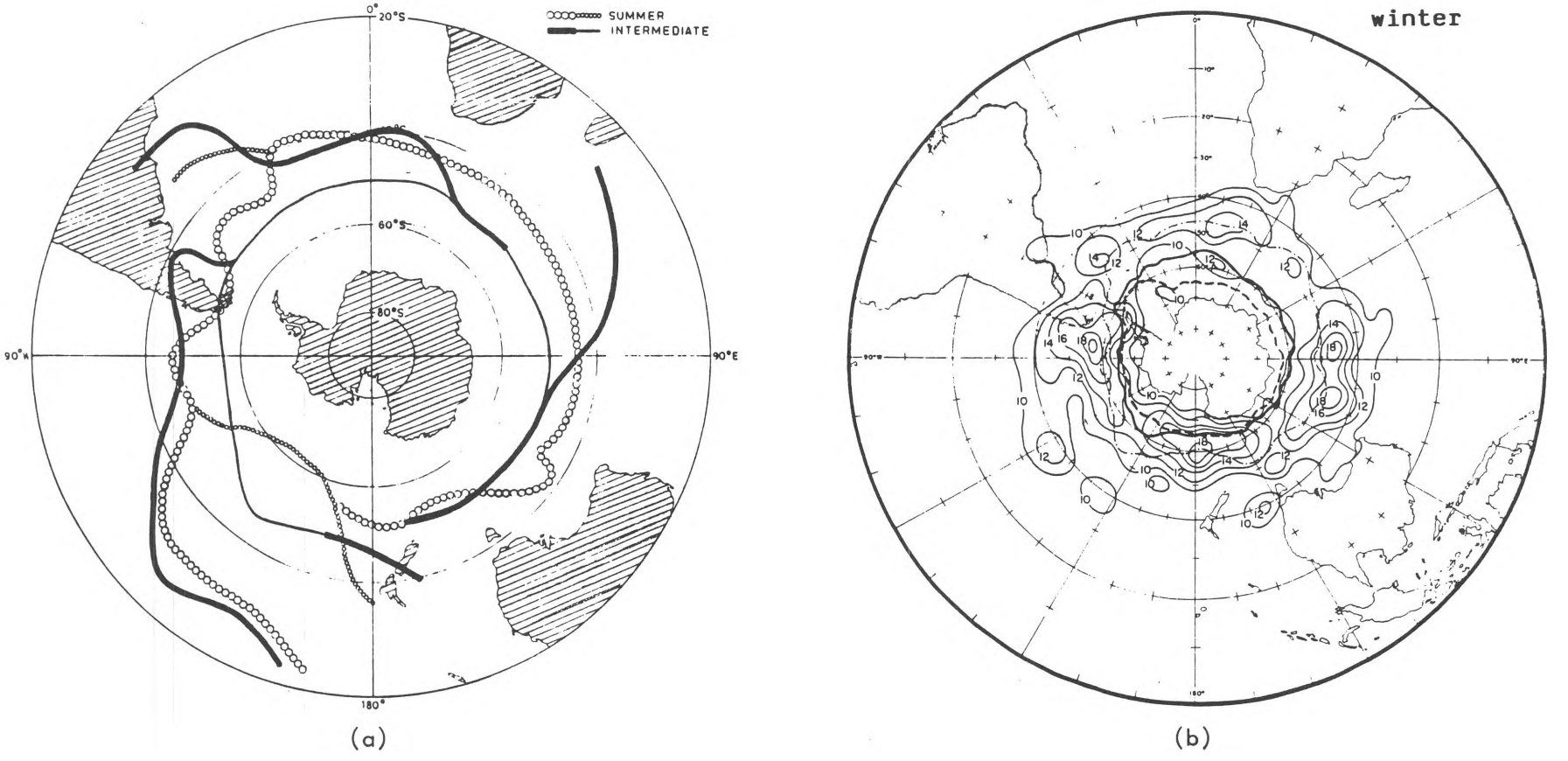

Figure 12 - (a) Axes of the zone of highest frequency of early development for summer (circles) and intermediate season (full line). Where a secondary maximum occurs, it is shown as a finer line (from Streten and Troup 1973); (b) Winter cyclogenesis isopleth values refer to the monthly normalized vortex frequencies in each 5° latitude by 10° longitude unit for the winters (from Carleton, 1981)

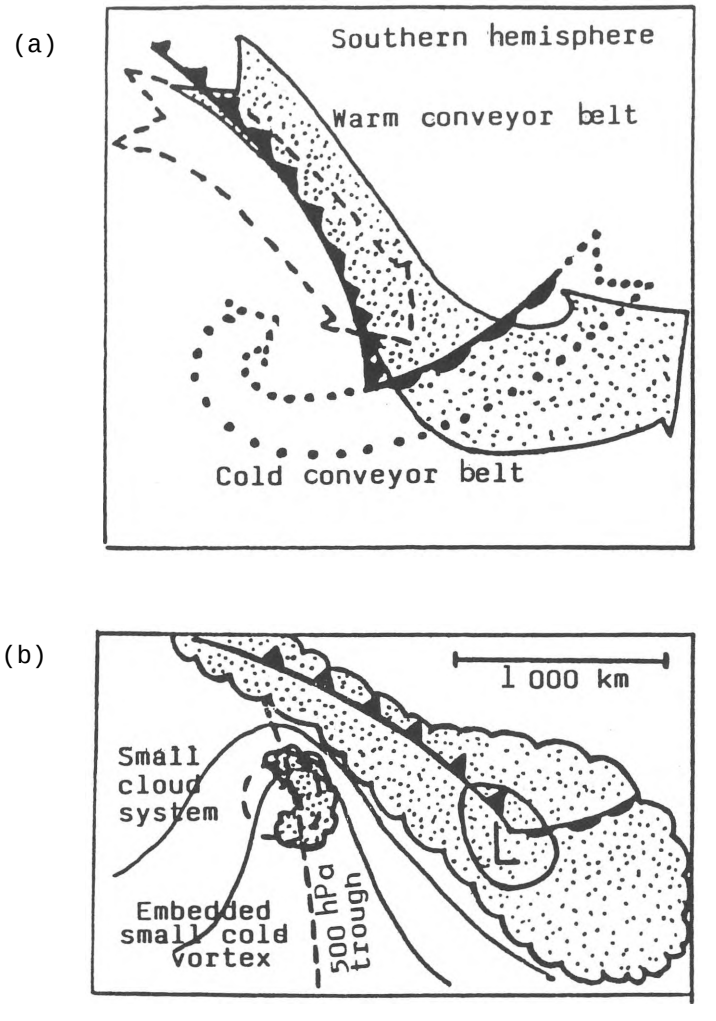

Figure 13 - Schematic portrayal of airflows in a mid-latitude, southern hemisphere cyclone in which the warm conveyor belt (solid arrow with stippled shading) is undergoing forward-sloping ascent ahead of a kata cold front before moving above a flow of cold air ahead of the warm front (dotted arrows) referred to as the cold conveyor belt. Cold middle-tropospheric air with low θ_w (dotted arrow) is shown overrunning the cold front and generating potential instability in the upper portions of the warm conveyor belt. Flows are shown relative to the moving frontal system (adapted from Browning, 1987)

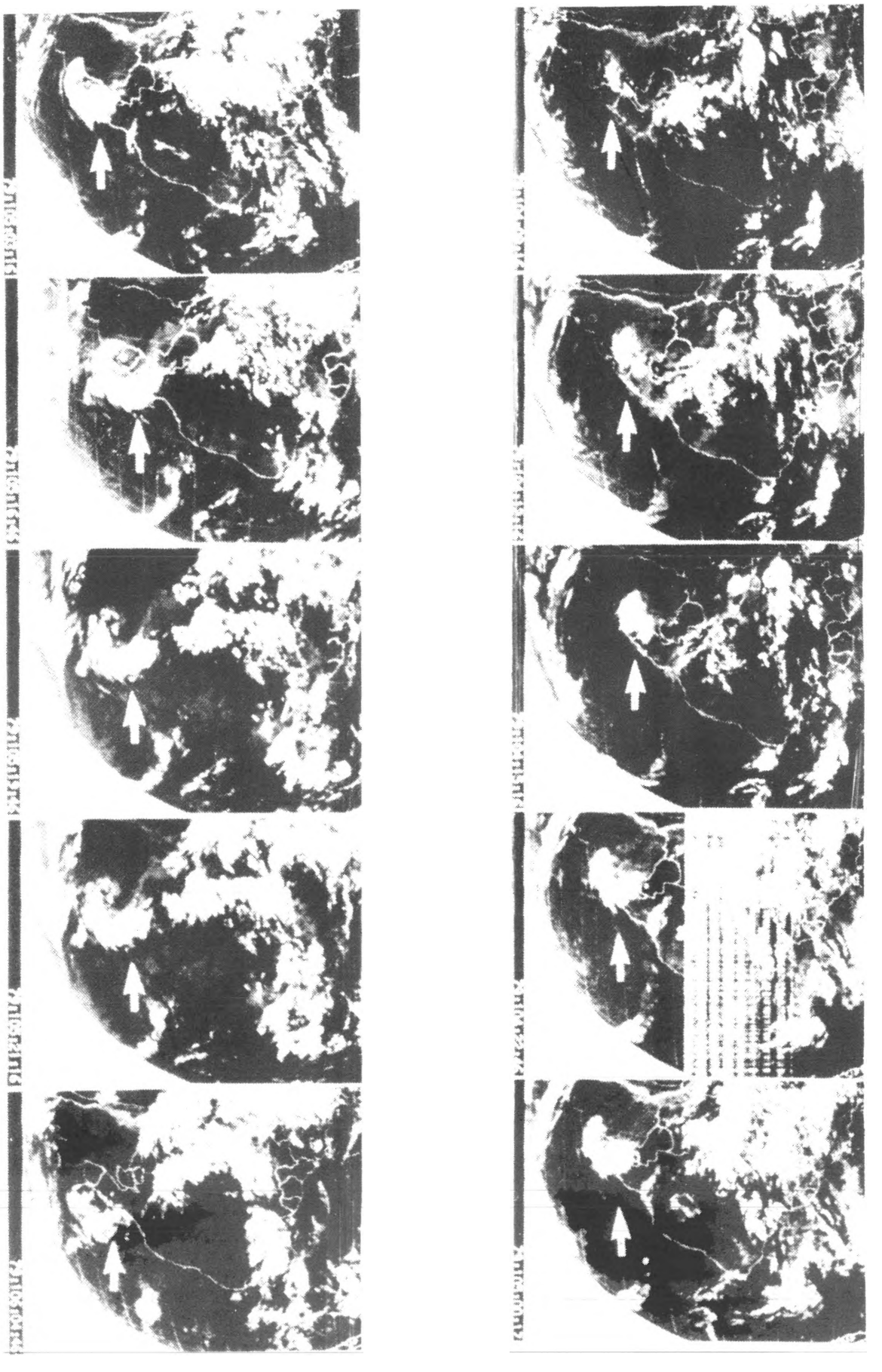

Figure 14(a) - Sequence of infra-red images from GOES-W for 14 and 15 April 1979, showing the formation of an inverted-comma cloud over north-east Argentina, Uruguay and southern Brazil

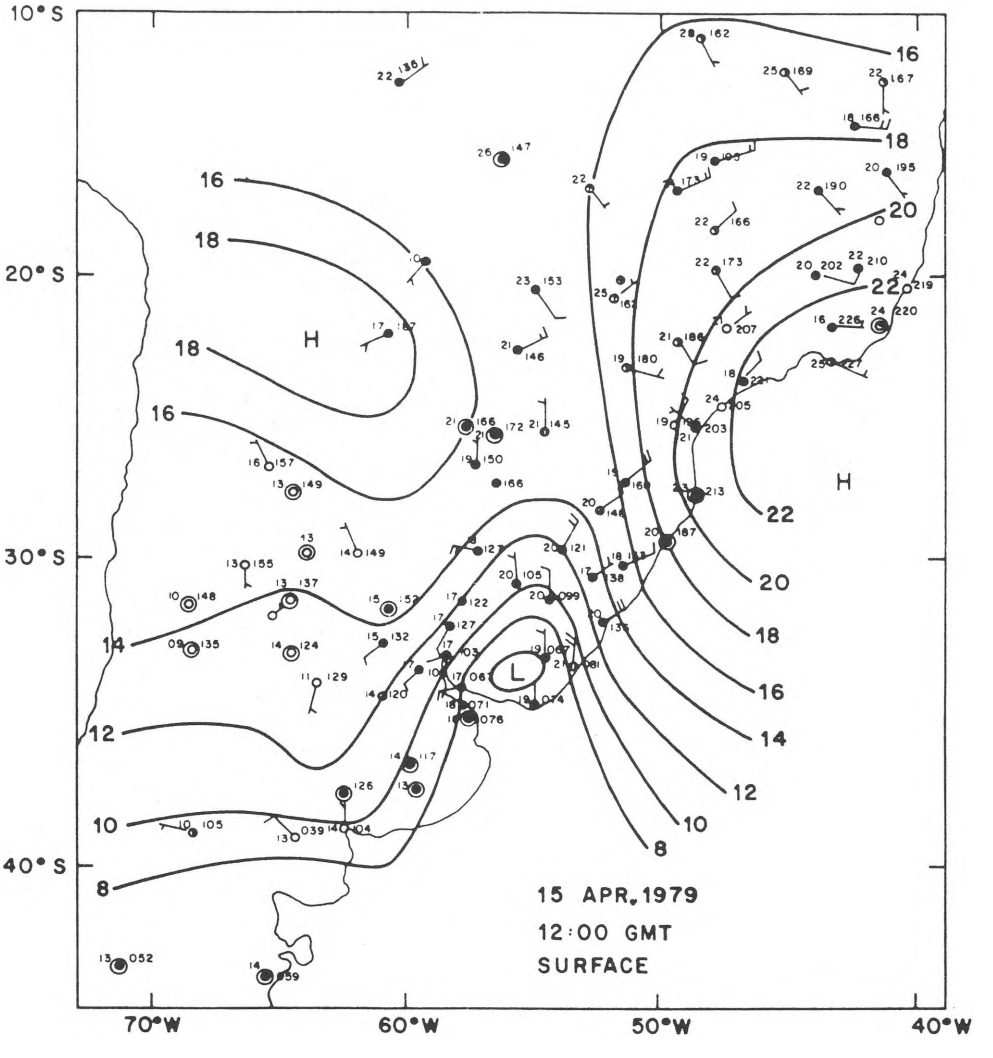

Figure 14(b) - Surface chart for 1200 GMT on 15 April 1979 (from Bonatti and Rao, 1987)

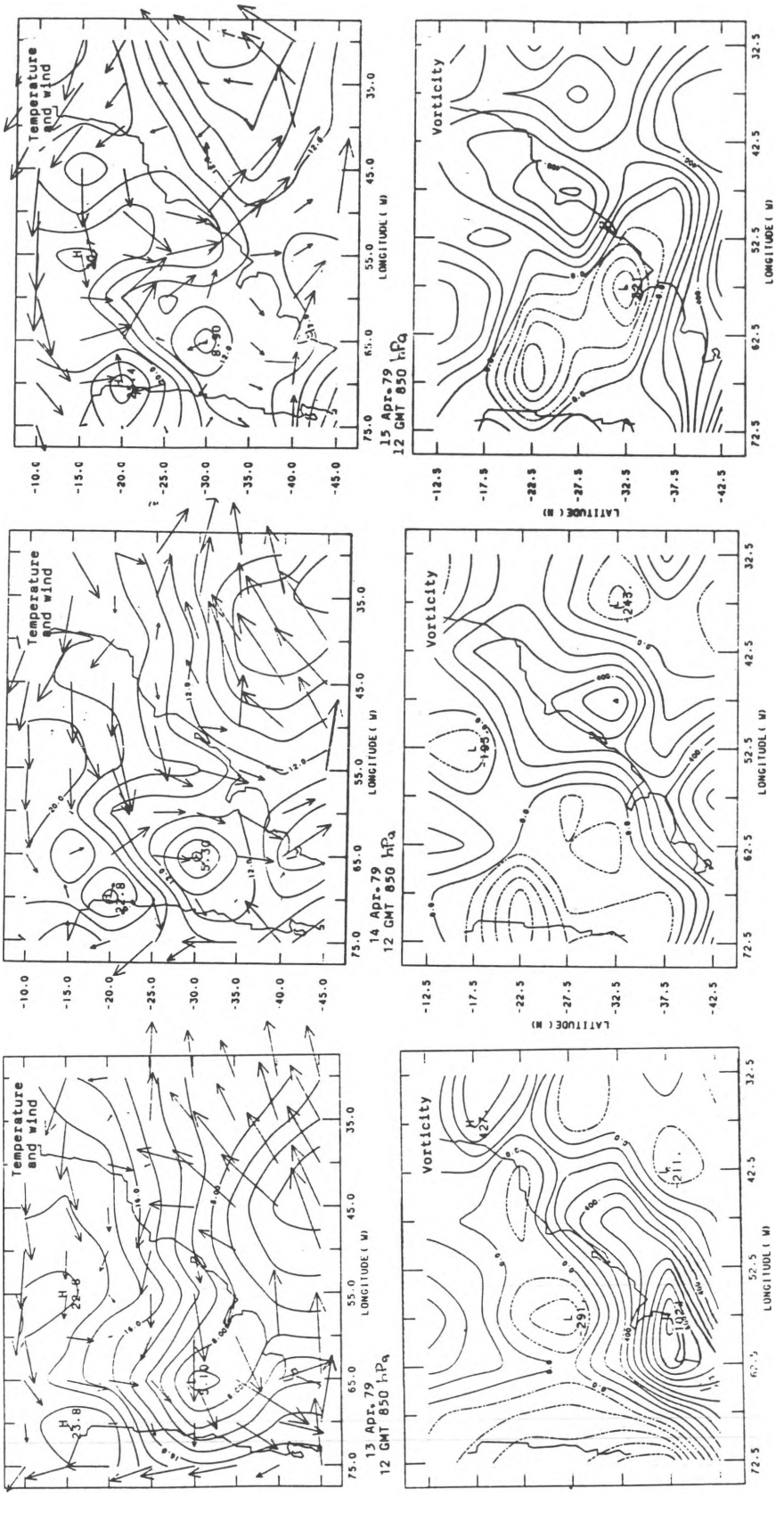

Figure 15 - Temperature, wind and vorticity fields, for 850 hPa at 1200 GMT for 13, 14 and 15 April 1979 (source: J.P. Bonatti)

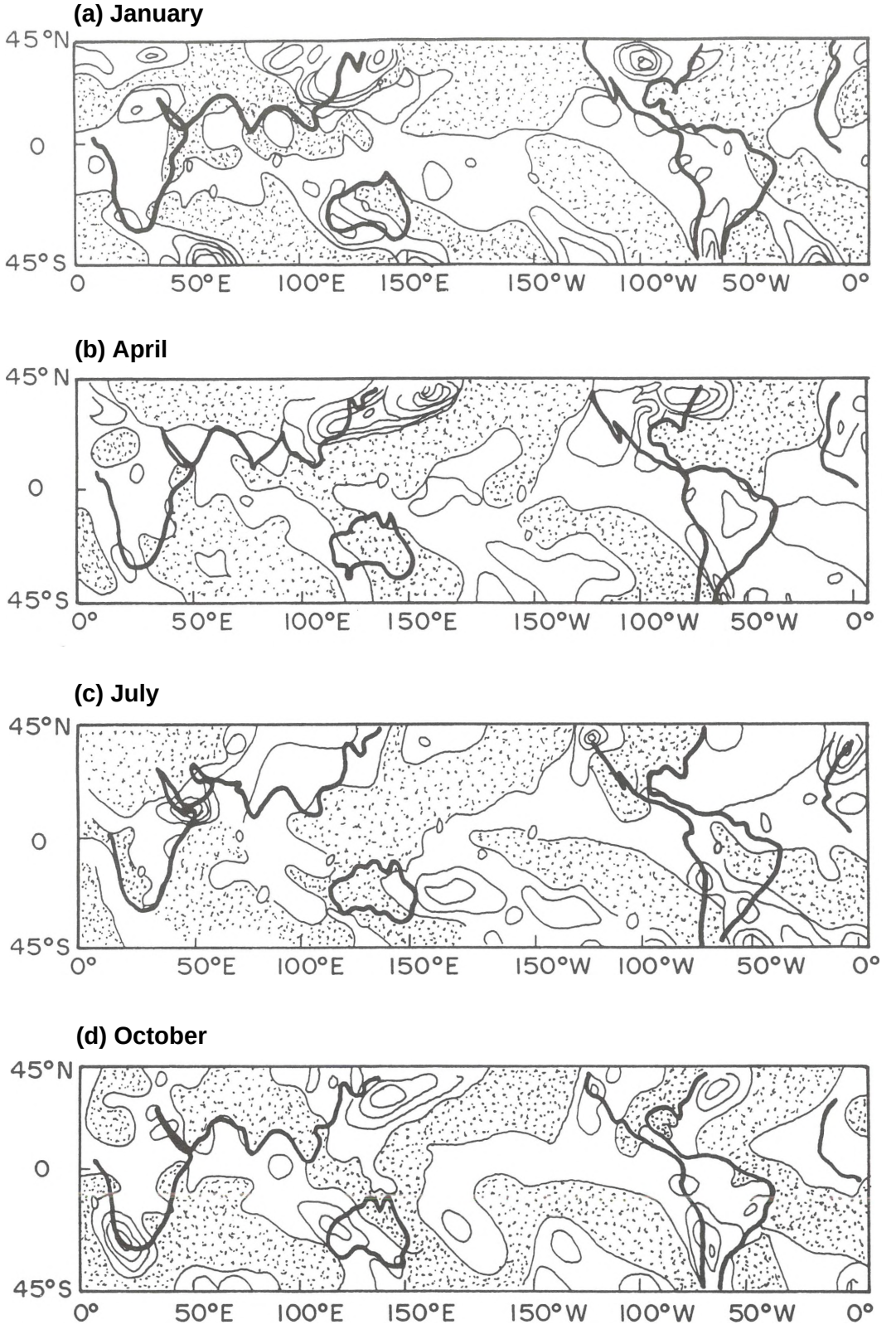

Figure 16 - Climatological frontogenetic functions at 850 hPa for the months of (a) January, (b) April, (c) July and (d) October. Shaded areas represent frontolysis. Isoline interval is 5 x 10^{-12} Km^{-1} s^{-1} (from Satyamurty and Mattos, 1987)

REFERENCES

Betts, A.K., R.W. Grover and M.W. Moncrief, 1976: Structure and motion of tropical squall-lines over Venezuela. Quart. Jour. R. Met. Soc., 102, 395-404.

Bonatti, J.P. and V.B. Rao, 1987: Moist baroclinic instability in the development of North Pacific and South American intermediate-scale disturbances. Jour. Atmos. Sci., 44(18), 21657-2667.

Browning, K.A., 1986: Conceptual models of precipitation systems. Weather and Forecasting, 1(1), 23-41.

Calheiros, R.V., 1976: Winter instability lines as detected by the Bauru C-band radar. 17th Conf. on Radar Meteorology, 26-29 October 1976, Seattle, Washington.

Carleton, A.M., 1981: Monthly variability of satellite-derived cyclonic activity for the southern hemisphere winter. Jour. Climatol., 1, 21-38.

Cavalcanti, I.F.A. and V.E. Kousky, 1982: Influences of the sea-breeze circulation over the N-NE coast of South America. (In Portugese). Proceedings, II Congresso Bras. Meteor. Pelotas, RS, 18-22 Outubro 1982. SBMET, Rio de Janeiro, 4, 409-425.

Climanalise - Monitoring and Climatic Analysis Bulletin, 1987. Instituto de Pesquisas Espaciais (INPE), Sao Jose dos Campos, Sao Paulo, Brazil, 2, 4 and 5 (in Portugese).

Cohen, J.P., 1988: Climatology of squall lines over northern Brazil. M.S. thesis (in preparation). INPE, Sao José dos Campos, Brazil.

Ferreira, R.N., 1988: Application of a linear spectral model to the study of squall lines over northern Brazil. M.S. thesis (in preparation), Institute of Astronomy and Geophysics, Univ. of Sao Paulo, Brazil.

Guedes, R.L. and M.A.F. Silva Dias, 1985: The observed synoptic scale structure in the presence of mesoscale convective complexes over South America. 2nd Meeting of the Brazil-USA Cooperative Program on the Role of Convection in the Amazon Region, Sao Jose dos Campos, Sao Paolo, 5-7 August 1985.

Houze, R.A. Jr., P.V. Hobbs, K.R. Biswas and W.M. Davis, 1976: Mesoscale rainbands in extratropical cyclones. Monthly Weather Review, 104(7), 868-878.

Kousky, V.E., 1979: Frontal influences on north-east Brazil. Monthly Weather Review, 107 (9), 1140-1153.

Kousky, V.E., 1980: Diurnal rainfall variations in north-east Brazil. Monthly Weather Review, 108 (4), 488-498.

Kousky, V.E. and L.C.B. Molion, 1981: Dynamic climatology of the troposphere over the Amazon Region. (In Portugese). Revista Brasileira de Hidrologia e Recursos Hidricos, 3, 199-211.

Lima, M.A. and M.A.F. Silva Dias, 1986: Mesoscale objective analysis: the network and characterization of organized precipitation systems. (In Portugese). Proceedings, I Congresso Interamericano de Meteorología, IV Congresso Brasileiro de Meteorología, Brasilia, DF, 20-24 October 1986, 2, 78-83.

Maddox, R.A., 1980: Mesoscale convective complexes. Bull. Amer. Meteor. Soc., 61, 1374-1387.

Miller, M.J. and A.K. Betts, 1977: Travelling convective storms over Venezuela. Monthly Weather Review, 105 (7), 833-848.

Oliveira, A.S. and C.A. Nobre, 1986(a): Interactions between South American frontal systems and convection in the Amazon region. Part I: Climatological aspects. (In Portugese). Proceedings, I Congresso Interamericano de Meteorología, IV Congresso Brasileiro de Meteorología, Brasilia, DF, 20-24 October 1986, 1, 311-316.

Oliveira, A.S. and C.A. Nobre, 1986(b): Interactions between South American frontal systems and convection in the Amazon region. Part II: Case studies. (In Portugese). Proceedings, I Congresso Interamericano de Meteorología, IV Congresso Brasileiro de Meteorología, Brasilia, DF, 20-24 October 1986, 1, 317-322.

Orlanski, I., 1975: A rational subdivision of scales for atmospheric processes. Bull. Amer. Meteor. Soc., 56(5), 527-534.

Paegle, J., J. Paegle, C. Ereno and E.A. Collini, 1982: Diurnal oscillation of convective weather and boundary layer flow in South America. II Congr. Bras. Meteor., Pelotas, RS, 18-22 October 1982. Anais, SBMET, 3, 132-146.

Riehl, H., 1979: Climate and weather in the tropics. Academic Press, 611 pp.

Satyamurty, P. and L.F. Mattos, 1987: Climatology of low level frontogenesis due to horizontal deformation and divergence fields. Proceedings, II Congreso Interamericano de Meteorología, V CONGREMET, Buenos Aires, Argentina, 30 November - 4 December 1987, T.3.1 - T.3.5.

Scolar, J. and M.A.F. Silvia Dias, 1982: Pre-frontal squall lines and their dependence on synoptic conditions. (In Portugese). Proceedings, II Congresso Bras. Meteor., Pelotas, RS, 18-22 October 1982, 4, 88-102.

Silva Dias, M.A.F., 1988: Mesoscale systems and short-term weather forecasting. (In Portugese). Accepted for publication in Revista Brasileira de Meteorología.

Silva Dias, M.A.F., A.K. Betts and D.E. Stevens, 1984: Linear spectral model of tropical mesoscale systems. Sensitivity studies. Jour. Atmos. Sci., 41 (10), 1704-1716.

Silva Dias, P.L., W.H. Schubert and M. De Maria, 1983: Large scale response of the tropical atmosphere to transient convection. Jour. Atmos. Sci., 40, 2690-2707.

Streten, N.A. and A.J. Troup, 1973: A synoptic climatology of satellite-observed cloud vortices over the southern hemisphere. Quart. Jour. R. Meteor. Soc., 99, 56-72.

Troup, A.J. and N.A. Streten, 1972: Satellite-observed southern hemisphere cloud vortices in relation to conventional observation. Jour. Appl. Meteor., 11.

Uccellini, L.W., 1980: On the role of upper tropospheric jet streaks and leeside cyclogenesis in the development of low-level jets in the Great Plains. Monthly Weather Review, 108 (10), 1689-1696.

Uccellini, L.W. and D.R. Johnson, 1979: The coupling of upper and lower troposphere jet streaks and implications for the development of severe convective systems. Monthly Weather Review, 107 (6), 682-703.

Velasco, I. and J.M. Fritsh, 1987: Mesoscale convective complexes over the Americas. Jour. Geophys. Res., 92 (8), 9591-9613.

Virji, H., 1982: An estimate of the summertime tropospheric vorticity budget over south America. Monthly Weather Review, 110 (13), 217-224.

ACKNOWLEDGMENTS

Some of the research presented in this review was supported by FINEP (Grants 53.84.0043.00 and 4.2.86.0922.00) and by FAPESP (Grant 85/1928.5) and by a CNP_q research fellowship received by the author.

THE MONITORING AND PREDICTION OF RAINSTORMS AND SEVERE CONVECTIVE WEATHER SYSTEMS IN CHINA

by
Zou Jingmeng

State Meteorological Administration
Beijing, China

1. THE GENERAL CHARACTERISTICS OF RAINSTORMS AND CONVECTIVE WEATHER SYSTEMS IN CHINA AND THE SIGNIFICANCE OF THEIR PREDICTION

China is situated in a monsoon-affected area. Each year, during spring and summer, the summer monsoon produces large quantities of water moisture which very often trigger off convective storms. The convective storm usually causes disastrous weather - including heavy rainfall, hailstorms, lightning and strong winds - occasioning heavy losses in terms of lives and property of the people, and to the national economy. Floods and thunderstorms are major natural disasters in China. Figure 1 gives the distribution of floods in China. East China is a flood-prone area. Each year the area flooded often covers several hundreds of thousands of square kilometres. In the 30 years from 1951 to 1980, 1 601 cases of floods occurred with an annual average of 53. The most severely affected areas are the valleys of the Chang Jiang (Yangtze) River, the Huai He (Yellow River), the Hai River, and the southern part of China. In some cases, the heavy rainfall and strong winds cause severe disasters. For instance, an exceptionally serious flood which took place from 5 to 7 August 1975 in Henan province, with the maximum rainfall of 1 605 mm within three days, caused a disastrous flood in the upper and middle reaches of the Huai He when a dam burst. About 100 counties were inundated, tens of thousands of people died, and the economic losses amounted to several hundreds of million US dollars. Another example is a short-lived but devastating squall line which occurred from 28 February to 17 March 1983 in Guangxi province, and led to heavy rain- and hailstorms accompanied by strong winds of 10.8 - 24.4 m s^{-1} in more than 20 counties. As a result, a passenger ship capsized with the loss of 147 passengers, and economic losses reached several million US dollars. Chinese meteorologists have therefore long paid great attention to the monitoring and prediction of heavy rainfall and convective weather systems as well as to the relevant research.

The rainstorm and convective weather patterns in China have three significant characteristics:

(a) They are influenced by monsoon and large-scale topography to a great extent. Thunderstorms occur mainly from March to May and hailstorms in spring and summer, while rainstorms occur in the period when typhoons affect or arrive at the east coast of China. Figure 2, which gives the annual average thunderstorm days from 1957 to 1970, shows that the southern part of China and the mountainous areas experience more thunderstorms than the northern part and the plains. Between 90 and 100 thunderstorm days were recorded in Guangdong, Yunnan and Guangxi provinces. In the North China plain, the annual thunderstorm days amount to 30 to 40 days. Figure 3 gives the annual mean distribution of hailstorms in China and indicates that the western part of China

suffers more from hailstorms with the maximum in the north-western mountainous areas, while the east suffers less. For instance, the hailstorm days in the Pleateau of Tibet are 15-35 days each year. Although hailstorms tend to be rare in the east plain areas, they cause more damage to crops, as they mostly occur during the crop-growing season and the diameter of the hailstones is bigger than that of the hailstones falling in the western mountainous areas;

(b) China is a country prone to rainstorms. The rainstorm in China is characterized by persistence and great severity (see Table I), with the one-hour and 24-hour maximum rainfall amount being 198.5 mm and 1 672 mm respectively. Although they have not broken the world record (3 240 mm in 24 hours in Reunion in the Indian Ocean), they are much more severe than those in the corresponding climatic zones of the USA, where the maximum rainfall in 24 hours is 983 mm (recorded in Florida).

In China, the average life cycle of rainstorms ranges from two to seven days but an exceptional case did occur in 1954 in the Chang Jiang valley, which lasted for two months. Figure 4 gives the geographic distribution of heavy rainfall from 1953 to 1977 with the 24-hour rainfall exceeding 1 000 mm, 800 mm and 400 mm respectively. The 24-hour rainfall of more than 1 000 mm occurred not only in coastal areas but also in areas far inland. A dividing line can be drawn running from the south of the Liaodong peninsula along the Yan Mountains, the Yin Mountains, the Great Bend of the Huang He, into Guangzhong and Sichuan provinces, and finally to Guangdong and Guangxi provinces. The vast area to the south and east of that line is prone to rainstorms. Within that area, three zones of relatively high rainstorm occurrence are identified: northern China, the Chang Jiang valley and southern China. In addition, heavy precipitation also occurs in coastal areas, caused by typhoons. It must be pointed out that, between the zones mentioned, there are two areas in between, which seldom experience rainstorms. This indicates that fronts usually jump over these two areas as they travel northward. In China, the precipitation systems can be classified into four major categories:

(i) The first which is caused by typhoons and their remnants, is considered to be the most important and strongest precipitation system in China. From 1931-1977, 26 cases of heavy rain were recorded, of which 56 per cent were the result of typhoons;

(ii) The second is caused by a vortex and shear line, which is a sort of mesoscale disturbance occurring frequently in the mei yü rain season;

(iii) The third is caused by the upper-level trough and cold front;

(iv) The fourth is caused by a quasi-stationary cold vortex which often brings about flash floods.

During the summer monsoon period, the inland area of northern China is supplied with abundant moisture. There, the mesoscale activities will produce a 24-hour rainfall of over 500 mm when they tend to be stagnant;

(c) In contrast with the USA, tornadoes seldom occur in China. Figure 5 gives the global distribution of tornado occurrence from 1963 to 1966: very few tornadoes occurred in continental east Asia while, in this same period in the USA, 2 600 tornadoes occurred.

Although the eastern parts of the USA and China both face oceans and are situated in approximately the same latitudes, the activity of convective storms differs greatly. This may be related to the differences in geography and general atmospheric circulation. In North America, the Rocky Mountains run from south to north. The airflows ascend and descend as they pass over the mountains. The genesis of severe cyclones tends to occur at the leeside. From April to June, the warm and humid lower-level south-east flow moves northwards from the Gulf of Mexico and is forced by the Rocky Mountains to change to a meridional direction. Over that flow, there is another prevailing flow starting to descend after crossing the Rocky Mountains. Between these two superimposed flows of different sources, a strong conversion layer forms, which we call a "warm lid" (see Figure 6). At the west edge of the warm lid, one often observes a dry line. The dry air to the west of this dry line comes from New Mexico and Arizona, while to the east there is the warm and moist tropical oceanic air, coming from the Gulf of Mexico. When the warm lid is destroyed, severe convective storms will quite often be generated along the dry line. The situation is completely different in eastern Asia, where the Plateau of Tibet is oval in shape and runs from east to west. When the westerly flow moves to the plateau, it splits into two branches and moves further east (see Figure 7). As a result, strong cyclones rarely occur in the area to the east of the Plateau of Tibet. In addition, as the southern part of Asia belongs to the monsoon region and is rather wet, neither do many dry lines occur over the Chinese continent.

In order to describe further the characteristics of the rainstorms and severe convective weather systems in China, some typical cases are given below.

1.1 The rainstorm of 5-7 August 1975 in Henan province

Heavy rainfall (1 605 mm in three days) was recorded in an area 120 km long and 50 km wide at the windward side of the Funiu Mountains (see Figure 8), which caused disastrous flooding in the upper and middle reaches of the Huai He. The statistics show that such a heavy rainfall event takes place about once every 400 years. The rainfall occurred in the period when a 500 hPa circulation pattern over eastern Asia changed from zonal to meridional. Figure 9 shows the analysis of 500 hPa at 1200Z on 7 August 1975. The rainstorm weather system was caused by a weakening typhoon (typhoon Nina). After landing in Fujian province, the typhoon kept moving slowly inland for two days. During this period, the zonal circulation was replaced by the meridional one, and a blocking high formed to the north of the

depression. The tropical depression slowed down towards the north-east and gradually turned west. Finally, it became quasi-stationary and made a small loop over the mountainous area to the south of Henan province. The depression interacted with the mid-latitude cold front and the local topography in the period of eratic movement for over 20 hours. As a result, exceptionally heavy-precipitation occurred in the north-east quadrant. The strong ascending motion was initiated by many factors: the mass convergence at the front of the wind maxima of the low-level easterly and southerly jets, the lifting effects of cold air, and the windward slope and the upper-level divergence (see Figure 10). The stable circulation allowed the well-organized mesoscale thunderstorm systems to grow and develop. As a result, exceptionally heavy rainfall occurred within a very limited mountainous area.

1.2 The flood of 11-15 July 1981 in Sichuan province

From 11 to 15 July 1981, a rainstorm caused severe damage to the lives and property of the people in Sichuan province. Figure 11 gives the 24-hour rainfall for 13 and 14 July. During the first 24 hours, the precipitation was caused by the development of a sustained mesoscale vortex (the so-called south-west vortex) and the precipitation mainly centred in the Sichuan Basin. During the subsequent 24 hours, the precipitation was produced by the front which concentrated along a narrow, elongated belt over the north-east of the basin. During these 48 hours, the precipitation appeared rather stable with the maximum six-hour rainfall being more than 100 mm. Most of the precipitation centred in the west of the basin, where the cyclonic circulation of the south-west vortex moved toward the plateau. The conclusion could therefore be drawn that such a lifting effect along the mountain slopes plays an important role in initiating convection.

During the entire rainstorm, two mesoscale vortices existed. Vortex P originated on 11 July over the central plateau, and moved eastward at 0000Z on 12 July (see Figure 12). At the same time, another mesoscale vortex, Vortex SW, was developing over the Sichuan Basin. The development of these two vortices could be seen clearly from the IR cloud images from a GMS satellite. The two vortices, located over the eastern edge of the plateau and the Sichuan basin respectively, were 500 km apart. Not long afterwards, they merged into a single, bigger mesoscale vortex (see Figure 13) and produced the first heavy precipitation. The mesoscale heat and moisture budget indicates that the release of latent heat caused by convective Cumulus played an important role in the development of vortex SW.

1.3 The rainstorm of 20-30 May 1987 in Guangdong province

The East Asian monsoon advances gradually, reaching the south-east coast of China in late May, the Chang Jiang valley in mid-June and the north of China in late July. The arrival of the summer monsoon is usually accompanied by rainstorms. From 20 to 22 May 1987 the onset of the summer monsoon in Guangdong province (south-east China) brought about a rainstorm. In Haifeng county, where the centre of the rainstorm was located, a total rainfall amount of 1 023 mm was recorded in 48 hours from 20 to 22 May, during which the 24-hour maximum reached 672 mm, and the one-hour maximum reached 113 mm. The occurrence of such a severe convective rainstorm was rather rare in that area: 114 people died, 320 000 hectares of farm land were flooded, and 25 000 houses collapsed.

Figure 14 gives the six-hourly rainfall variation from 19 to 22 May, from which we can identify three episodes of precipitation at 1800Z on 20 May, 0600Z on 21 May and 0000Z on 22 May, respectively. They were each caused by four mesoscale systems. Figure 15 gives the distribution of the 24-hour rainfall amount along the coastal area in Guangdong province from 1200Z on 20 May to 1200Z on 21 May which was the most intensive period. The heavy rainfall took place along a long and narrow belt running north-west to south-east. This rain belt was caused by three mesoscale cloud clusters (A, B, and C) which were formed in the mountainous area north-east of Guangdong province and which moved south-east. Heavy precipitation occurred along the paths of these cloud clusters with the most intensive precipitation being at the rear of each one. Figure 16(a) is the satellite cloud image at 2100Z on 20 May and shows cloud cluster A over Haifeng county. Figure 16(b) is the same image at 0600Z on 21 May and shows A moving out to sea with B over Haifeng county, followed by C. Both cloud clusters A and B left the six-hour maximum rainfall of 672 mm in Haifeng county.

After forming in the south-eastern part of Guizhou province at 1800Z on 20 May (see Figure 16(a)), cloud cluster C developed and moved east together with the comma-shaped cloud system in the north. At 0600Z on 21 May, cloud cluster D and the comma-shaped cloud system developed into a typical trough cloud system (see Figure 16(c)). Soon afterwards, cloud cluster D turned south-east and the third bout of precipitation affected Haifeng county. Figure 17 gives the IR image from NOAA-9 at 0700Z on 22 May, showing the peak of the last precipitation in Haifeng county. The image shows that the rainstorm area was covered by heavy Cumulonimbus clusters which were about 170 000 km^2 in area; the temperature of the cloud top was below -53°C and its area was 90 000 km^2.

From our experience in rainstorm analysis and forecasting, we consider that satellite cloud imagery - IR cloud imagery in particular - is an effective tool for rainstorm monitoring and forecasting.

1.4 The intense squall line on 17 June 1974

At 1100Z on 17 June 1974, a severe squall line hit Jiangsu province, causing great damage. At 0000Z that day, there was a cold front moving southwards. In the frontal warm sector, there was a mesoscale warm low developing, within which the squall line generated and developed and moved southwards in a regular way (Figure 18). At 0600Z, the squall line had developed to a certain degree of intensity; the horizontal gradients of temperature and humidity along it were very large and a thunderstorm high had developed behind. The squall line passed over Nanjing at 1100Z (Figure 19). In Figure 20, the trace curves indicate the pressure, temperature and wind speed in Nanjing while the squall line was passing. The wind speed reached 30.1 m s^{-1}, precipitation amounted to 30.6 mm in 10 minutes, and the temperature dropped by 11°C in 15 minutes. The severe thunderstorm and gale caused enormous losses in Nanjing. Trees with trunks 30 cm in diameter were even uprooted and broken. The biggest hailstone measured was 10-11 cm in diameter and weiged 0.6 kg.

This kind of squall line occurred in a situation of ladder-like upper troughs in East Asia, i.e. from the north to south, with several troughs being arranged in a trapezoid, as shown in Figure 21. On the 500 hPa chart at 1200Z the same day, there were three troughs running from south to north to the

north of 30°N. One was over the lower reaches of the Chang Jiang; another - a diffluent short-wave trough - was over northern China; and the third was south of Lake Baykal (USSR). The trough over the lower reaches of the Chang Jiang was a perturbation in the westerly flow over the southern side of the Plateau of Tibet. The disturbance caused large amounts of precipitation in the lower reaches of the Chang Jiang when the trough passed; the descending motion behind the trough formed an inversion layer favourable for severe convection. During the daytime of 16 June, the strong insolation caused a rise in temperature under the warm lid, thus increasing convective instability. The diffluent trough at the 500 hPa level over northern China indicated this intense development. The ascending motion ahead of the trough was favourable for the release of unstable energy, causing the intense development of the squall line. This kind of flow field of ladder-like troughs from south to north usually leads to hail in northern China, and thunderstorms and gales in the Chang Jiang Basin.

2. THE OPERATIONAL FORECASTING OF EXCESSIVE RAINFALL AND SEVERE CONVECTIVE WEATHER

The forecasting of rainstorms and severe convective weather is a question of mesoscale prediction. There are two prerequisites for the forecast: one is a denser observing network on the spatial and temporal scales to monitor the genesis and development of meso-a scale and meso-β scale weather systems; the other is a large and powerful computer. As these two requirements have not yet been fully provided in China, however, several rainstorm-forecasting methods have been developed, based on our existing conditions and requirements with which very good results have been obtained.

2.1 Monitoring and forecasting rainstorms and severe convective weather by means of radar and satellite data

Since 1980, a method combining the data from weather radar, satellite imagery and enhanced surface observation has been applied in the monitoring and forecasting of rainstorms and severe convective weather in China. Currently, we have 187 sets of weather radar (10, 5 and 3 cm) with which the eastern parts of our country - where the severe convective weather often occurs - are well covered (Figure 22). About 60 satellite ground receiving stations have been established in China to receive satellite images from the GMS and NOAA satellites. In some areas (such as Beijing and the middle and lower reaches of the Chang Jiang), the conventional surface observations are intensified in the seasons of rainstorms and severe convective weather. Based on these data, very-short-range (0-12 hours) methods for predicting rainstorms and severe convective weather have been developed.

2.2 The expert system of rainstorm forecasting

In recent years, with the wide application of microcomputers (IBM series) in the meteorological field, the artificial intelligence technique has been introduced in many provincial meteorological forecasting offices and stations for the forecasting of rainstorms and severe convective weather. Based on the accumulated experience of forecasters over more than 30 years, and combined with NWP products, the system is realized on microcomputers and is very suitable for local observatories and stations. The practice of operational prediction has proved that this method is useful to a certain degree. It can produce "yes or no" forecasts of rainstorms as well as area

and intensity for 12-48 hours in advance. Figure 23 is a flowchart of this approach, from which one can see that the forecasting method is able to consider all kinds of information and techniques comprehensively (particularly the forecasters' experience), to simulate the logical thinking procedure of analysis, reduction and inference, and to deduce the local rainstorms and severe convective weather. It has been used in 21 provinces in China, including the meteorological forecasting offices in Sichuan and Anhui provinces, which have obtained very good results. For instance, in the "yes or no" forecasts of rainstorms within 12-48 hours in the Sichuan Basin during the period May to September 1987 made by the Sichuan Provincial Forecasting Office, the average CSI (critical success index) was 43/54 = 79.6 per cent. The technical score (TS) was 24.1 per cent. The average technical score for the rainfall area and intensity forecasting within 36 hours (100 mm h^{-1} 1) was 31.8 per cent. Hence, this forecasting method plays a more and more important role in China's rainstorm and severe convective weather forecasting.

2.3 The diagnosis of physical quantities and forecasting of rainstorms

Since 1982, the National Meteorological Centre (Beijing) has provided 20 kinds of products of analysis and numerical weather prediction to various forecasting offices and stations all over the country every day. They are mainly produced with the northern hemisphere model and the regional precipitation model (Figure 24). The main forecasting methods using these fields are as follows:

(a) Establishing the model output statistics (MOS) equation for local rainstorm forecasting with these products as predictors;

(b) Perfect prediction (PP) method for rainstorm forecasting;

(c) Model index method, i.e. several models are divided according to grid data and the forecasting index is defined. A correlation equation is then established for predicting the local rainstorm. The above forecasting methods are all realized on microcomputers and the results - especially the prediction of rainfall areas - are rather successful.

2.4 The numerical weather prediction method

The operation of numerical precipitation prediction in China began in 1984 and was a major step towards an objective and quantitative goal. At present, there are two models of numerical precipitation prediction: one is the limited-area precipitation prediction model operated at the National Meteorological Centre, Beijing - mainly for the prediction of precipitation distribution and timing over a rather large area - and the products are disseminated all over China. The other is the operational model of limited-area numerical rainstorm prediction for the Chang Jiang and Huai He Basins (Jiang-Huai) operated by the Wuhan Forecasting Office, which has been designed and developed mainly for forecasting rainstorms in the mei yü season. The Jiang-Huai Basin is one of the main precipitation areas in China. Table II is the comparison of the two models.

A preliminary test has been made on the forecasting capability and the performance of these two models. Table III gives the results of five rainstorms in central China in June 1986. The figures represent the proximity between the predicted and the observed: 1, 2 and 3 stand for bad, moderate and good forecasts respectively.

We can see from the table that these two models are all capable of forecasting precipitation in central China, and all are successful in "yes or no" forecasting as well as predicting rainfall areas. Their common problem, however, is that the predicted rainfall areas are too large and the intensity, particularly the maximum intensity, is too small. Relatively speaking, the rainfall area predicted by the Wuhan model is smaller, with fewer ommissions of forecasting cases, and the location of rainfall area, maxima and intensity are all better than the forecasts made by the Beijing limited-area model for the same areas, especially the 12-36 hour forecasts of maximum and rainfall amount. It is therefore obvious that the reduction of the horizontal grid spacing (Table II) can improve precipitation forecasts to a certain degree, as well as having a capability of rainstorm forecasting.

We then made a further strict verification on the Jiang-Huai Basin limited-area forecasting model. In the past four years, 26 rainstorm forecasts were made for the middle reaches of the Chang Jiang. Based on the results of 24 hours forecasts (Table IV), the average technical score for forecasting 50 mm d^{-1} (TS = C/P + 0-C) was 25.4 (normally the precipitation TS is about 20) and the TS for 25 mm d^{-1} is 38.1, where C is the correctly predicted rain area. The average error for the prediction of the maxima of 54 rainstorms is 90 km, and the average error for rainfall amount is (103 - 87)/103 = 15.5 per cent. Through operational forecasting practice over the last four years, we have learned that the meso-α scale ascending motion is the key factor to success. Therefore, it is very important to make a good forecast of the moisture flux convergence $(\nabla \cdot \vec{vq})$, which determines the area and the amount.

I would like to cite two examples. The first one is prediction of the shear line associated with precipitation. In Figure 25, we can see that the predicted area of the rainstorm and the maximum are quite consistent with the observed, but the amount is smaller, only half (56 mm d^{-1}) of the observed. The next 24-hour forecast is also basically comparable. Figure 26 shows a rainstorm in the Chang Jiang Basin caused by the eastward movement of a south-west vortex. The precipitation areas are predicted fairly well, while the vortex moves eastward. Between 0000Z and 1200Z on 15 June, the rainstorm was to the east of Sichuan and west of Hubei; 12 hours later, it had moved to the middle reaches of the Chang Jiang (Wuhan). Figure 23(c) shows the 24-hour precipitation forecast. There were, altogether, three rainstorms along the Jiang-Huai Basin. Of these, A and B were predicted, and their locations and rainfall amounts agreed with the observed.

Numerical precipitation prediction in China needs to be improved further, including the horizontal and vertical resolutions, the processing of the initial data, knowledge of the physical processes in the planetary boundary layer and topography.

3. THE DISASTROUS WEATHER MONITORING SYSTEM AND THE VERY-SHORT-RANGE WEATHER FORECAST RESEARCH PROGRAMME IN CHINA

Although in the past four years significant progress has been made concerning the ability and skill of large-scale weather forecasts, much needs to be done in forecasting those meso- and small-scale weather systems which might bring about great disasters. At present, many difficulties remain in forecasting certain sudden developments of weather processes. Along with the development of economic activities of all kinds, Chinese meteorologists are facing a new challenge, i.e. to develop a warning system for effectively forecasting and monitoring disastrous weather 12 hours ahead. In order to

achieve this goal, the State Meteorological Administration (SMA) has designed a research programme (1986-1990) for monitoring and making very-short-range forecasts of disastrous weather systems. This programme, linking operations and research together, was first implemented in 1986. The SMA has realized that the implementation of such a five-year plan is just the first step towards establishing an effective monitoring and forecasting system of meso- and small-scale disastrous weather. Its main objectives are:

(a) In operations:

(i) To establish a moderately advanced disastrous weather monitoring system which can be used to monitor the activities of meso- and small-scale weather systems;

(ii) To establish a data-acquisition and dissemination system, in order to acquire, process and disseminate data and forecast products;

(iii) To establish a very-short-range forecast and warning system for prompt and timely delivery of the severe weather warning bulletins to users;

(b) In research:

(i) To work out a conceptual model for the occurrence, development and structure of severe storms on the basis of observation and diagnostic analysis;

(ii) To develop an improved regional numerical forecast model which is able to forecast the possible location and timing of occurrence of a mesoscale weather system;

(iii) To study cloud models in order to improve the schemes of Cumulus parameterization;

(iv) To develop and test the new observing system including automatic surface stations, Doppler radar systems, atmospheric profiler (UHF wind-finding Doppler radar, microwave radiometer and Sodar, etc.);

(v) To carry out the basic and theoretical studies of mesoscale meteorology, including mesoscale dynamics, predictability of mesoscale weather systems and the parameterization of its physical process, the optimal design of a mesoscale observation network.

Four experimental sites were selected for establishing the monitoring and forecasting system (see Figure 27):

(a) The experimental area of Beijing, Tianjing and Hebei province

The major research effort in this area is directed at hailstorms, local rainstorms and strong winds caused by squall lines. This area is prone to flooding. Figure 28 shows the Doppler radar system installed in Beijing and the digitized radar products. Figure 29 shows the domestically developed automatic surface weather station system. UHF radar is currently under development;

(b) The experimental area of the Chang Jiang delta region

Thunderstorms, tornadoes, hailstorms, and rainstorms in the mei yü season are studied as first priority;

(c) The experimental area of the Sanxia dam on the Chang Jiang

Research is mainly conducted on rainstorm prediction, with special emphasis on the rainstorms caused by the south-west vortex;

(d) The experimental area of the Pearl River delta region

The major research subject is the cause of the pre-summer rainstorm and its prediction.

This programme has been carried out for two years and we plan to start the field observation experiment and the forecast experiment in 1990.

The study of rainstorms and convective weather is a complex issue which deserves our continuous efforts. At present, the cause of occurrence, development and structure of mesoscale weather systems are not fully understood and many scientific issues remain to be solved. Currently, mesoscale meteorology and very-short-range weather forecast are listed as high-priority items in the development plans of many countries. As a result, much has already been achieved. We certainly believe that the long-term, continuous efforts of meteorologists from different countries will bring about a solution to this issue.

*

* *

TABLE I

Major heavy rainfall in China during the past 50 years, in descending order of precipitation amount

Province or city	Location	Time of occurrence	Maximum rainfall (mm) 24 h	3 days	Entire period	Main rain-producing synoptic systems
Taiwan	Xinliao	17-19 Oct. 1967	1 672	2 749	2 749	An easterly wave disturbance in the northern section of typhoon Carla
* Many provinces in central China	Chang Jiang and Huai He	June and July 1954	Not available		2 000	8-9 low-pressure disturbances
Taiwan	Baixin	10-12 Sept. 1963	1 248	1 684	1 684	Typhoon Gloria
* Henan	Linzhuang	5-7 Aug. 1975	1 060	1 629	1 631	Weakening typhoon Nina
'Hebei	Zhangmao	1-10 Aug. 1963	950	1 458	1 600** (or 2 050)	Low-level SW vortices
*Guangdong	Tai shan	24-30 May 1973	850	Not available 1 268		Shear lines
Hubei and Hunan	Wufeng	3-8 July 1935	Not available		1 200	Low-level vortices
Shanxi and Inner Mongolia	Maousu Desert	1-2 Aug. 1977	1 050	1 050	1 050	Shear line and upper cold front
Guangxi	Laohutan	11 July 1960	634	1 036	1 036	Vortices and upper trough
Jiangsu	Chaoqiao	3-4 Aug. 1960	653	934	934	Typhoon Shirley
Fujian	Fengchao	18-19 Sept. 1956	593	871	871	Typhoon Freda
Anhui	Zhilaichao	15-17 Aug. 1975	539	809	809	Typhoon Ora
* Shanxi	Yangquan	22-24 Aug. 1966	Not available	800	800	Remnants of typhoon Tess

(cont.)

* Cases selected for further study

** Cumulative rainfall given is not very accurate; should be taken as rough estimate.

TABLE I (cont.)

Province or city	Location	Time of occurrence	Maximum rainfall (mm) 24 h	3 days	Entire period	Main rain-producing synoptic systems
Liaoning	Hei gou	7-8 Aug. 1962	657	794	794	Extra-tropical cyclone transformed from typhoon Opal
Hubei	Duzhenwan	9 Aug. 1975	629	629	629	Typhoon Nina
Shanxi	Middle Huang He	6-9 Aug. 1933	400	Not available 600	800**	Two upper troughs
Many provinces in central China	Middle and lower Chang Jiang	July 1931	Not available		800**	Six low-pressure disturbances
Many provinces in central China	Middle Chang Jiang	17-29 June 1973	Not available		718	Shear lines and mei yü stationary front
Zhejiang	Shiling	1-2 Aug. 1956	565	688	688	Typhoon Wanda
Shanghai	Tangqiao	21 Aug. 1977	581	592	592	Mesoscale cloud clusters north of typhoon Amy
Shandong	Shifuzhi	12 Aug. 1974	499	572	572	Shear line in the northern section of typhoon Lucy
Jiangxi	Dongxiang	17 Aug. 1953	499	533	533	Typhoon Nina
Beijing	Zaoshulin	26-28 July 1972	479	518	518	Typhoon Rita
*Henan	Yuanqu	14-19 July 1958	367	Not available 500		Upper trough and cold front
*Shanxi	Ansai	5-6 July 1977	400	400	400	Two upper troughs
Beijing	Beijing	1-2 July 1973	169	200	200	Low-level SW vortices

* Cases selected for further study

** Cumulative rainfall given is not very accurate; should be taken as rough estimate.

TABLE II

Comparison between two models

	Wuhan	Beijing
Validity	0-24 h 12-36 h	0-24 h 12-36 h
Initial time	0000Z	OOOOZ
Time of issue	0700Z	0800Z
Area	Limited E-W 2 900 km N-S 2 3000 km	Limited 5 000 km 3 400 km
Projection	Lambert	Polar-conical
Equation	Primitive	Primitive
Grid space	100 km	190.5 km
Layers	5	5
Initial windfield	Observed	Derived
Topography	Included	Not included
Boundary	Fixed	Nested

TABLE III

Comparison of skill for June 1986

Forecast period	Rainfall area		Maxima		Intensity forecast score				
	Wuhan	Beijing	Wuhan	Beijing	Wuhan		Beijing		Observed
0000Z/15-0000/16	3	2	3	2	92	3	47	2	96
1200/20-1200/21	1	2	3	1	51	3	29	2	254
0000/21-0000/22	3	2	3	3	50	3	36	2	263
0000/27-0000/28	3	2	3	2	32	3	23	3	215
4900/28-0000/29	2	3	3	2	50	3	22	2	175
Total	12	11	15	10	15		11		

TABLE IV

Forecast score for rainstorms (1983-1986)

Date OOOOZ	TS (25 mm d^{-1})	TS (50 mm d^{-1})	Observed (mm)	Predicted (mm)	Difference between maxima predicted and observed
1983					
June					
24	42	50	108	83	50
			75	65	100
25	27	26	132	104	100
			66	72	50
			60	79	50
26	49	36	106	82	100
			54	60	50
			62	83	150
27	41	50	51	63	50
28	27	17	52	80	50
			118	67	100
29	29	6	176	76	100
			105	66	100
30	32	9	73	61	50
July					
1	42	35	102	121	100
			69	68	50
2	0	0	15	109	
3	3	0	148	66	200
4	62	53	112	124	50
			250	153	100
			100	125	50
				170	
5	59	29	92	41	80
			119	83	50
			56	102	50
6	78	85	108	52	50
			223	110	50
1984					
June					
5	21	0	102	164	300
6	64	26	147	92	50
			152	49	
			69	95	80
			129	50	100
1985					
April					
9	40	31	67	94	50
			157	91	100
May					
11	35	12	47	91	120
			193	132	100
11	(1200 GMT)		116	166	50

(cont.)

Table IV (cont.)

Date 0000Z	TS (25 mm d^{-1})	TS (50 mm d^{-1})	Observed (mm)	Predicted (mm)	Difference between maxima predicted and observed
June					
5	20	10	73	72	200
			36	59	50
21	4	0	152		
			30	65	100
July					
3	29	29	61	132	50
			50	77	50
			52	25	50
5	34	19	122	88	150
			222	65	50
		153	65	50	
6	29	0	79	63	250
	71	55	62	57	50
1986					
June					
15					
			96	92	100
			97	42	50
21	67	31	263	184	200
23	47		45	42	100
Average:	38.1	25.4	103	87	90

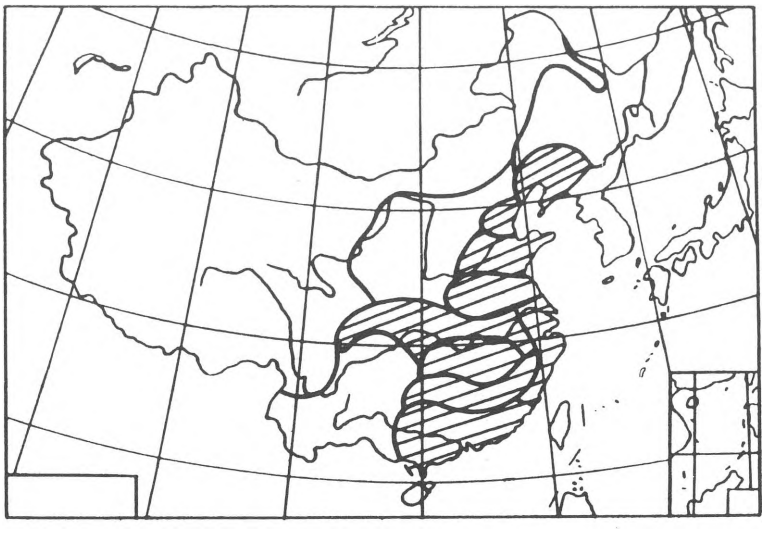

Figure 1 - Distribution of floods in China

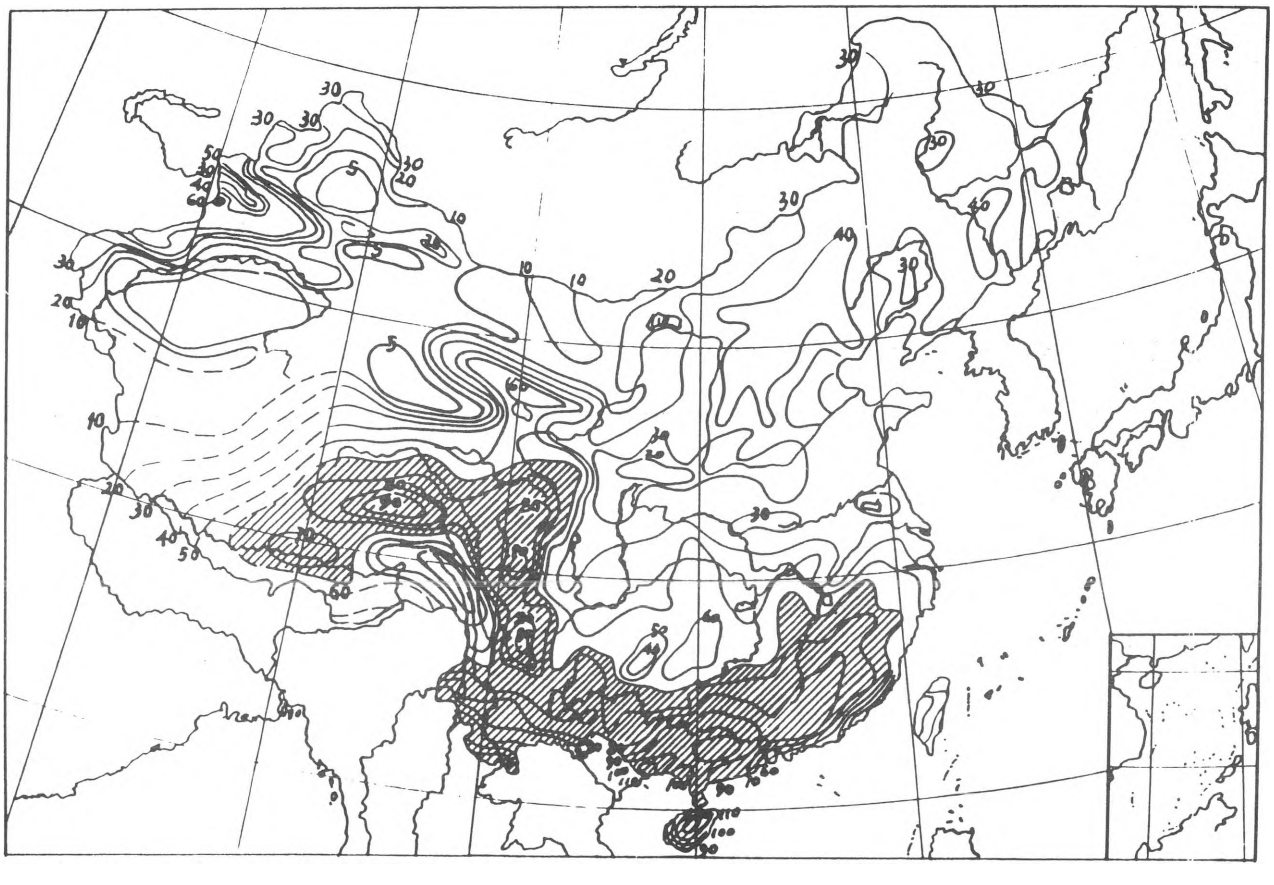

Figure 2 - Annual average thunderstorm days in China, 1957-1970

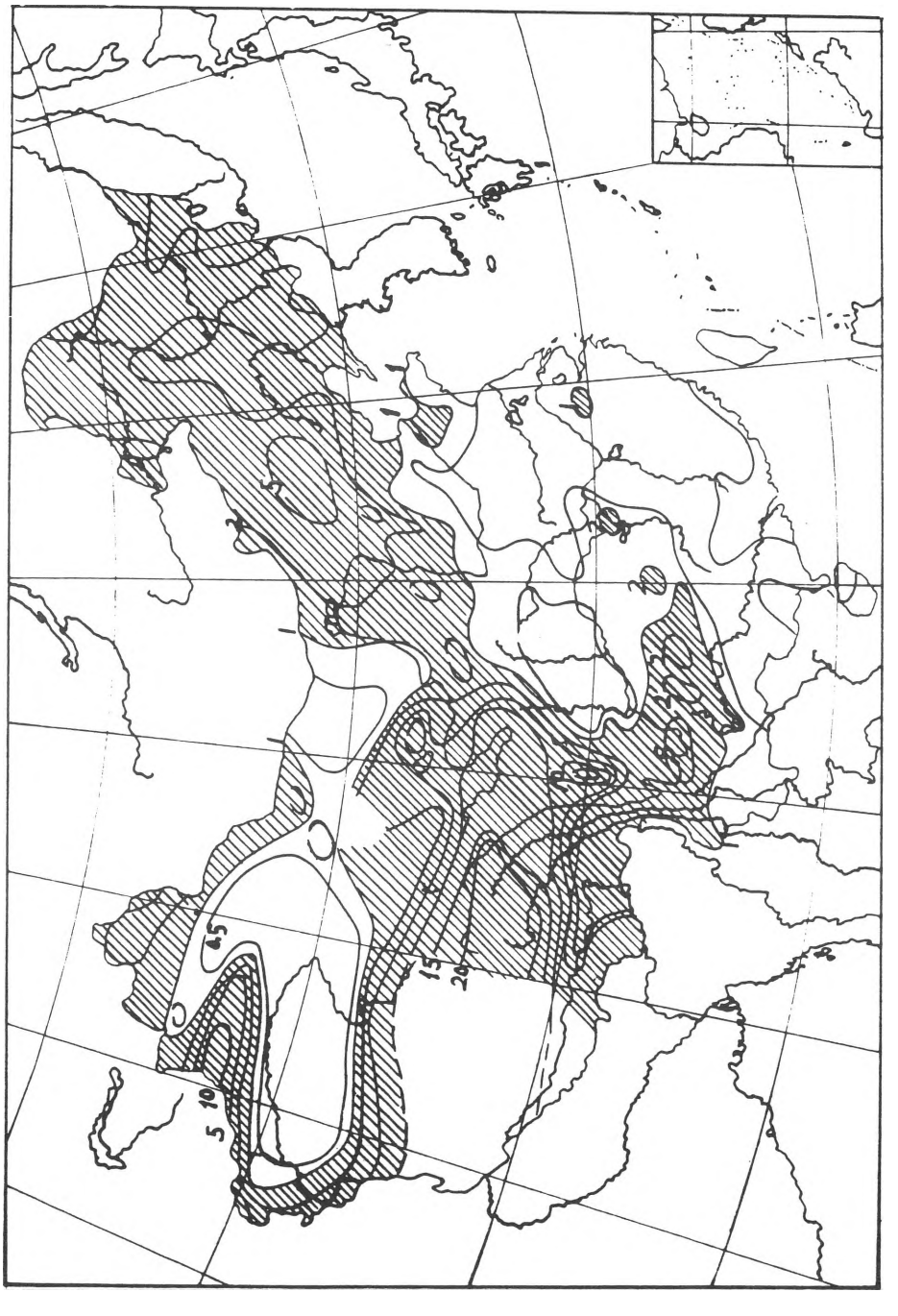

Figure 3 - Annual mean distribution of hailstorms in China

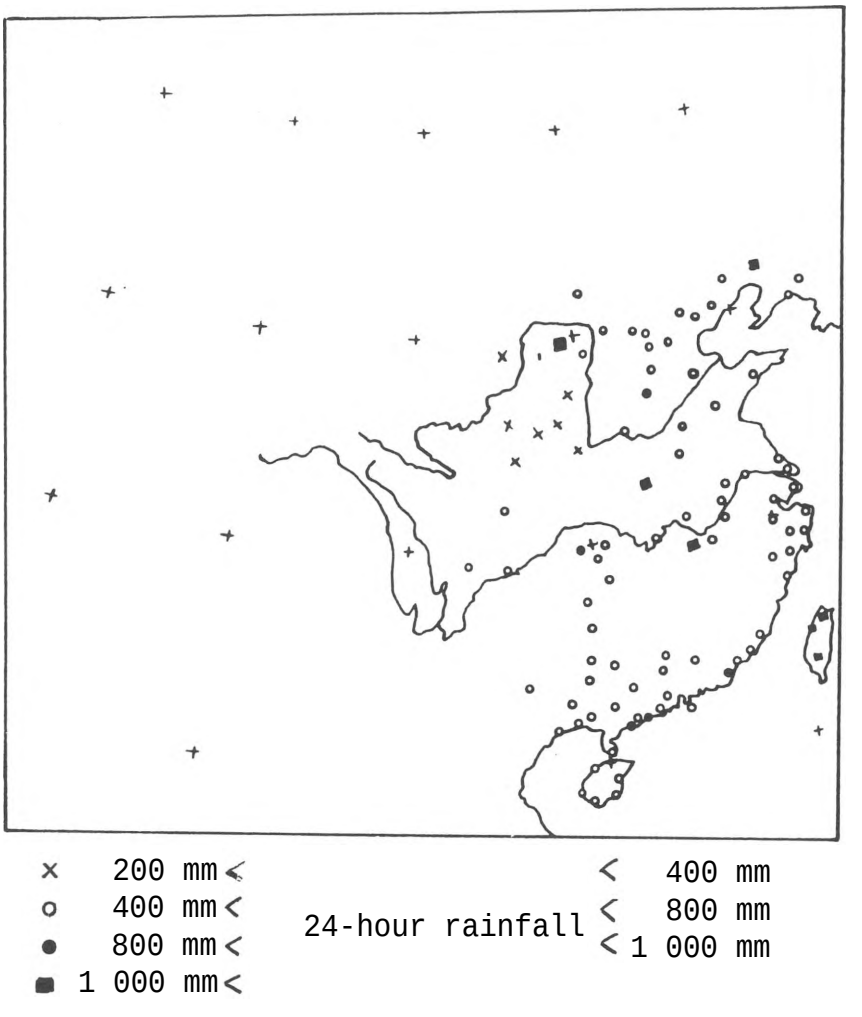

Figure 4 - Geographic distribution of heavy rainfall in China from 1953 to 1957 with the 24-hour rainfall exceeding 1 000 mm, 800 mm and 400 mm, respectively

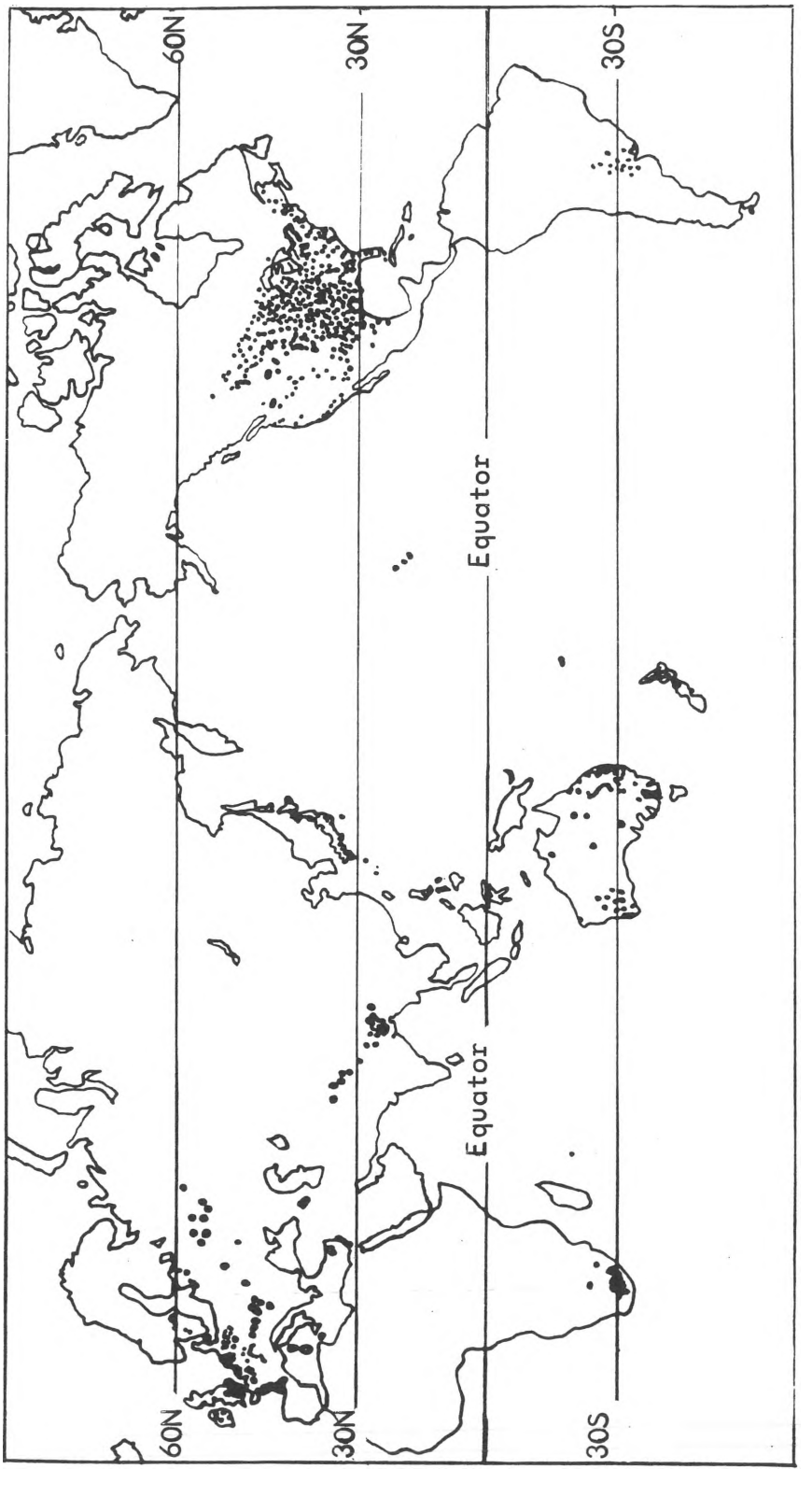

Figure 5 - Global distribution of tornado occurrence, 1963-1964

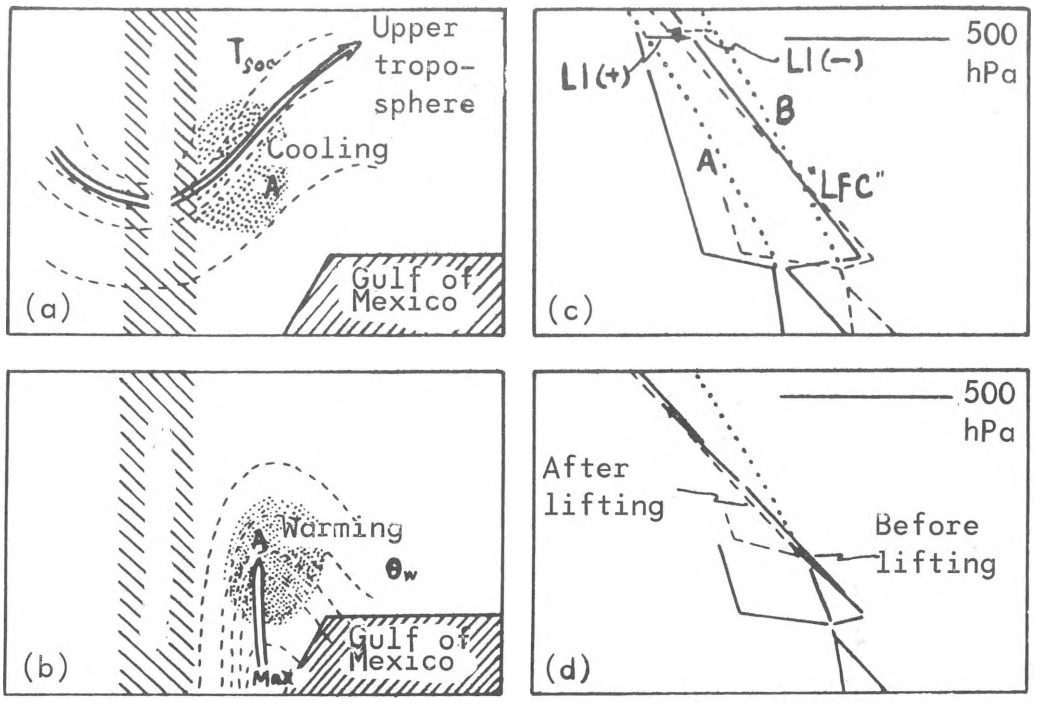

Figure 6 - Airflows over the Rocky Mountains, USA

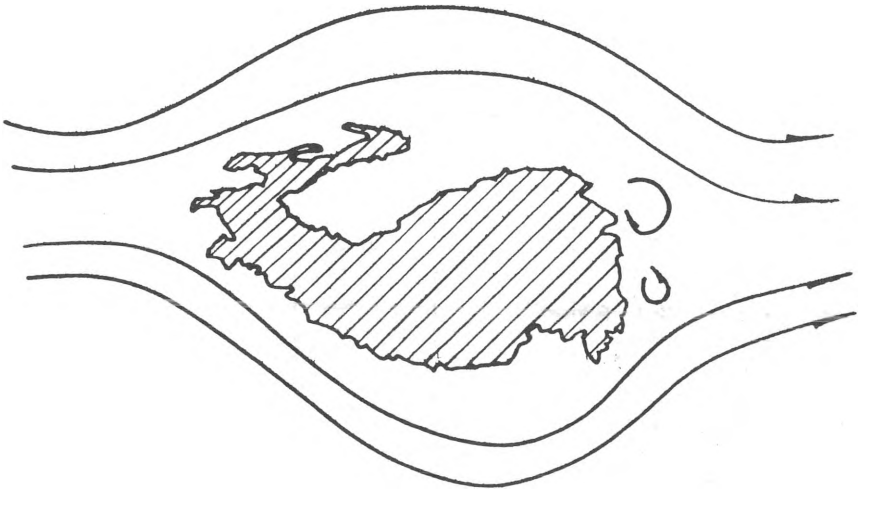

Figure 7 - Airflows over the Plateau of Tibet

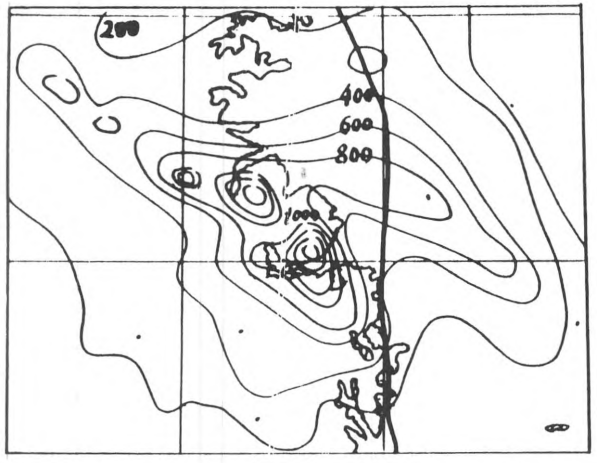

Figure 8 - Analysis of rainstorm at 500 hPa at 1200Z on 7 August 1975

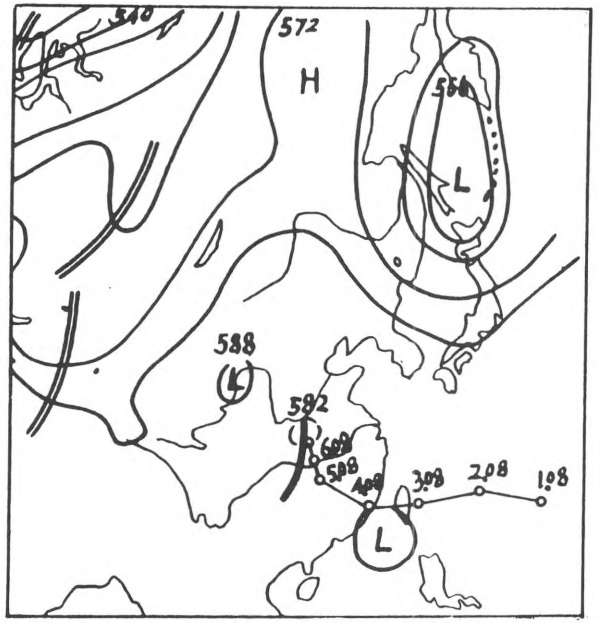

Figure 9 - Rainfall of 1 605 mm in three days was recorded in an area 120 x 50 km at the windward side of the Funiu mountains (5-7 August 1975)

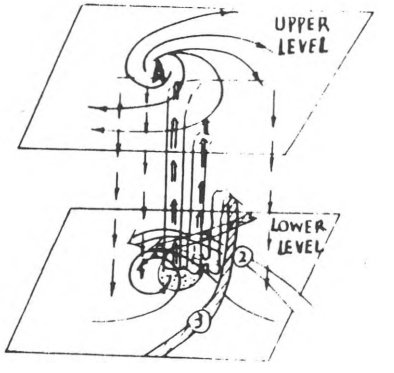

Figure 10 - Development of meso-scale thunderstorm system

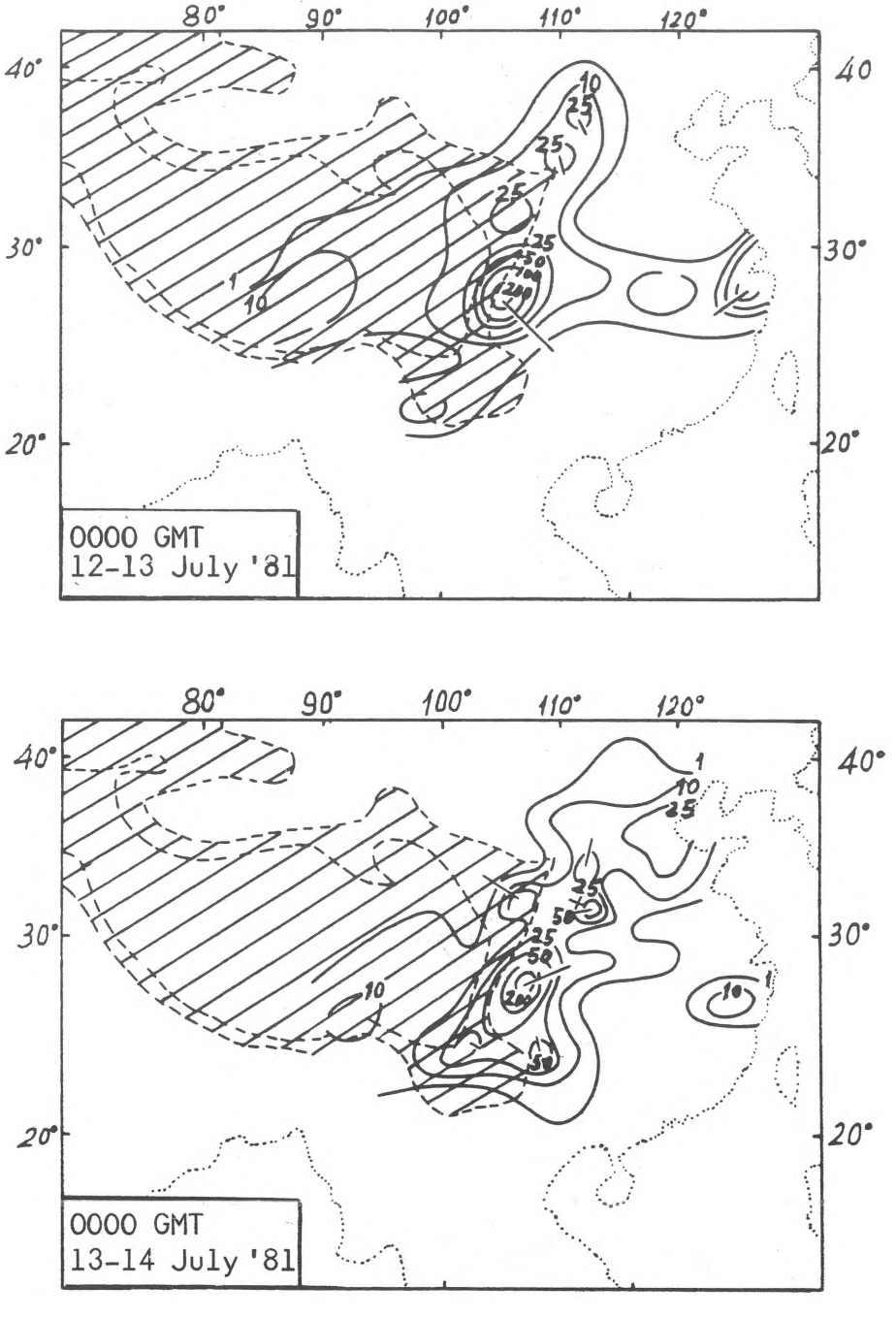

Figure 11 - Flood of 11-15 July 1981 in Sichuan province - 24 hour precipitation

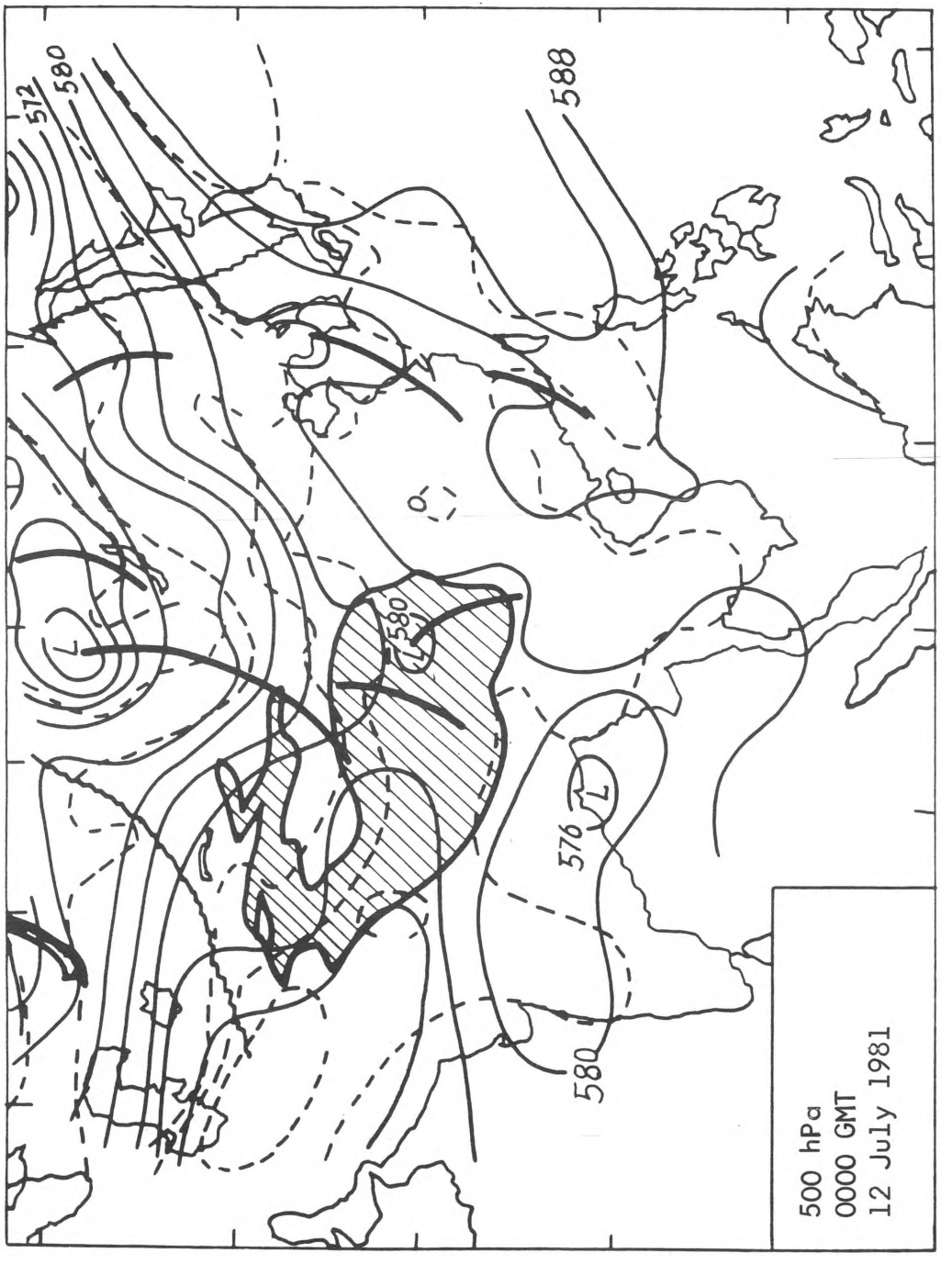

Figure 12 - Vortex P, which originated on 11 July 1981 over the Plateau of Tibet, moves eastward

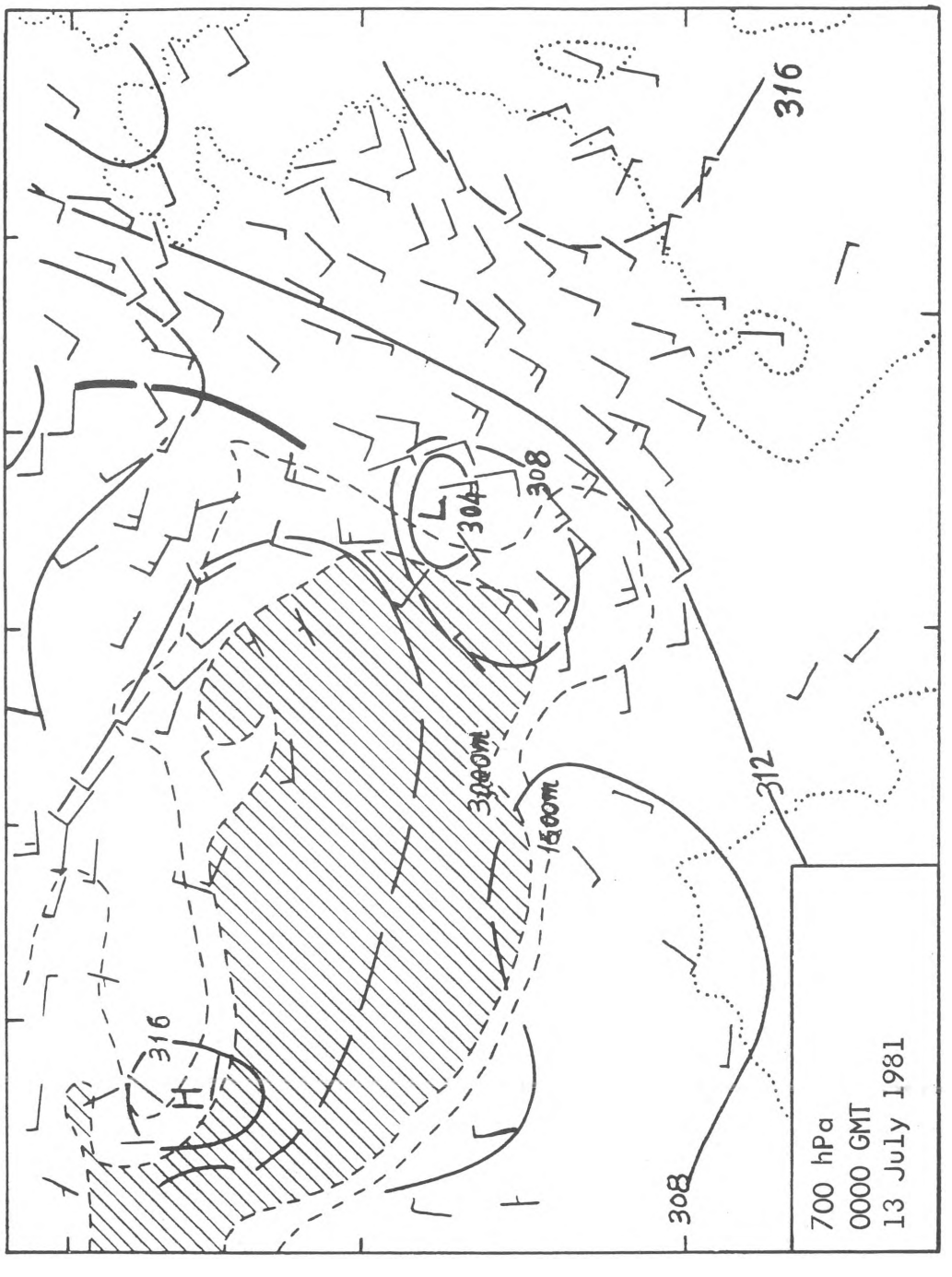

Figure 13 - Vortices P and SW merge into a single, bigger mesoscale vortex and produce the first heavy precipitation

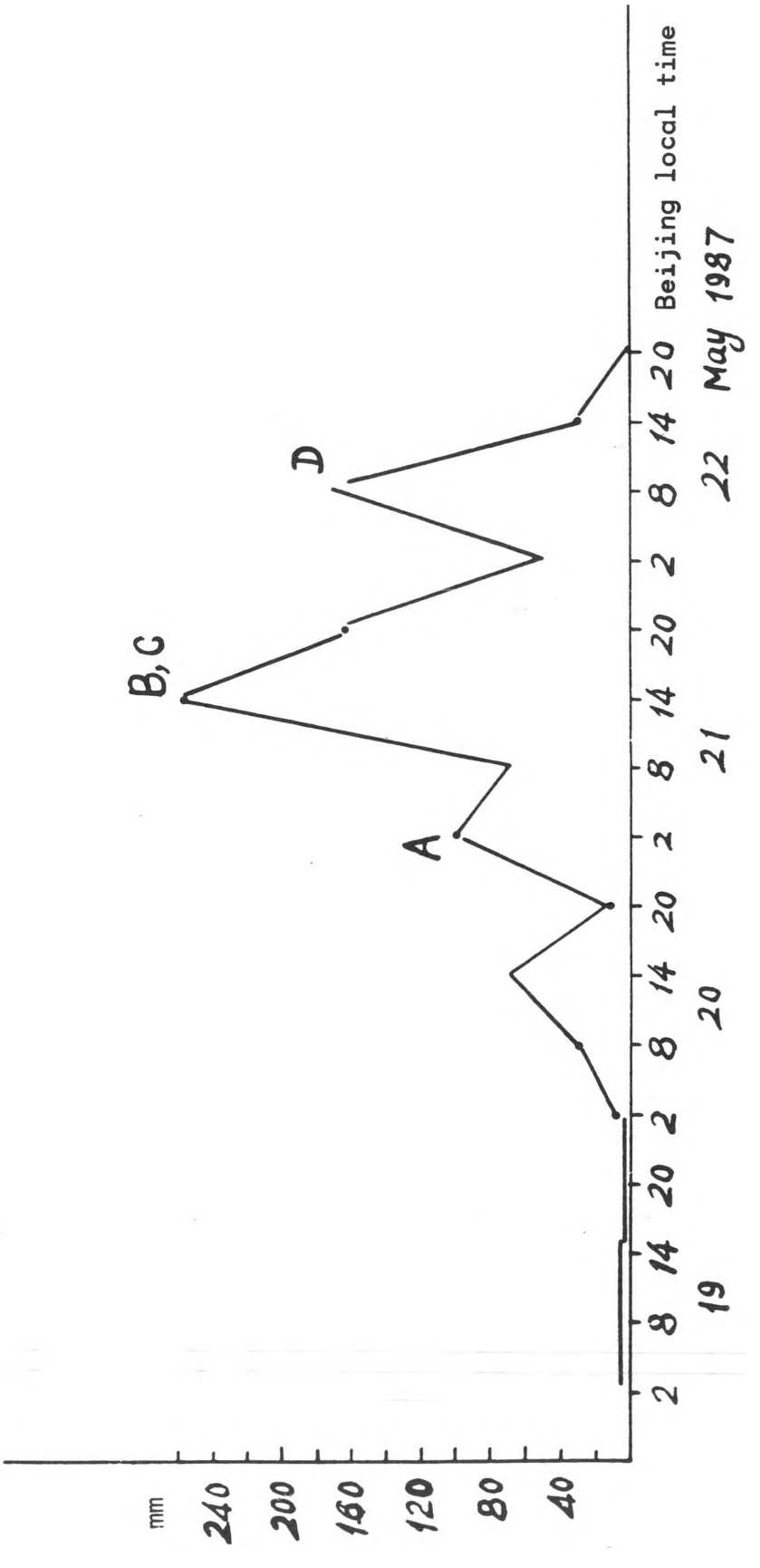

Figure 14 - Six-hourly rainfall variation, 19-22 May 1987

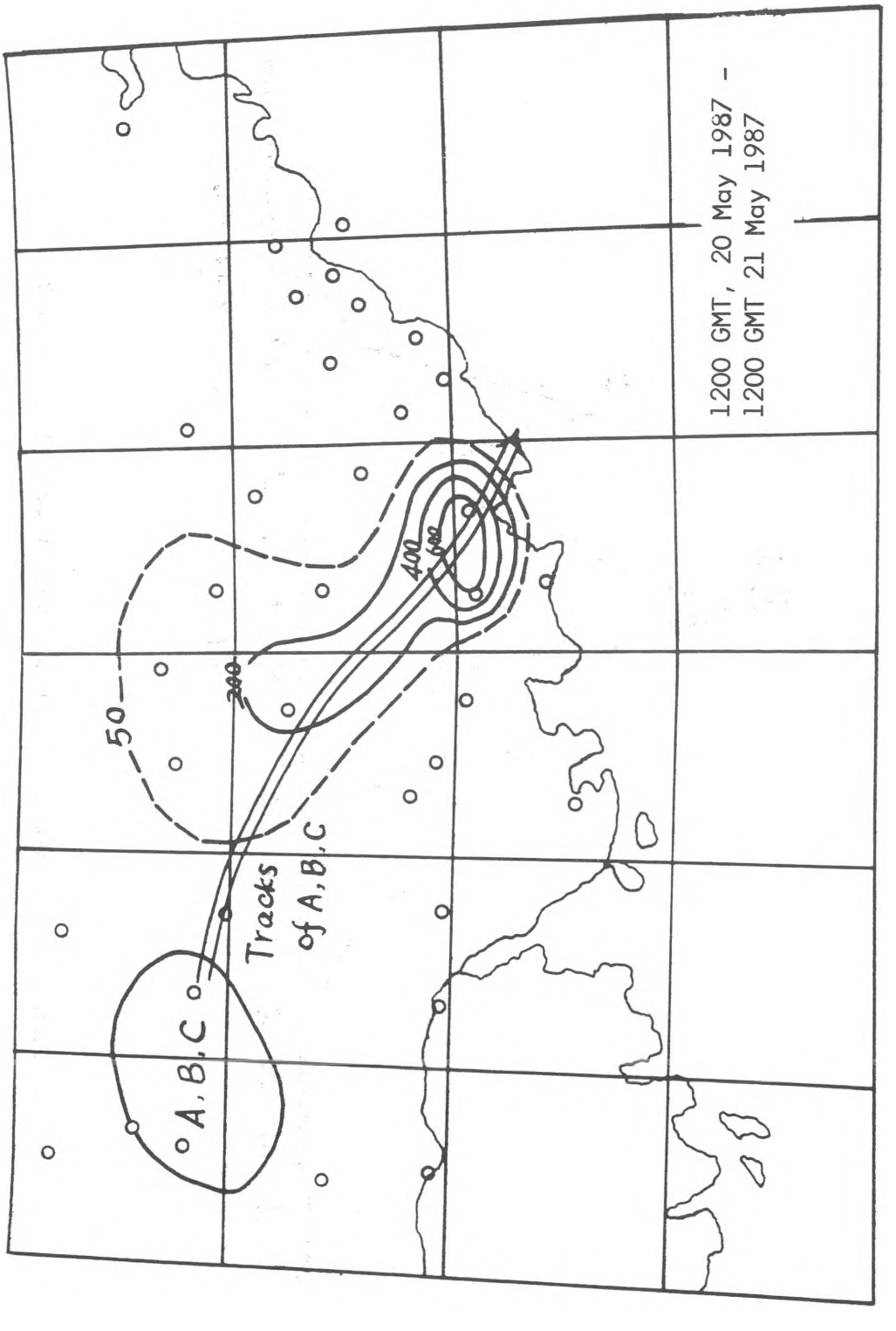

Figure 15 - 24-hour rainfall amount in coastal area, Guangdong

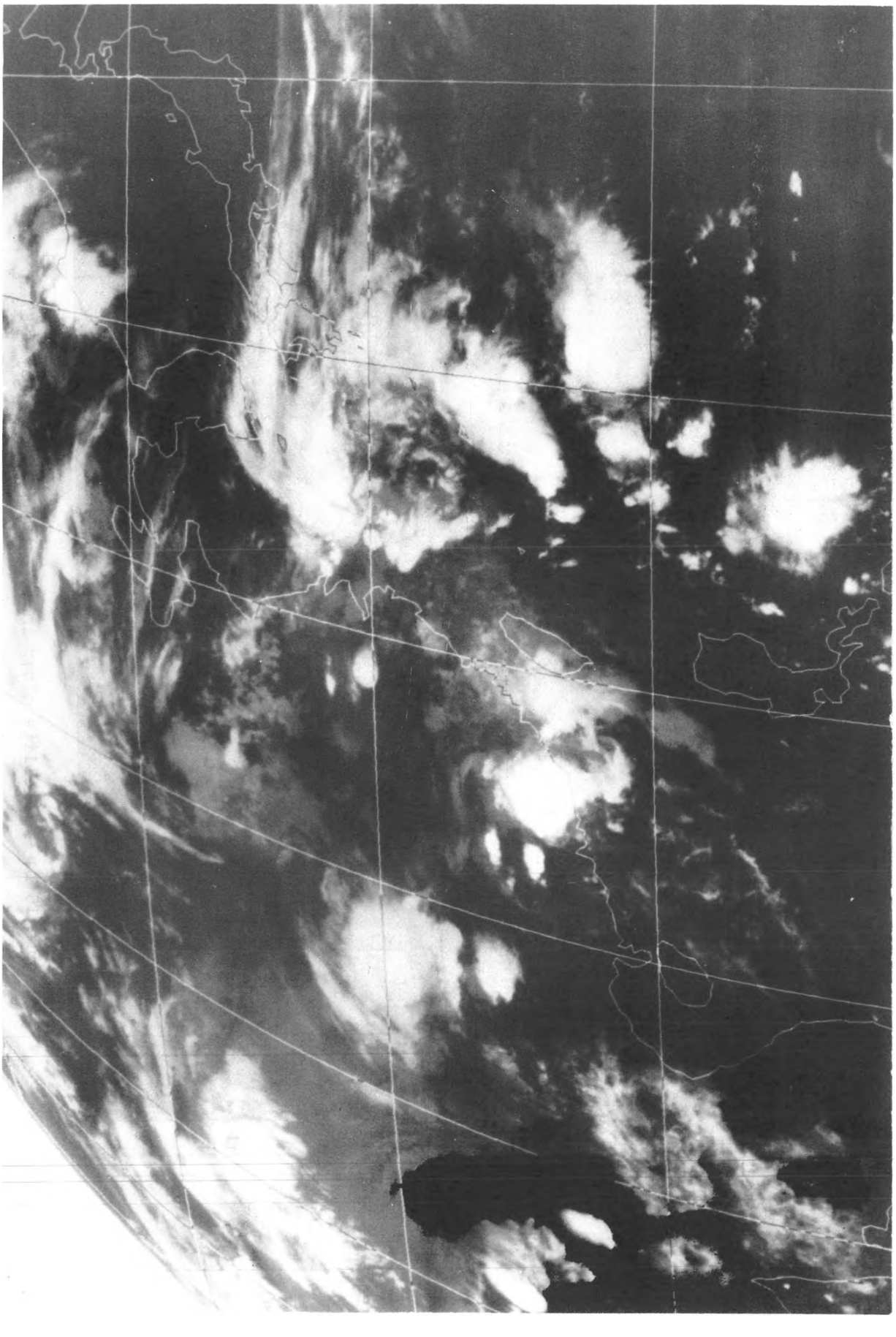

Figure 16(a) - Satellite cloud image at 2100Z on 20 May 1987

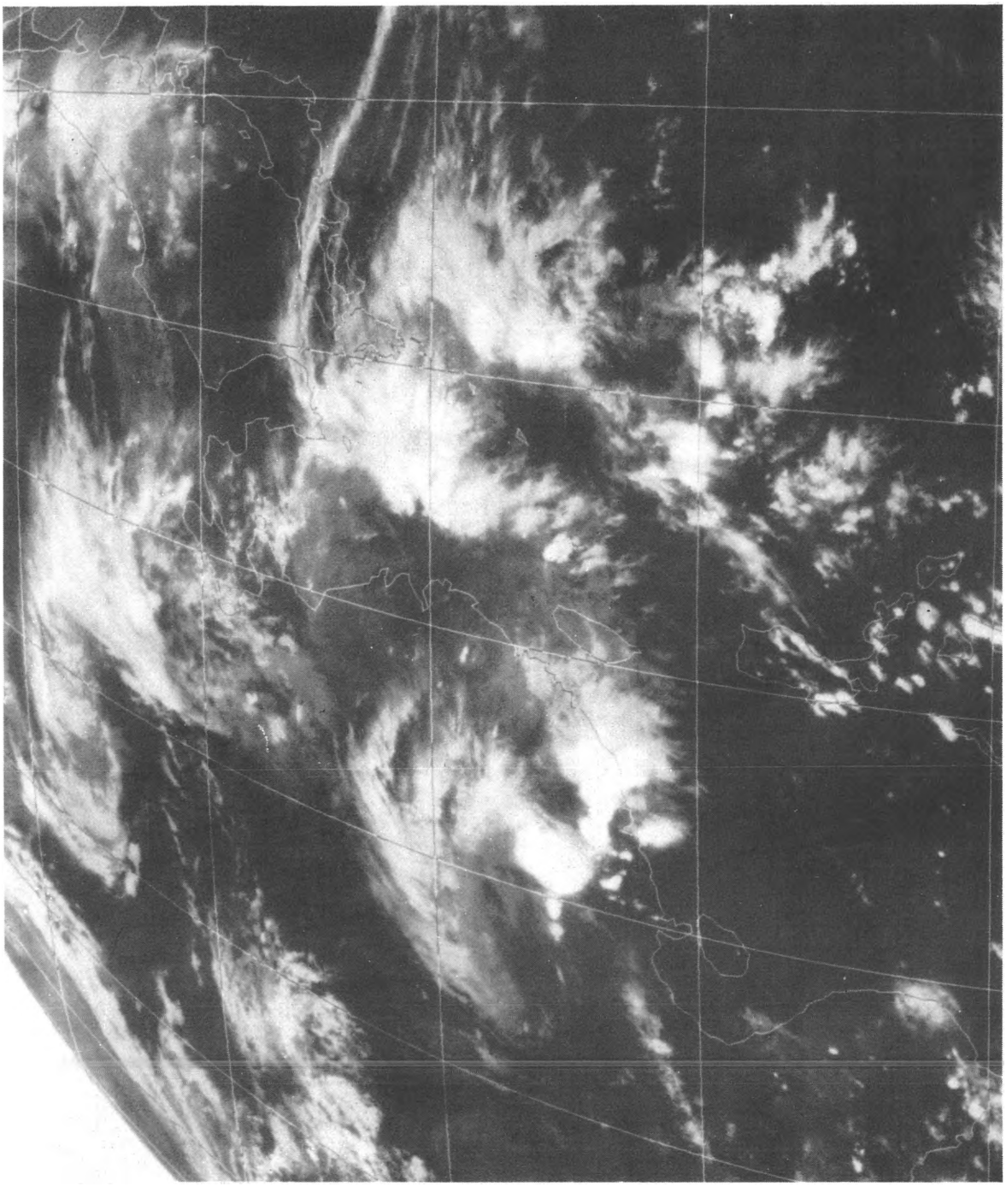

Figure 16(b) - Satellite cloud image at 0600Z on 21 May 1987

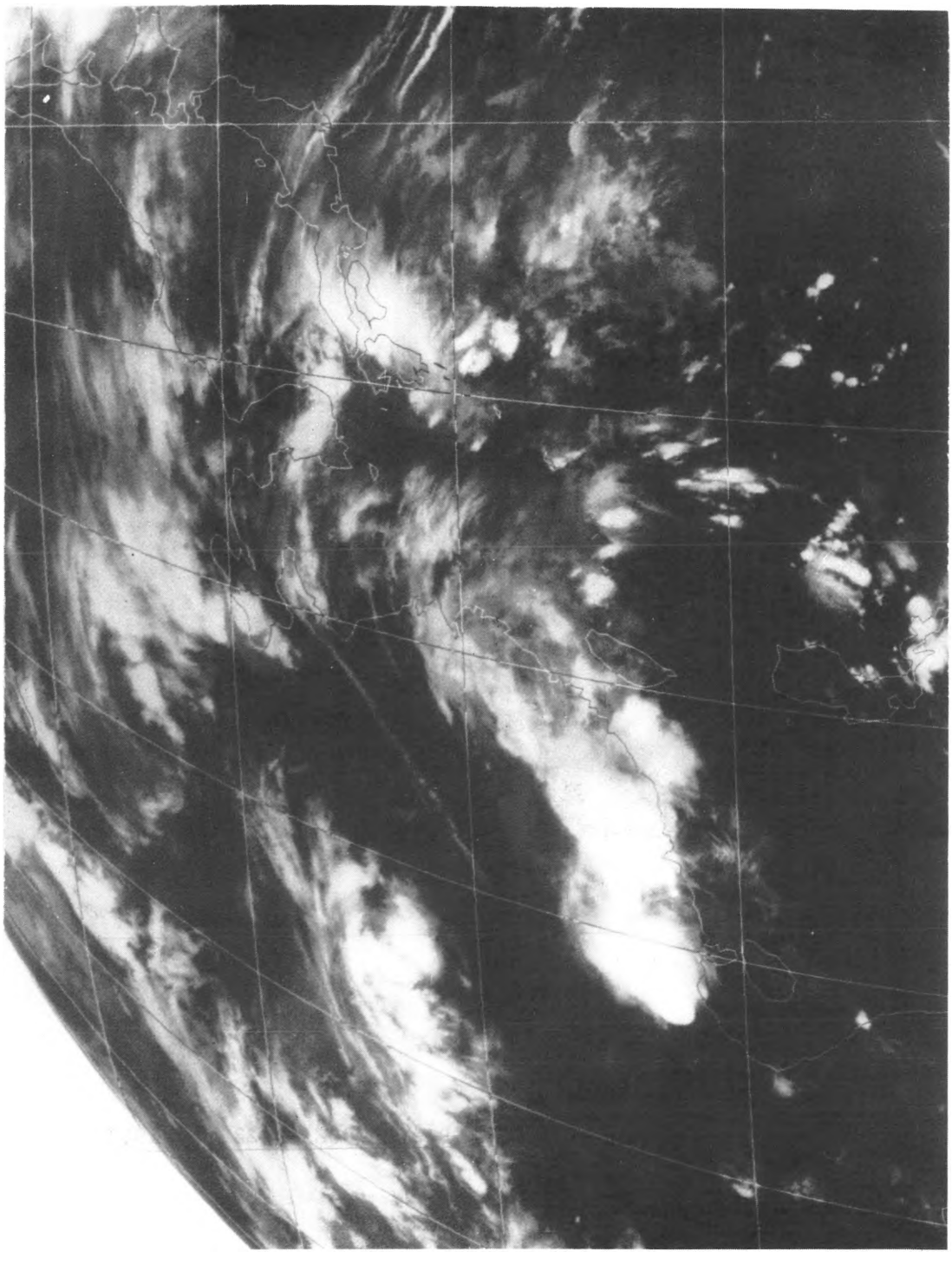

Figure 16(c) - Satellite cloud image at 1800Z on 21 May 1987

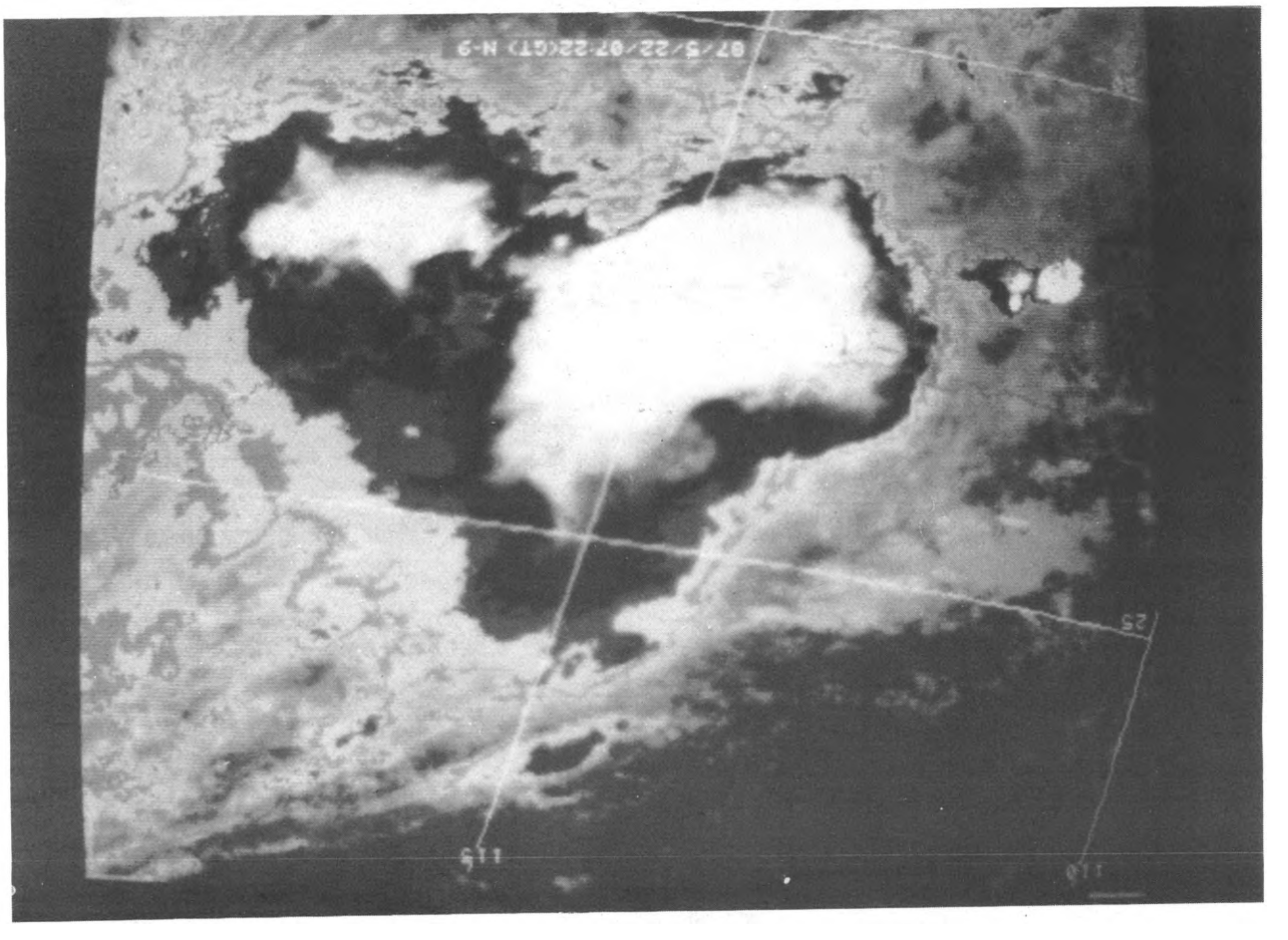

Figure 17 - IR image from NOAA-9 at 0700Z on 22 May 1987

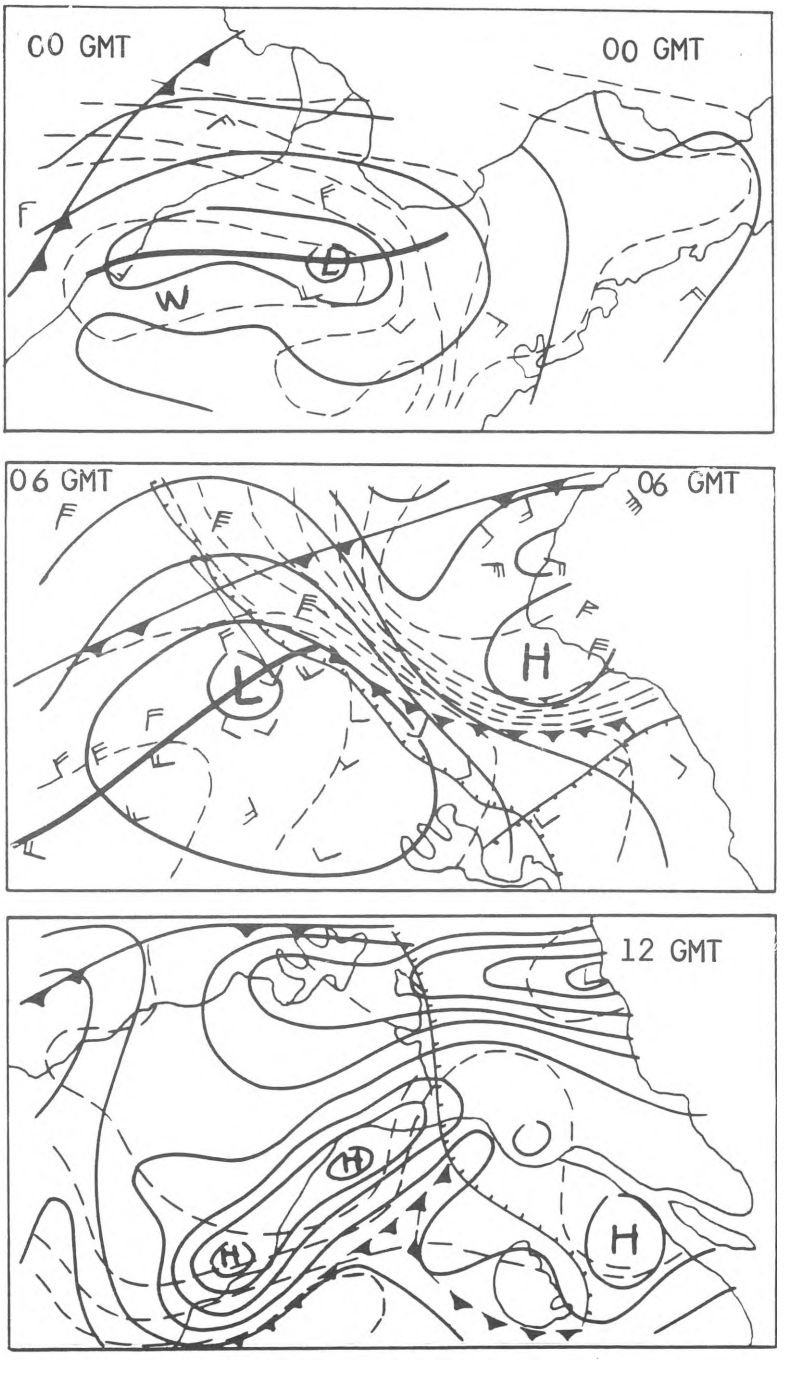

Figure 19 - Squall line of 17 June 1974 over Nanjing at 1100Z

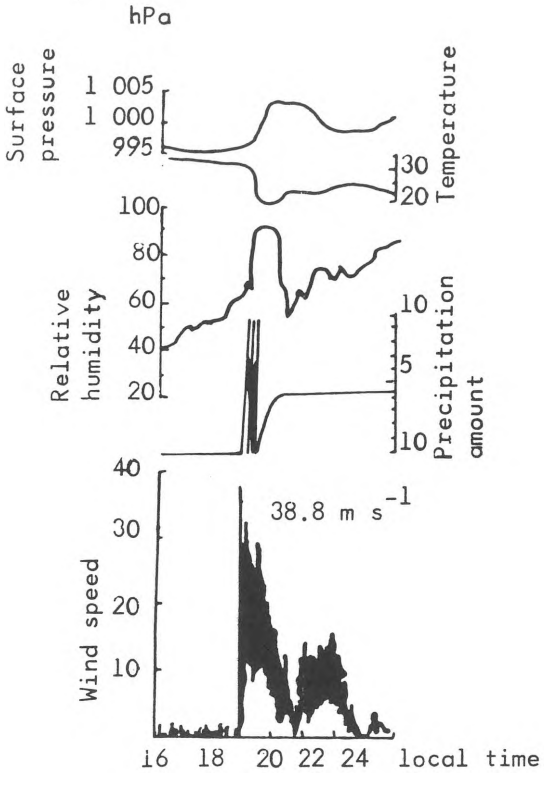

Figure 20 - Pressure, temperature and wind speed in Nanjing during passage of squall line

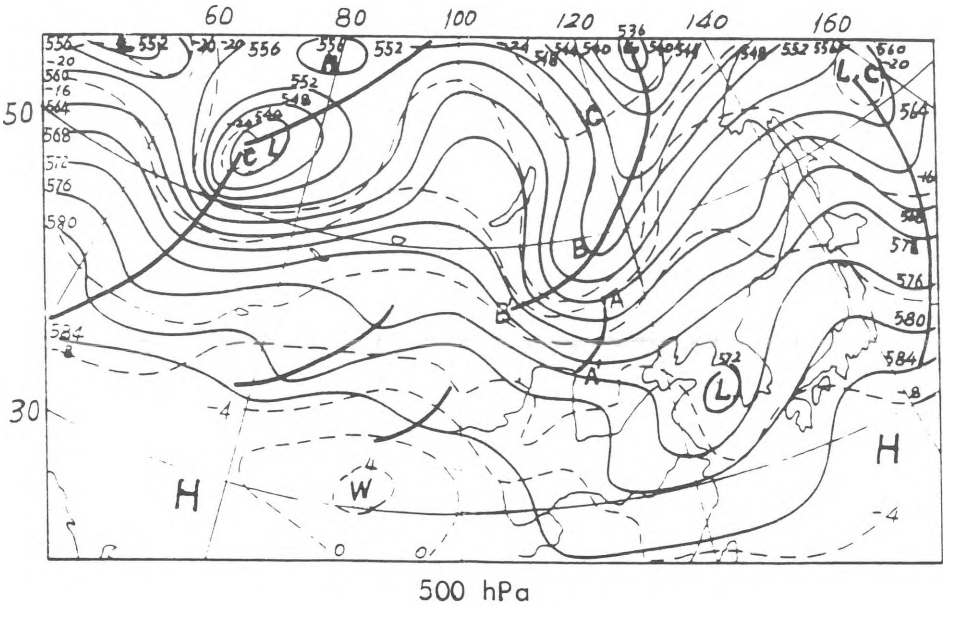

Figure 21 - Trapezoidal upper troughs over eastern Asia at 1200Z on 17 June 1974 at 500 hPA

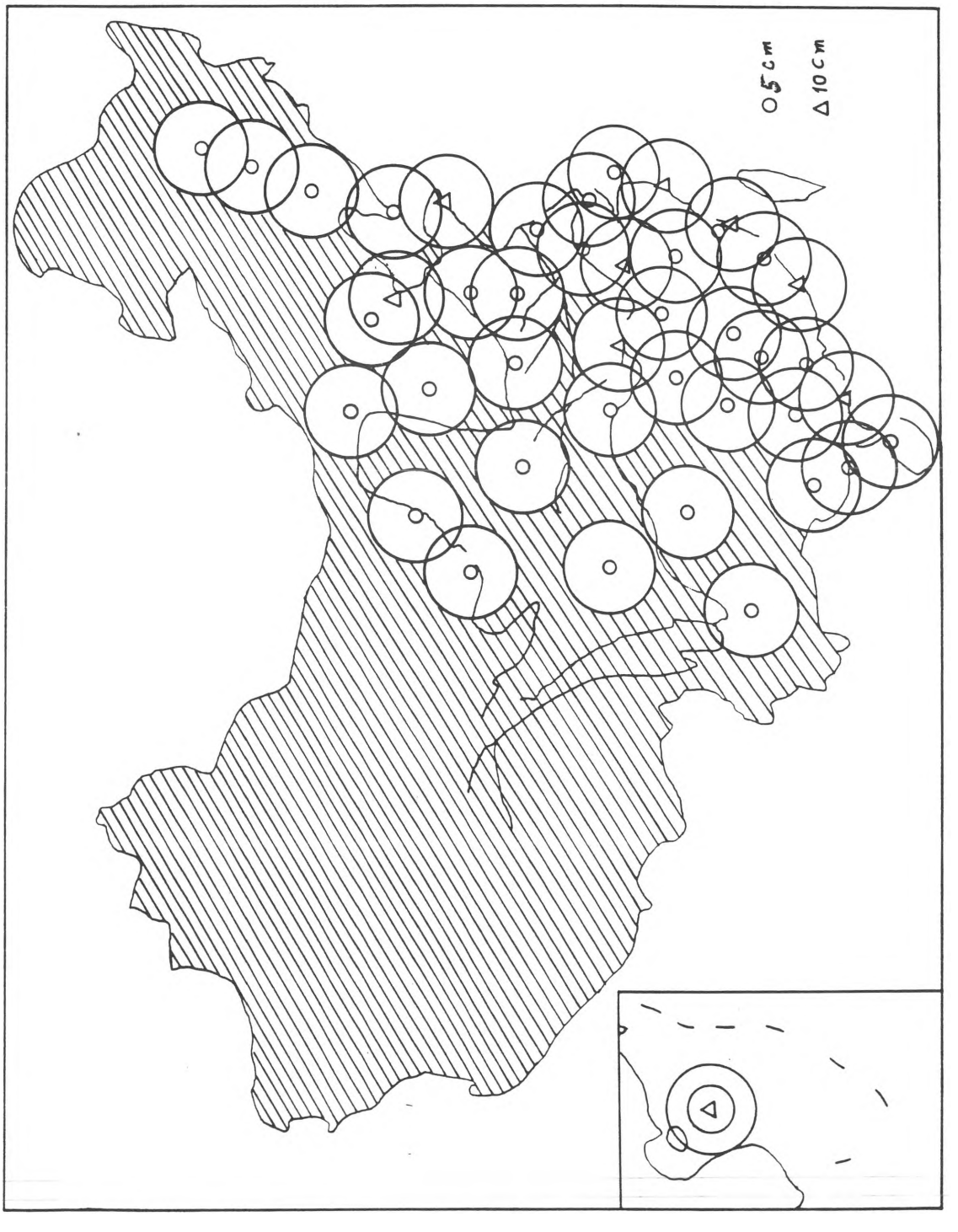

Figure 22 - Coverage of rainstorms and severe convective weather in eastern China by method combining data from weather radar, satellite imagery and enhanced surface observations

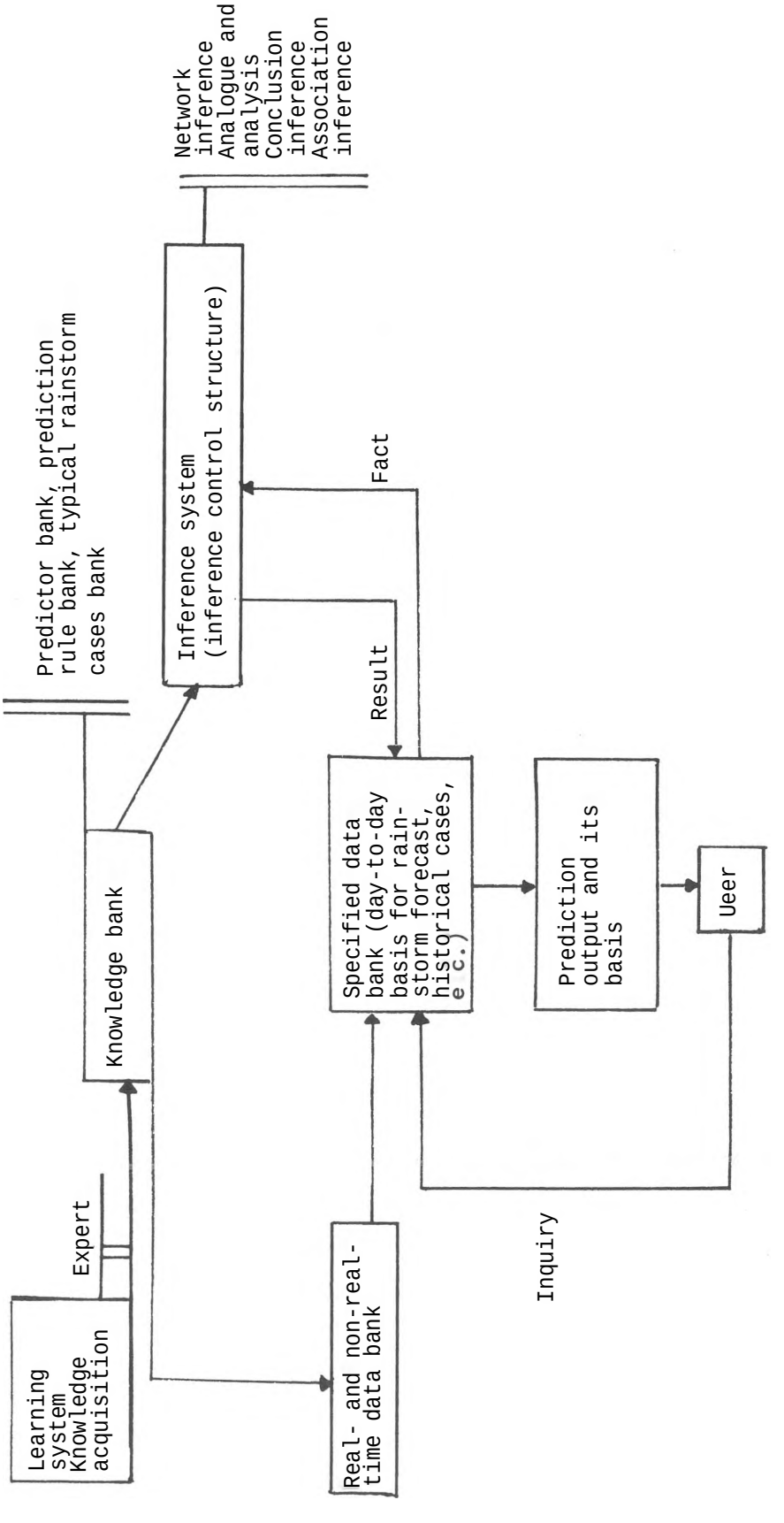

Figure 23 - Flowchart of expert system of rainstorm prediction

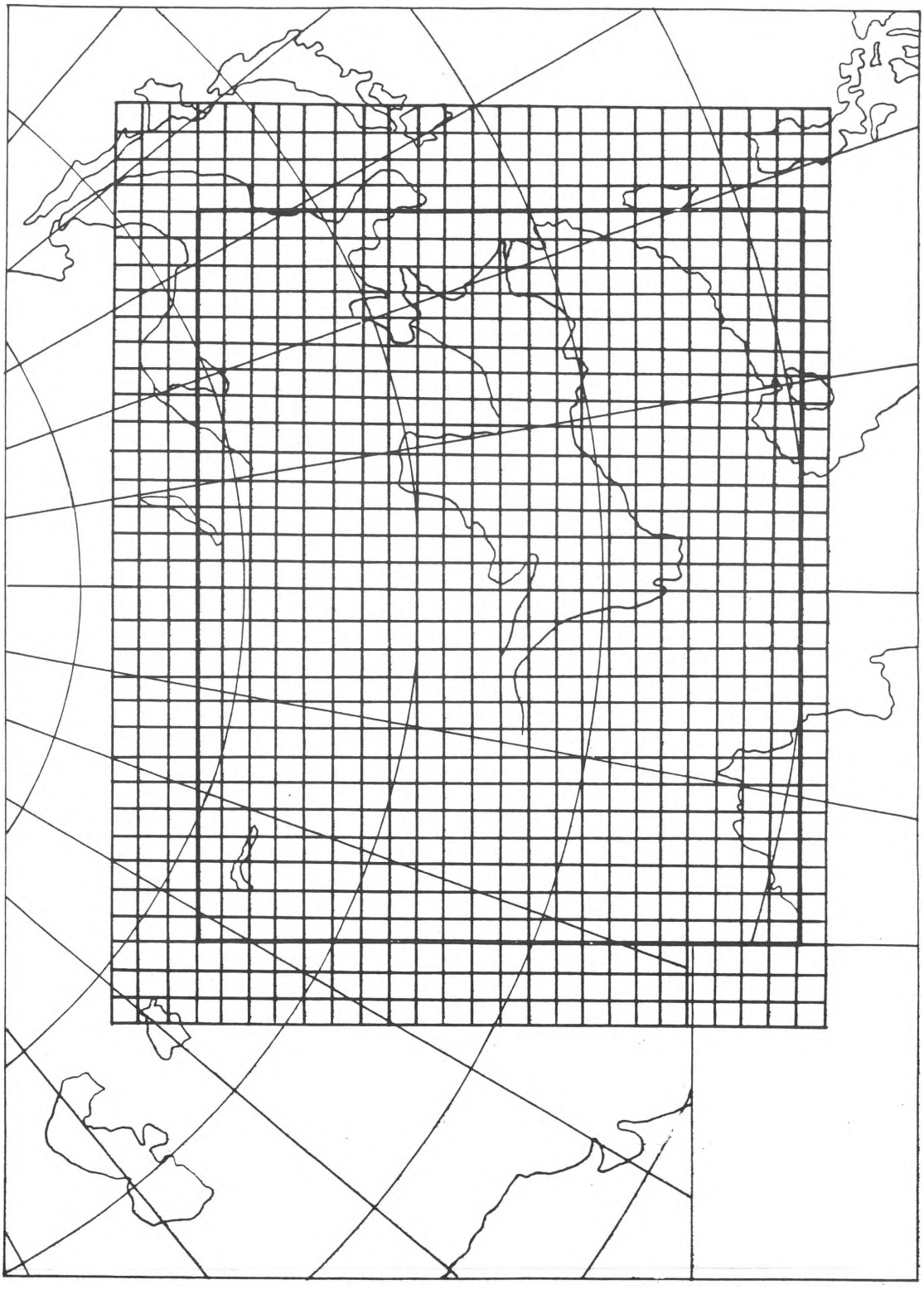

Figure 24 Product of northern hemisphere model and regional precipitation model

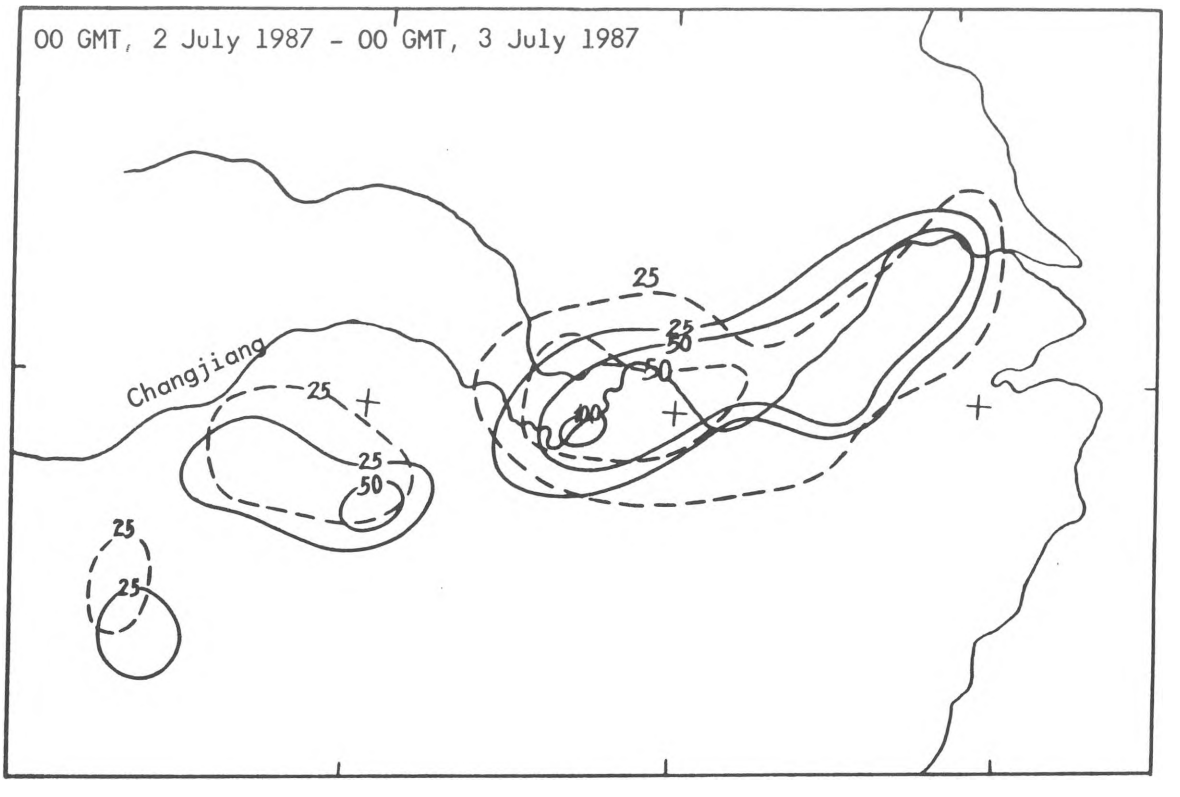

(a)

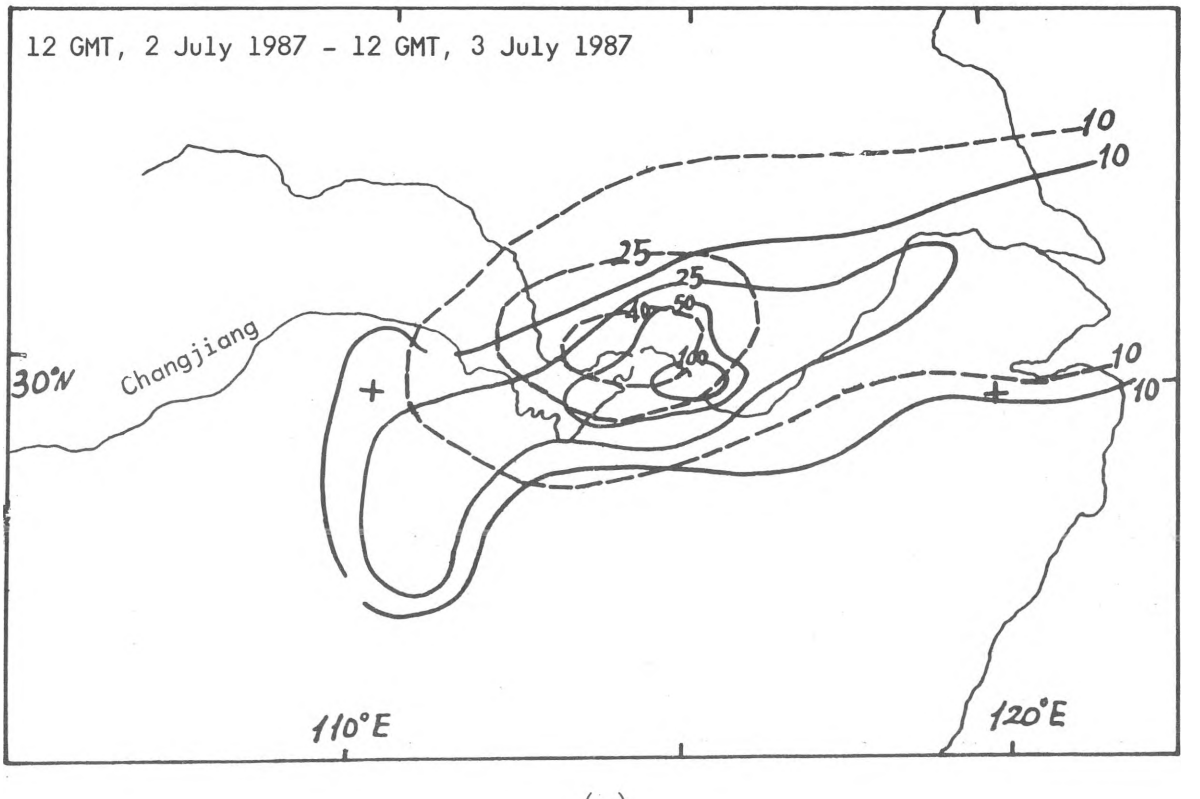

(b)

Figure 25 - Predicted and observed shear line associated with precipitation for 24 hours

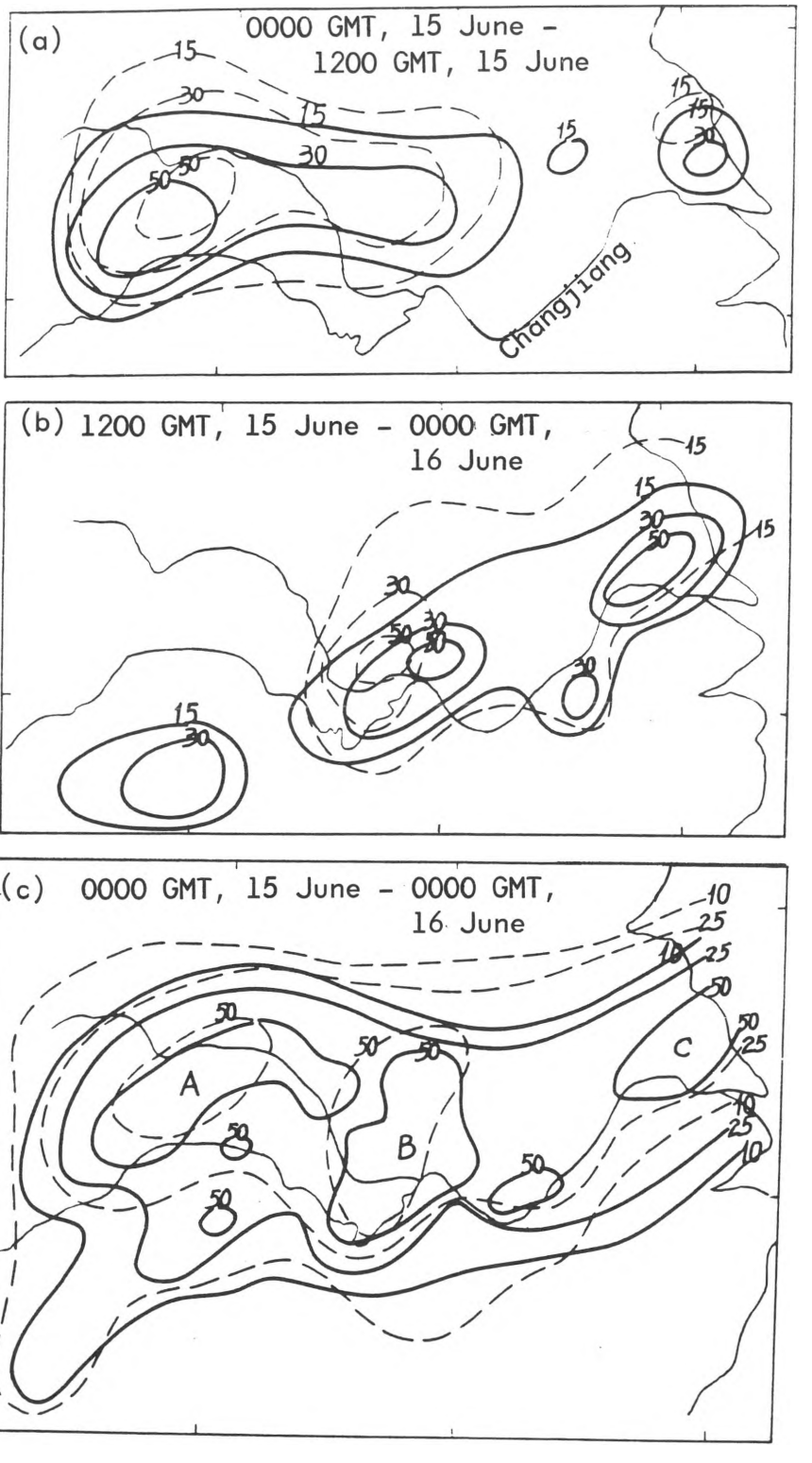

Figure 26 - Rainstorm in Changjiang Basin caused by eastward movement of a south-west vortex

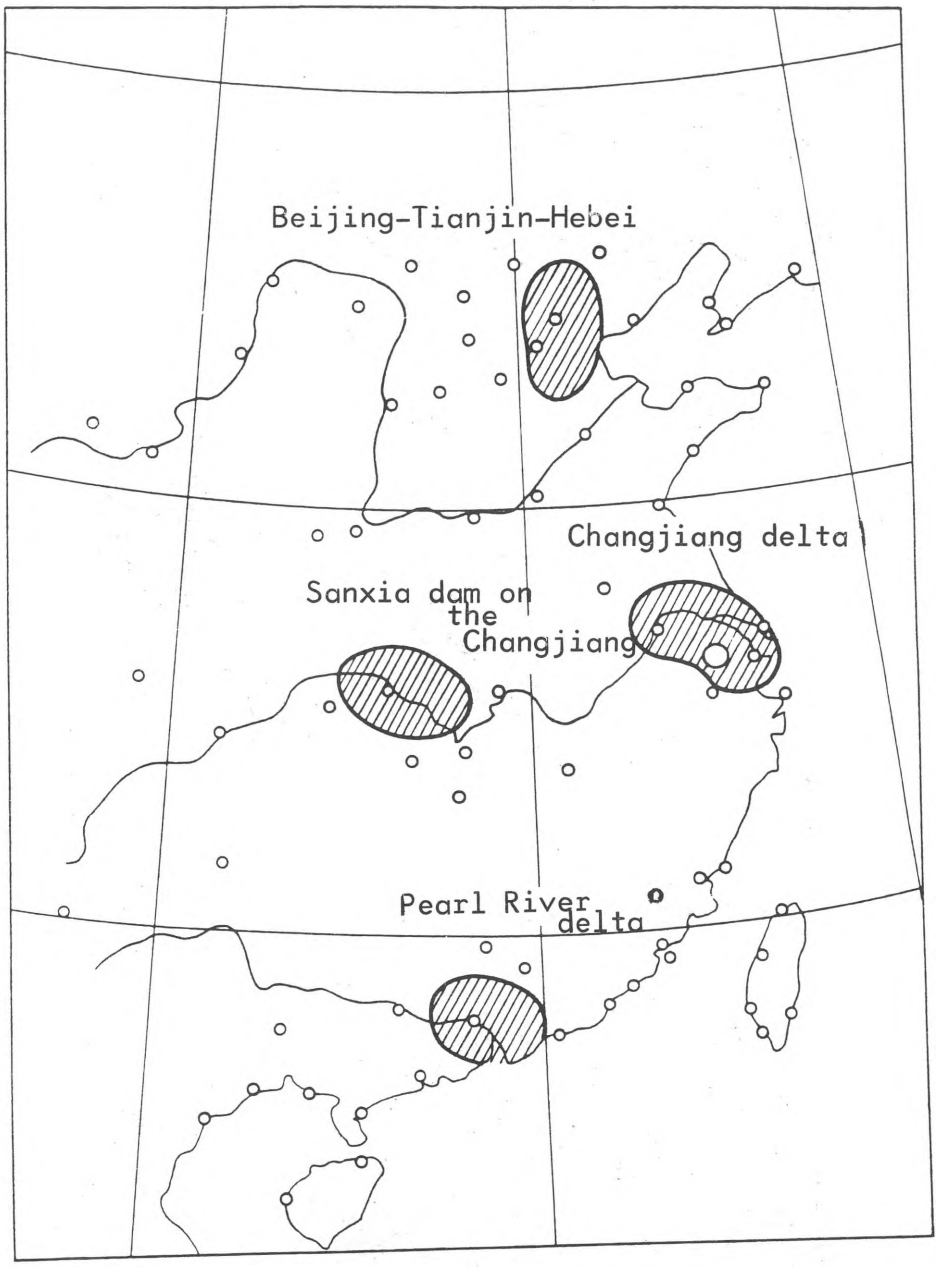

Figure 27 - Four experimental sites for establishing a monitoring and forecasting system in China

РАЗРАБОТКА МЕЗОМАСШТАБНЫХ МОДЕЛЕЙ ПРОГНОЗА МЕТЕОРОЛОГИЧЕСКИХ ЭЛЕМЕНТОВ

Н.Ф. Вельтищев
Гидрометцентр СССР

многие явления погоды, угрожающие человеческой жизни и наносящие ущерб экономике (интенсивная грозовая деятельность, катастрофические осадки, шквалистые ветры, интенсивная турбулентность), являются результатом мезомасштабных процессов, протекающих в атмосфере. К ним относятся организованная конвекция, тропические циклоны и взрывной циклогенез во внетропических широтах, интенсивные фронты и некоторые вилы орографических циркуляций (фен, бора, горные волны).

Естественно, что проблема точного и своевременного прогнозирования мезомасштабных систем в атмосфере и связанных с ними явлений погоды существовала всегда, однако ло недавнего времени из-за отсутствия соответствующих наблюла тельных средств и ограниченных возможностей вычислительной техники не представлялось возможным идентифицировать мезо-масштабные возмущения в атмосфере и осуществлять их численное прогнозирование.

С развитием спутниковых, радиолокационных и других методов дистанционных измерений наземного и космического базирования с большим пространственно-временным разрешением, а также наземных сетей станций с большой плотностью наблюдений стало возможным идентифицировать мезо масштабные атмосферные возмущения по данным о структуре облачного покрова, осадков, влажности. Значительная часть этой информации носит пока что качественный характер и не может быть использована непосредственно в задаче численного прогноза, однако прогрессивное совершенствование техники дистанционных измерений в инфракрасном и микроволновом диапазонах, развитие допплеровской техники свидетельствует о том, что информационная база мезо масштабных численных моделей будет постепенно расширяться и более полно удовлетворять нужды моделей на мелких сетках в исходных данных.

Параллельно с развитием наблюдательных систем происходило совершенствование методов численного решения уравнений гидротермодинамики и методов параметризации различных физических процессов, происходящих в атмосфере. Последнее осуществлялось как в рамках разработки прогностических региональных и глобальных моделей, так и пои изучении отдельных мезомасштабных явлений в атмосфере.

В результате расширения информационной базы, совершенствования методов численного прогнозирования и увеличения возможностей вычислительной техники в настоящее время создались предпосылки для разработки мезомасштабных моделей, предназначенных для прогнозирования основных элементов погоды: температуры, ветра, давления, влажности, облачности и осадков на очень мелких сетках.

Основное отличие этих моделей состоит в том, что они должны ВОСПРОИЗВОДИТЬ мезомасштабные системы течений и на основе этого давать более детализированные ПРОГНОЗЫ метеорологических величин на ограниченной территории .

ВОПРОС О ТОМ, где проходит граница между крупномасштабными, мезомасштабными и микромасштабными движениями, обсуждался в литературе многими авторами (см., например, Орланский, 1975, Уайт, 1978, Аткинсон, 1981). Я не буду останавливаться на этом вопросе подробно, поскольку спектр атмосферных движений является более или менее непрерывным, а выбор разрешаемого масштаба диктуется, как правило, не только теоретическими, но и практическими соображениями.

Поскольку в литературе наиболее широкое распространение приобрела классификация, предложенная Оршанским (1975), я буду пользоваться в дальнейшем ею. В соответствии с этой классификацией в мезо масштабном участке спектра выделяются три интервала:

мезо-**α** (200-2000 км): фронты и тропические циклоны:
мезо-β (20-200 км): низкоуровенные струйные течения, линии шквалов, внутренние волны, скопления конвективных облаков, орографические возмущения:
мезо-γ (2-20 км): грозы, внутренние гравитационные волны, городские эффекты.

Нетрудно заметить, что определенный таким образом диапазон мезомасштабных движений является весьма широким и практически сложно реализовать модель, которая разрешала бы одновременно движения, горизонтальный масштаб которых отличается на два порядка. Представляется, что на первом этапе мезомасштабные прогностические модели будут ориентироваться в основном на воспроизведение атмосферных возмущений масштабов мезо-α и мезо-β, хотя в принципе не исключен подход с иерархией вложенных друг в друга моделей с непосредственным разрешением масштаба мезо-γ в районах, подозрительных на развитие грозовой деятельности.

На вопросе выбора исходных уравнений для мезо масштабных прогностических моделей я остановлюсь подробнее позднее. Здесь лишь отмечу, что появившиеся в последнее время прогностически ориентированные модели отражают две основные тенденции.

Первая из них состоит в том, что при формулировке задачи численного мезо масштабного прогноза используются гидростатические модели, применяющиеся в задачах регионального и глобального прогноза. При этом усовершенствуются алгоритмы параметризации подсеточных процессов и вводится повышенное разрешение по горизонтали и вертикали, особенно в пограничном слое атмосферы. Перечень такого рода гидростатических моделей с горизонтальным шагом сетки менее 50 км, заимствованный из обзора Вмо (1987), приведен в табл. 1.

Вторая тенденция состоит в построении мезо масштабных прогностических схем на основе опыта работы с негидростатическими моделями, предназначенными для изучения отдельных мезо масштабных циркуляций в атмосфере. Список такого рода схем, заимствованный из обзора Вмо (1987), дается в табл. 2. В эту таблицу включены как полностью прогностически ориентированные негидростатические модели, так и некоторые исследовательские модели, которые по своему физическому содержанию весьма близки к прогностическим.

Естественно, что при постановке задачи численного мезо масштабного прогноза возникает ВОПРОС - можно ли детерминированными методами прогнозировать мезо масштабные циркуляции с достаточной степенью заблаговременности, иди какова предсказуемость мезо масштабных явлений. Этот вопрос является важным для численного мезо масштабного прогнозирования, поскольку

мы никогда не знаем точного начального состояния атмосферы. Если окажется, что при весьма близких начальных состояниях через небольшой промежуток времени вследствие имевшихся незначительных отличий в начальный момент развиваются сильно отличающиеся системы движений, то мезо масштабный прогноз является безнадежным. Если же зависимость развивающихся со временем циркуляций не очень чувствительна к начальному состоянию атмосферы, то при их краткосрочном прогнозировании можно надеяться на определенный успех.

Вопрос о предсказуемости мезомасштабных движений в настоящее время еще недостаточно разработан, и по этому поводу существуют как пессимистические, так и оптимические точки зрения, которые вытекают в основном из методов применявшегося анализа (Антее и др., 1985).

Так, например, на основе анализа спектра атмосферных движений с позиций однородной турбулентности получается вывод о том, что в мезомасштабе происходит быстрый перенос энергии от меньших к большим длинам волн, поэтому неизбежные ошибки и неопределенности в движениях малого масштаба будут распространяться в движения большего масштаба и сокращать предсказуемость. Таким образом, с позиций однородной турбулентности прогнозирование мезомасштабных движений представляется весьма безнадежным.

Против такого рода выводов можно выдвинуть, однако, ряд контраргументов. во-первых, наблюдаемые атмосферные спектры представляют статистическое описание структуры атмосферы и включают осреднение по пространству и времени, в то время как атмосферные структуры, когда они образуются, являются хорошо организованными и не являются такими случайными, как трехмерная турбулентность инерциального диапазона. Наиболее ярким примером такой структуры мезо-**α** может служить тропический циклон, движения в котором являются турбулентными, а сама вихревая структура иногда существует в течение нескольких недель. Фронты в подвижных циклонах, линии шквалов также могут существовать в течение нескольких дней, хотя отдельные элементы их строения претерпевают существенные изменения на Солее коротких временных масштабах. То же самое можно сказать об интенсивных вращающихся грозовых облаках в потоке со сдвигом, мезомасштабных конвективных комплексах, которые имеют жизненный цикл и предсказуемость намного большую, чем можно было бы ожидать, исходя из теории турбулентности. Лилли (1984) предполагает, что причиной такого увеличения предсказуемости

является спиральность, представляющая собой скалярное произведение ВИХРЯ и скорости. моделирование трехмерной турбулентности (Андре и лесюр, 1977) указывает на то, что потоки, обладающие большими значениями спиральности, противостоят турбулентному разрушению.

ВТОРЫМ важным Фактором, влияющим на повеление многих мезомасштабных систем, является возмущающее воздействие подстилающей поверхности. Термические и механические неоднородности генерируют многие мезомасштабные системы (бризы, орографические циркуляции, конвекцию).

Исходя из генезиса мезомасштабных явлений, большинство авторов подразделяют их на три основные группы:

системы, возникающие пол действием термической и механической неоднородности подстилающей поверхности (бризовые циркуляции, горно-долинные ветры, горные волны, вихри с подветренной стороны препятствий);

системы, возникающие под действием мезомасштабных неоднородностей крупномасштабного потока (атмосферные ФРОНТЫ, ЛИНИИ шквалов (линии неустойчивости), мезомасштабные конвективные комплексы);

системы, возникающие в свободной атмосфере в результате разрешения мезомасштабной неустойчивости в горизонтально ОДНОРОДНОМ воздушном потоке (гравитационные волны, системы мелкой и глубокой конвекции).

Отличительная особенность систем первой группы состоит в том, что будучи локально возбужденными, они развиваются также локализованно и поведение их наиболее предсказуемо, так как возбуждающие силы являются или постоянными (механическое возбуждение), или имеет суточный цикл (термическое возбуждение).

Наиболее сложной с точки зрения прогнозирования является ситуация, когда турбулентность развивается в однородном по горизонтали крупномасштабном потоке. Примером такой почти ОДНОРОДНОЙ турбулентности может служить внутримассовая конвекция, когда хотя и можно предсказать уровень

конвекции, но точно предсказать местоположение каждого конвективного элемента с достаточной заблаговременностью вряд ли окажется возможным.

исходя из сказанного выше и существующего опыта, можно констатировать, что наиболее простыми для численного прогнозирования являются мезомасштабные орографические циркуляции. Большую сложность представляет прогнозирование мезомасштабных систем, локализованных в пространстве неоднородностью крупномасштабного потока (фронты, линии шквалов, мезомасштабные конвективные комплексы). Наименее перспективным является, по-видимому, прогнозирование мезомасштабных систем, развивающихся в однородном по горизонтали крупномасштабном потоке (отдельных кучево-дождевых облаков и внутренних гравитационных волн).

К счастью, большинство мезомасштабных систем не относится к последнему типу (почти однородной турбулентности), поэтому их краткосрочное прогнозирование имеет определенную перспективу.

Выше уже отмечалось, что в мезомасштабных прогностических моделях используются как гидростатические, так и негидростатические модели. Вопросам использования различных исходных систем уравнений для мезомасштабного моделирования посвящено достаточно много работ. Они базируются, как правило, на масштабном анализе исходных уравнений, и получающиеся выводы в определенной мере зависят от выбранного подхода к масштабированию и отличаются в деталях. Не останавливаясь на подробностях, укажем, что при использовании в качестве основных масштабов масштаба длины в векторном варианте (L_x, L_y, L_z) и масштаба времени ($_t$) нетрудно получить (при L_x = $L_x = L_r$), что $\omega/\nu = L_z/L_r$, где со- вертикальная скорость, L_r - горизонтальный масштаб движений, а ν_r - один из горизонтальных компонентов СКОРОСТИ. Применение оператора индивидуальной производной к компонентам скорости не изменяет выписанного выше соотношения между вертикальным и горизонтальным компонентом СКОРОСТИ, поэтому отношение ускорений вертикальной и горизонтальной скорости также оказывается пропорциальным отношению масштабов движений вдоль этих координат. Отсюда вытекает, что для систем, горизонтальные и вертикальные размеры КОТОРЫХ одинаковы, вертикальные ускорения имеют тотже порядок, что и горизонтальные, и пренебрегать ими нельзя. По мере увеличения неизотропности в горизонтальной и вертикальной плоскости (например, $L_r \gg L_z$) относительный вклад вертикальных ускорений убывает. Таким образом, пои моделировании атмосферных циркуляций,

горизонтальные и вертикальные масштабы которых соизмеримы, несомненным преимуществом облапают негидростатические уравнения, а при моделировании атмосферных циркуляций, горизонтальные размеры КОТОРЫХ немного превышают вертикальные, приближение гидростатики является вполне оправданным. Указать конкретное соотношение L_z/L_r, при КОТОРОМ целесообразно переходить от гидростатических систем к негидростатическим, довольно сложно. Если иметь в виду возмущения, развивающиеся во всей толще тропосферы, такой переход целесообразен, по видимому, при желании адекватного моделирования систем масштабов мезо-β и мезо-γ. Системы масштаба мезо-**α** могут быть воспроизведены достаточно успешно и гидростатической системой. В целом для моделирования мезомасштабных циркуляций более перспективными являются негидростатические уравнения, поэтому можно предположить, что их удельный вес среди мезомасштабных прогностических схем будет постепенно расти.

Негидростатические системы уравнений можно подразделить на две группы: (1) полные, эластичные уравнения, в которых уравнение сохранения массы остается в своем полном виде с сохранением локальной ПРОИЗВОДНОЙ ОТ плотности ($\boldsymbol{\delta}p/\boldsymbol{\delta}t=0$), и (2) неэластичные уравнения, в КОТОРЫХ локальные изменения плотности считаются малыми и не учитываются ($\boldsymbol{\delta}p/\boldsymbol{\delta}t=0$).

Неэластичные уравнения фильтруют акустические волны, включая волны лэмба, чего не делают гидростатические уравнения. Это приближение ПРИВОДИТ также к нарушению (в пределах 20%) фазовой СКОРОСТИ внутренних гравитационных волн (увеличивает ее при сильно устойчивой стратификации и уменьшает ПРИ малой неустойчивости). Нарушение увеличивается с РОСТОМ горизонтальной длины волны и в меньшей степени с РОСТОМ длины волны по вертикали (Кадышников, 1984).

Преимущество неэластичных уравнений состоит в том, что из-за отсутствия быстрых волн представляется возможным использовать достаточно большие шаги по времени ПРИ численном решении эволюционных уравнений. Недостаток этих уравнений состоит в том, что для отыскания в них давления требуется решать диагностическое уравнение эллиптического типа. Для этого можно использовать итерационные процедуры, быстрое преобразование Фурье или прямые методы решения. В прогностической модели желательно пользоваться последним подходом с тем, чтобы время расчета прогноза сохранялось одинаковым. Он оказывается, однако, чувствительным к характеристикам аппроксимаций: неоднородности расчетной сетки, использованию конечно-разностных аппроксимаций более высокого порядка и т.д. Ситуация

усложняется, если в задаче прогноза учитывается орография. В этом случае увеличивается число итераций при решении уравнения для давления, и эффективность вычислительного алгоритма быстро падает с ростом КРУТИЗНЫ рельефа. Поэтому неэластичные системы являются достаточно эффективными лишь в районах, где орография не играет существенной роли, из этих соображений неэластичные уравнения были использованы для мезомасштабной модели Гидрометцентра СССР (Вельтишев и др., 1982, Кисельников и др., 1984), предназначенной для прогнозирования погоды над центром Европейской части СССР, где рельеф не играет существенной роли.

В связи с тем, что при численной реализации неэластичных уравнений, особенно в условиях крутого рельефа, возникают определенные трудности, с середины 70-х годов для моделирования мезомасштабных процессов начали применяться полные уравнения, в КОТОРЫХ отсутствуют и акустические волны. В полной системе эволюционные уравнения имеются для всех переменных, поэтому включение дополнительных физических факторов и численных модификаций не вызывает принципиальных трудностей. Естественно, что одновременно возникают сложности вычислительного характера, связанные с наличием в системе быстрых волн.

исторически первая мезомасштабная модель, основанная на полных уравнениях, была развита в метеорологической службе Великобритании (Тапп и Уайт, 1976). Позднее полные уравнения использовались РЯДОМ авторов в моделях конвекции и осесимметричного циклона. В настоящее время мезомасштабная прогностическая модель, базирующаяся на полных уравнениях, функционирует оперативно в метеорологической службе Великобритании (Голдинг, 1984, 1987).

Таким образом, в прогностических целях в настоящее время используются как гидростатические, так и негидростатические (эластичные и неэластичные) мезомасштаоные модели.

Ниже я останавлюсь на некоторых результатах, полученных с помощью моделей разного типа. При изложении результатов по гидростатическим моделям основное внимание будет уделено экспериментам или оперативной работе с моделями, горизонтальный шаг в КОТОРЫХ не превышал 50 км, т.е. позволял воспроизводить по крайней мере возмущения масштаба мезо-α.

Гидростатические прогностические мезомасштабные модели составляют в настоящее время подавляющее большинство. Часть из них используется, в основном, для научных исследований (см., например, Каплан и др., 1982, Орланский и Полинский, 1984, Ниномия, 1985, Калб, 1985, Сашеги, 1987, Каплан и др., 1987, Чу и др., 1987, модика, 1987, Стауффер и Симен, 1987), а некоторыое внедрены в оперативную практику (Жуванон Дю Наша и др., 1987, Гронас и др., 1987).

На основании численных экспериментов, проведенных с такого рода моделями, имеющими разрешение лучше 50 км, получены следующие основные выводы. Увеличение пространственного разрешения моделей до 30-50 км, даже при сохранении их физического содержания, как у моделей с шагом ~ 150 км, приводит к повышению качества прогноза. прежде всего это относится к прогнозированию интенсивных циклонических возмущений. Хотя модели пока что не воспроизводят наблюдаемой экстремальной глубины таких циклонов, однако дают заметно лучшие результаты, чем более грубые модели. Повышение пространственного разрешения приводит также к улучшению прогноза осадков: предсказанные зоны осадков становятся более узкими, увеличивается интенсивность осадков, что приближает их к наблюдаемым.

в области параметризаций наибольшее внимание уделялось параметризации конвекции. Были получены выводы о том, что параметрический учет конвекции заметно улучшает качество прогноза. Зто относится как к прогнозированию интенсивности циклонических возмущений, так и к ПРОГНОЗУ осадков.

Эксперименты по влиянию качества исходных данных на мезомасштабный прогноз (см., например, Дюран и жуванон дю ваша, 1983, Кало, 1985, Такано и Сегами, 1986, Голдинг, 198/, Диак и миллс, 198/) показывают, что наличие в начальном поле мезомасштабного возмущения в значительной мере влияет на успешность краткосрочного численного прогноза. В цитированных выше работах было показано, что использование дистанционных измерений температуры и влажности со спутников, спутниковых данных о ветре, данных о ветре, полученных с помощью профилемеров, а также наземных наблюдений за облачностью на стадии анализа исходных полей лает ощутимое повышение качества прогнозов.

Наиболее полная статистика по успешности прогнозов погоды с помощью мезомасштабной гидростатической модели имеется в Метеорологической службе Франции, где численная прогностическая схема ПЕРИДОТ функционирует оперативно с 1 января. 1985 года, а ежемесячная статистика качества прогнозов аккумулируется с июня 1985 года (см. Жуванон Дю Ваша и др., 1986, 1987, Имбард и др., 1986). Эта модель имеет горизонтальное разрешение 35 км, нижний ее уровень находится на высоте 20 м. Ниже я приведу несколько основных выводов о качестве прогнозирования элементов погоды у поверхности земли с помощью этой модели, которые заимствованы, в основном, из последней публикации Жуванона Дю Ваша и др. (1987). Статистика основана на 300 днях 1986 года по 120 станциям на территории Франции. В части прогнозирования температуры на уровне будки получено, что среднеквадратическая ошибка при прогнозе на 36 ч не превышает 3°С, а средняя абсолютная ошибка - 2°С. Смещение прогноза температуры практически отсутствует. Здесь необходимо отметить, что при сравнении прогностических значений температуры в узлах сетки с данными наблюдений на станциях в дисперсию и среднюю абсолютную ошибку неизбежно входит сигнал, появляющийся вследствие неоднородности поля температуры в пределах шага сетки (35 км). Такие неоднородности могут быть вызваны различиями микрорельефа, мелкомасштабной неоднородностью облачности и другими эффектами подсеточного масштаба. Изучение изменчивости поля приземной температуры по трем станциям в районе Парижа показало, что 80 процентов ошибки прогноза температуры объясняется такими вариациями.

В прогнозах влажности, нижней облачности и скорости ветра присутствует пока что смещенность. Направление ветра предсказывается достаточно хорошо, и смещенность отсутствует. Мелкомасштабная изменчивость поля влажности и скорости ветра объясняют 80 процентов и почти 100 процентов ошибки, соответственно.

Сопоставление прогнозов по модели ПЕРИДОТ и по крупномасштабной модели ЕМЕРОД показало, что использование мезомасштабной модели дает выигрыш при прогнозе молей давления, температуры и скорости ветра у поверхности земли. Для температуры, например, среднеквадратическая ошибка убывает на 0,5°С, уменьшается также и смещенность.

Сравнение прогнозов минимальной температуры по модели ПЕРИДОТ со статистическим прогнозом, базирующимся на модели ЕМЕРОД, обнаружило их примерно одинаковое качество.

Наиболее полная статистика по успешности прогнозов с помощью негидростатической мезомасштабной модели имеется в Метеорологической службе Великобритании, где такая модель функционирует в оперативном режиме с осени 1984 года (Голдинг, 1984, Голдин и Махин, 1984, Голдин, 1986, Голдинг, 1987). Эта модель имеет горизонтальное разрешение 15 км, а нижний прогностический уровень находится на высоте 10 м. Ниже будут приведены основные выводы относительно успешности прогноза наземных полей некоторых метеорологических элементов, полученные в результате сравнения прогнозов с данными наблюдений на синоптических станциях Великобритании.

Прогноз температуры имеет в целом высокое качество, за исключением тех случаев, когда имеется серьезная ошибка в прогнозе облачности, особенно в ночные часы. В таблице 3 показан процент различных ошибок прогноза максимальных/минимальных температур осенью 1985 года. С наблюдениями на станциях сравнивались расчеты во всех узлах сетки, в том числе и находящихся над морем. Получено, что большая часть крупных ошибок максимальной температуры (более 4°С) связана с различиями топографии. Более детальные оценки прогноза температуры в январе 1986 года на отдельных станциях в сравнении с субъективными прогнозами приведены в таблице 4. Сравнения численного и синоптического прогнозов показали, что модель дает лучшие результаты, если рассматривать процент ошибок 2°С. Процент больших ошибок в модели больше, чем у синоптиков. Здесь следует заметить, что прогнозист выпускал прогноз через 5 ч после выпуска численного прогноза.

Оценка прогноза влажности показала, что прогнозируемые значения относительной влажности систематически (в среднем на 5 процентов) превышает фактические значения. Это хуже результатов, получаемых по региональной модели, однако число крупных ошибок по мезомасштабной модели оказалось меньшим. Смещенность прогнозов влажности определенно связана со смещенностью прогноза нижней границы облаков.

Оценки прогноза ветра на 12 ч в декабре 1985 года показали, что среднеквадратические ошибки скорости ветра не превышают 2,5 м/с. Качество прогноза ветра по мезомасштабной модели лучше, чем по региональной. Наиболее плохо мезомасштабной моделью предсказываются слабые ветры (< 2 м/с).

Весьма сложной оказалась задача прогнозирования нижней границы облачности. В целом в модели нижняя граница облачности получается систематически ниже, чем наблюдаемая. При наиболее часто наблюдаемой высоте нижней границы облаков 600 м в январе 1986 года, прогностические значения получаются чаще всего на высотах ниже 180 м. Тенденция изменения высоты нижней границы облаков предсказывается моделью удовлетворительно.

В целом области осадков по мезомасштабной модели совпадают с областями осадков по региональной модели. Однако мезомасштабная модель гораздо лучше воспроизводит орографическое усиление осадков.

Сравнение фактических и спрогнозированных сумм осадков за 12 ч в декабре 1985 года показало, что зоны осадков, спрогнозированные по мезомасштабной модели, хорошо совпадают с наблюдаемыми, в то время как региональная модель почти вдвое недооценивает количество осадков в западном холмистом районе. Основной недостаток в прогнозе осадков состоит в том, что малое количество осадков прогнозируется слишком часто.

Резюмируя статистику качества мезомасштабных моделей, накопленную к настоящему времени, можно сделать следующие основные выводы.

Мезомасштабные модели дают возможность лучше воспроизвести внутреннюю динамику объектов синоптического масштаба, а также орографические эффекты. Наибольший эффект от их использования получается при прогнозировании метеорологических элементов, имеющих большую пространственную изменчивость: облачности и осадков. Но качеству прогнозирования температуры и ветра мезомасштабные модели приближаются к качеству прогноза синоптическими методами. Таким образом, они обладают высоким потенциалом для прогнозирования элементов погоды на ограниченной территории, и развитие мезомасштабных моделей представляет, по-видимому, магистральное направление, по которому будет происходить улучшение качества прогноза с заблаговременностью от 6 до 36 ч.

На этом пути существует, однако, ряд проблем, которые будет необходимо решить в процессе разработки и совершенствования систем мезомасштабного прогнозирования.

Первая из них состоит в подготовке начальных полей. В настоящее время сеть радиозондирования, даже в районах с наиболее густой сетью

станций, совершенно недостаточна для получения сведений о мезомасштабных возмущениях в свободной атмосфере. Привлечение к анализу спутниковых данных о температуре и влажности, особенно последних, несколько улучшает качество исходного анализа, однако не изменяет его радикально. В перспективе можно надеяться на повышение плотности ветрового зондирования путем создания сети профилемеров, однако в ближайшее время нужно, по-видимому, ориентироваться на более полное использование уже существующей информации. Из доступных средств наблюдений мезомасштабный сигнал дают в настоящее время спутниковые и радиолокационные системы, поэтому в ближайшей перспективе необходимо более полно усваивать эти типы данных в процедурах мезомасштабного анализа и инициализации. Помимо непосредственной информации о трехмерном распределении облачности и осадков (с дополнительным привлечением наземных наблюдений), эти виды наблюдений посредством процедур динамической инициализации позволят распространить мезомасштабный сигнал из термодинамических характеристик в динамические и тем самым повысить качество исходного анализа всех полей. Эксперименты в этой области уже начинаются. При более детальном описании процессов тепло- и влагообмена между атмосферой и подстилающей поверхностью в мезомасштабных моделях ощущается серьезная нехватка в исходной информации о состоянии деятельного слоя почвы, его температуре и влажности. Число таких измерений намного меньше, чем измерений в атмосфере, а производятся они, особенно в части влажности почвы, гораздо реже, чем это требуется для задачи краткосрочного прогноза. Интегральные характеристики влажности могут быть получены, в принципе, методами дистанционных измерений со спутников, но оперативное получение профилей влажности будет представлять в обозримом будущем определенную проблему.

Вторая проблема, которую теоретически невозможно преодолеть и которая свойственна всем моделям на ограниченной территории, состоит в том, что мы никогда не имеем информации о проникновении мезомасштабного возмущения, возникшего за пределами области расчетов, на территорию, по которой дается прогноз. Эта трудность носит принципиальный характер и решить ее частично можно лишь расширением области прогноза, для чего понадобится существенное расширение ресурсов на ЭВМ. Проблему задания "нефизических" условий на боковых границах, минимально искажающих решение внутри области, также нельзя считать полностью решенной.

Третья проблема состоит в совершенствовании процедур параметризации подсеточных процессов. Применение процедур параметризации конвекции,

особенно в негидростатических моделях, не представляется, например, столь очевидным, как в крупномасштабных моделях, поскольку горизонтальные масштабы глубокой конвекции оказываются соизмеримыми с масштабом вычислительной сетки. Этот вопрос нуждается в дальнейшем изучении и проведении численных экспериментов и тестов.

Заслуживает дальнейшей проработки вопрос создания сбалансированных процедур параметризации мелкомасштабной турбулентности и радиационных притоков тепла, особенно в условиях образования облачности, поскольку оба этих процесса особенно трудно моделировать на границах с резким изменением оптических свойств среды (поверхности земли, верхней границе облаков), где обычно создаются узкие зоны больших градиентов метеорологических элементов, требующие повышенного разрешения вычислительной сетки по вертикали.

В части процедур параметризации микрофизических процессов в облаках в настоящее время имеется достаточно широкий выбор, однако необходимо более полное тестирование предложенных методик в рамках прогностических моделей.

С точки зрения вычислений в мезомасштабных моделях ощущается особенно большая необходимость в вычислительных алгоритмах, сохраняющих узкие области больших градиентов переменных (фронтальные зоны). Определенный опыт использования такого рода вычислительных схем имеется в задачах моделирования ударных волн и других задачах гидродинамики. Этот опыт необходимо, по-видимому, адаптировать к задачам мезомасштабного численного прогноза.

*

* *

Таблица Т

Гидростатические мезомасштабные модели

модель, источник	система ур-ний, вертикальная координата	шаг по горизонтали (км)	число уровней	шаг по времени (с)	орография	параметризация физических процессов			
						атмосферная влага	конвекция	радиация	турбулентность
1	2	3	4	5	6	7	8	9	10
Будра (1981)	полные уравнения z	40	15	50	нет	критерий насыщения ПРИ 100%, осадки определяются диагностически	есть, Байер и ДР. (1976)	нет	$K(R)$
МАСС-3 Каплан и ДР. (1982)	полные уравнения σ	47,6	14	51	есть	критерий насыщения при 95%, осадки определяются диагностически	модификация метола Фритша и Чэппела (1980)	есть у поверхности земли	фильтр
ПЕРИДОТ Жуванон Дю Ваша и др. (1983)	полные уравнения σ	35	15	240	есть	облака, осадки по Кесслеру (1969)	Желен и др. (1982)	есть в атмосфере и на поверхности земли	к формулировке Прандтля при устойчивой стратификации, $K=100$ см^2/с при неустойчивой стратификации

(ПРОДОЛЖ.)

модель, источник	Система ур-ний, вертикальная координата	Шаг по горизонтали (км)	Число уровней	Шаг по времени (с)	Орография	Параметризация Физических процессов: атмосферная влага	конвекция	радиация	турбулентность
1	2	3	4	5	6	7	8	9	10
Орланский Полинский (1984)	неэластичные уравнения z	50	17	-	есть	критерий насыщения при 95%, осадки определяются диагностически	рассчитывается явно	нет	$K(R)$
ЛАМПС Калб (1985)	полные уравне- σ	35	15	40	есть	критерий насыщения пои 100%, осадки по Кесслеру (1969)	метол Крайцберга и Перки (1976)	неявно у поверхности земли	$K\square_4$ ПО Г0РИЗ0Н- тали, $L\square_2$ по вертикали
метеорологическое агентство Японии, Ниномия (1985)	полные уравнения σ	42	13	-	есть	критерий насыщения при 100%, облака и осадки определяются диагностически	влажное конвективное приспособление	есть у поверхности земли	модель замыкания Дуровня 2

(продолж.)

модель, источник	Система ур-ний, вертикальная координата	Шаг по горизонтали (км)	Число уровней	Шаг по времени (с)	Орография	Параметризация физических процессов			
						атмосферная влага	конвекция	радиация	турбулентность
1	2	3	4	5	6	7	8	9	10
Норвежский метеорологический институт Вмо тд № 79 (1985)	полные уравнения σ	50 (10)	11 (20)	-	есть	крупномасштабная конденсация, осадки определяются диагностически	типа Куо (1965) или влажное конвективное приспособление	есть в атмосфере и у поверхности земли	К-теория
Курихара и др. (1986)	полные уравне- σ	25	13		есть		конвективное приспособление	есть у поверхности земли	модель замыкания уровня 2, мэллор и Ямала (1974)

Таблица 2

Трехмерные негидростатические модели

модель, источник	Система ур-ний, вертикальная координата	Шаг по горизонтали (км) 1)	Шаг по вертикали	Число уровней	Шаг по времени (с)	Орография	Параметризация физических процессов			
							атмосферная влага	конвекция	радиация	турбулентность
1	2	3	4	5	6	7	8	9	10	11
Пастушков, 1970а,в. 1973, 1975	неуругая 2) Z	1	1 км	11	20	нет	облака: осадки опрелеляются лиагностически	рассчитывается явно	нет	упрошенный вариант нелинейной турбулентной вязкости (НТВ)
ДИРДОРФ, 1972а: Соммерия, 1976; Редельспергер и Соммерия, 1981, 1982 а,в 3	неупругая Z	1	0,4 км	25	10:20	нет	облака: вероятностная модель распределения влаги в расчетной ячейке (ДирдорФ, 1976а: Соммерия и ДирдОРФ, 1977)	рассчитывается явно	есть только в атмосфере	уточненная НТВ (с учетом стратификации тепла и влаги) с прогностическим уравнением для $
Штайнер, 1973: Яу, 1980; Терпайнен и Яу и МИШО, 1982: Теопайнен, 1982	неупругая Z	0,5	0,3 км	16	20	нет	облака: осадки по Кесслеру	рассчитывается явно	нет	НТВ с упрошенным учетом стратификации тепла

(ПРОДОЛЖ.)

модель, источник	Система ур-ний, вертикальная координата	Шаг по горизонтали (км) 1)	Шаг по вертикали	Число уровней	Шаг по времени (с)	Орография	Параметризация физических процессов			
							атмосферная влага	конвекция	радиация	турбулентность
	2	3	4	5	6	7	8	9	10	11
миллер и Пирс, 1974; монкрифф и миллер, 1978: Беннет и Рауллинс, 1981; Беннет и Бэйдер, 1982	неупругая P	1	50 мб	19	15	нет	облака: осадки по Кесслеру, 1969: Лиу и Орвиллу, 1969	рассчитывается явно	нет	диффузия с постоянным коэффициентом: преимущественно для КОНТРОЛЯ устойчивости
Шлезингер. 1975, 1978, 1980, 1982, 1984а,в	неупругая z	1,8	0,7 км	20	50	нет	облака; осадки по Такеда, 1966	рассчитывается явно	нет	НТВ
Тэпп и Уайт 1976; Карпентер , 1979; Голдинг, 1984, 1986; Голдинг и мэхин, 1984	полная 4) ζ	15	переменный, 0,1 км $<\Delta z<$ 1,5 км; нижний уровень 10 м	16	60	есть	облака; осадки по Сандквисту, 1978	параметризация по Фритшу и чеппелю, 1980	есть только у земли	одномерная, с прогностическим уравнением для Е

(ПРОДОЛЖ.)

модель, источник	Система ур-ний, вертикальная координата	Шаг по горизонтали (км) 1)	шаг по вертикали	Число уровней	Шаг по времени (с)	Орография	параметризация физических процессов			
							атмосферная влага	конвекция	радиация	турбулентность
1	2	3	4	5	6	7	8	9	10	11
Липс, 1977; Липс и хемлер, 1982	неупругая Z	0,375	0,25 Км	40	5:10	нет	облака; осадки по Кесслеру, 1969	рассчитывается явно	нет	уточненная НТВ, с учетом стратификации тепла и влаги
Кларк, 1977 1979; хо и Кларк, 1981 Кларк и Гэлл, 1982; Пелтайр и Кларк, 1983	неупругая 5) ζ	1	0,3 км	35	20	есть	облака: осадки по Кесслеру, 1969	рассчитывается явно	нет	нТв с упрощенным учетом стратификации тепла и влаги
Клемп и Вильхельмсон, 1978а, в; Клемп и ДР., 1981; Вильхельмсон и Чен, 1982	полная Z	1	переменный, 0,1 км $<\Delta Z<$ 0,9 км; нижний расчетный уровень 40 м	25	10	нет	облака; осадки по Кесслеру, 1969	рассчитывается явно	нет	НТВ с прогностическим уравнением для Е

(ПРОДОЛЖ.)

модель, источник	Система ур-ний, вертикальная координата	шаг по горизонтали (км) 1)	шаг по вертикали	ЧИСЛО уровней	Шаг по времени (С)	Орография	Параметризация Физических процессов			
							атмосферная влага	конвекция	радиация	турбулентность
1	2	3	4	5	6	7	8	9	10	11
Коттон и Триполи, 1978; Юи-поли и коттон, 1980, 1982, 1986; КОТТОН и ДР., 1982	полная 0,5 5) ζ	0,5	0,5 КМ	3/	5	есть	облака; осадки в жидкой и твердой фазах	рассчитывается явно	нет	НТВ с упрощенным учетом стратификации тепла и влаги
Вельтишев и ло., 1982; Кисельникова и ДР., 1984; Прессман, 1984	неупругая Z	10	переменный, 2 м <ΔZ< <800 м НИЖНИЙ расчетный уровень 2 м	15	200	нет	облака; осадки по Кесслеру, 1969	рассчитывается явно	есть в атмосфере и у земли	нТв с упрощенным учетом стратификации тепла и влаги

(ПРОДОЛЖ.)

модель, ИСТОЧНИК	Система ур-ний, вертикальная координата	шаг по горизонтали (км) 1)	Шаг по вертикали	Число уровней	шаг по времени (с)	орография	Параметризация физических процессов: атмосферная влага	конвекция	радиация	турбулентность
1	2	3	4	5	6	7	8	9	10	11
Алоян, 1984; Пененко и АЛОЯН, 1	неупругая 5)	1	переменный, 0,1 км <ΔZ< U,3 км; нижний расчетный уровень 1UU м	2U	180	есть	облака; осадки определяются диагностически	рассчитывается явно	нет	НТВ с упрощенным учетом стратификации тепла

1) Выбор шагов сетки по пространственным и временной координатам и число уровней варьируют в пределах каждой модели от эксперимента к эксперименту и от публикации к публикации, иногда значительно, мы ПРИВОДИМ некоторые характерные показатели.

2) Гермины "неупругая" и "полная" системы уравнений разъясняются в 1.2, 1.3.

публикации по этой и последующим моделям даются лишь выборочно.

4) $\zeta = Z - \Gamma$

5) $\zeta = (Z - \Gamma)\, H / (H - \Gamma)$

6) Авторы приводят алгоритм расчета также и для варианта с полными уравнениями, однако образцы и параметры расчетов в этом варианте нам неизвестны.

Таблица 3

Процент ошибок максимальной и минимальной температуры по месяцам с августа 1985 г. по январь 1986 г.

	максимальная температура			минимальная температура		
	10	20	40	10	20	40
август	45	77	98	47	79	98
сентябрь	45	75	97	44	73	94
октябрь	53	82	98	40	68	93
нояорь	53	85	98	38	63	88
декабрь	58	85	97	43	70	93
январь	58	88	99	45	74	95

Таблица 4

Процент ошибок по модели (МЕЗ) и прогнозиста (ПР) в 6 пунктах в январе 1986 г.

	ошибка в °С	Саутгемп-тон		ЛВС		Уогнол		Манчестер		Нью-Кастл		Глазго	
		ПР	МЕЗ	ПР	МЕЗ	ПР	МЕЗ	ПР	МЕЗ	ПР	МЕЗ	ПР	МЕЗ
15 Гр	1	68	83	83	76	91	73	67	80	77	70	80	70
	2	96	100	90	97	100	97	97	93	93	90	100	93
	3	100		97	100		100	100	100	93	97		100
	4			100						100	100		
17 Гр	1	74	70	77	68	83	83	74	84	77	77	68	65
	2	96	89	97	94	92	92	97	94	87	94	81	90
	3	96	96	100	100	96	100	100	100	97	100	97	100
	4	100	100			100				100		97	
	5									100		100	
09 Гр	1	67	67			71	52	57	69	64	71	61	79
	2	96	92			95	81	82	85	79	86	82	89
	3	100	100			95	95	100	96	89	89	96	93
	4					100	100		100	100	96	100	96
	5										100		100

ЛИТЕРАТУРА

Вельтищев Н.Ф. и др., 1982: Мезомасштаоный прогноз погоды. - метеорология и гидрология, № 4, с. 5-15.

Кадышников В.М., 1984: Фильтрующая роль уравнений глубокой конвекции в модели политропной атмосферы. - Метеорология и гидрология, № 1, с. 11-19.

André, J.C. and M. Le Sieur, 1977: Influence of helicity on the evolution of isotropic disturbance at high Reynolds number. Jour. Fluid Mech., 81, 187-207.

Anthes, R.A. et al., 1985: Predictability of mesoscale atmospheric motions. Advances in Geophys., 28B, 159-202.

Atkinson, R.W. 1981: Mesoscale atmospheric circulations. Academic Press, 495 pp.

Diak, G.R. and G.A. Mills, 1987: Methods of incorporating satellite data into mesoscale numerical forecast models. Proc. Int. Symp. on Mesoscale Analysis and Forecasting, Vancouver, Canada, 17-19 August 1987, 579-588.

Durand, Y. and R. Juvanon du Vachat, 1983: Mesoscale analysis using satellite information. Tech. Proc. First Int. TOVS Study Conference, 80-93.

Golding, B.W., 1984: The Meteorological Office mesoscale model: its curent status. Meteor. Mag., 113, 288-302.

Golding, B.W., 1986: The Meteorological Office mesoscale model: an overview. Version 1. February 1986. Met. 011 Mesoscale Documentation Paper, 12, 16 pp.

Golding, B.W., 1987(a): Strategies for using mesoscale data in an operational mesoscale model. Proc. Int. Symp. on Mesoscale Analysis and Forecasting, Vancouver, Canada, 17-19 August 1987, 569-578.

Golding, B.W., 1987(b): The Meteorological Office mesoscale model: an overview. Version 6. November 1987. Met. 011 Mesoscale Documentation Paper, 12, 35 pp.

Golding, B.W. and N.A. Machin, 1984: The United Kingdom Meteorological Office mesoscale forecasting system. Proc. Second Int. Symp. on Nowcasting, Norrköping, Sweden, 3-7 September 1984, 309-314.

Gronas, S. et al., 1987: The Norwegian mesoscale NWP system. Proc. Int. Symp. on Mesoscale Analysis and Forecasting, Vancouver, Canada, 17-19 August 1987, 481-486.

Imbard, M. et al., 1986: Experiments and results with PERIDOT in French limited-area model. Extended abstracts WMO/IUGG Int. Symp. Short-and Medium-range NWP, Tokyo, 4-8 August 1986.

Juvanon du Vachat et al., 1986: The PERIDOT fine-mesh numerical weather prediction system. Description and evaluation. Ibid.

Juvanon du Vachat et al., 1987: Evaluation of a mesoscale prediction system with surface weather observations and comparison with a large-scale prediction system. Proc. Int. Symp. on Mesoscale Analysis and Forecasting, Vancouver, Canada, 17-19 August 1987, 475-480.

Kalb, M.W., 1985: Results from limited area mesoscale numerical simulation for 10 April 1979. Monthly Weather Review, 113, 1644-1662.

Kaplan, M.L. et al., 1982: Initial results from mesoscale atmospheric simulation system and comparisons with AVE-SESAME 1 data set. Monthly Weather Review, 110, 1564-1590.

Kaplan, M.L. et al., 1987: A numerical simulation of meso-beta-scale mid-tropospheric frontogenesis resulting from the interaction between a jet streak and mountain range. Proc. Int. Symp. On Mesoscale Analysis and Forecasting, Vancouver, Canada, 17-19 August 1987, 501-502.

Kiselnikova, V.S. et al., 1984: Application of mesoscale numerical model to local weather prediction. Proc. Second Int. Symp. on Nowcasting, Norrköping, Sweden, 3-7 September 1984, 301-307.

Lilly, D.K., 1984: Some facets of the predictability problem for atmospheric mesoscales. In: Predictability of fluid motions. G. Holloway and B.J. West (Eds.), 287-294.

Modica, G.D., 1987: The impact on short-term prediction forecast skill of time-dependent lateral and lower boundary conditions within meso-beta numerical cloud prediction models. Proc. Int. Symp. on Mesoscale Analysis and Frecasting, Vancouver, Canada, 17-19 August 1987, 521-526.

Ninomiya, K., 1985: Predictability of mesoscale phenomena. ESA Journal, 2, 195-206.

Orlanski I., 1975: A rational subdivision of sales for atmospheric processes. Bull. Amer. Meteor. Soc., 56, 527-530.

Orlanski, I. and L. Polinsky, 1984: Predictability of mesoscale phenomena. Proc. Second Int. Symp. on Nowcasting, Norrköping, Sweden, 3-7 September 1984, 271-280.

Sashegyi, K.D. et al., 1987: Preliminary results from real data experiments with the NRL mesoscale numerical model. Proc. Int. Symp. on Mesoscale Analysis and Forecasting, Vancouver, Canada, 17-19 August 1987, 497-500.

Stauffer, D.R. and N.L. Seaman, 1987: A real-data numerical study and four-dimensional data assimilation application for meso-beta-scale flow in complex terrain. Ibid.

Takano, I. and A. Segami, 1986: Impact of high resolution satellite winds on the regional forecasts. Extended abstracts WMO/IUGG Int. Symp. Short- and Medium-Range NWP, Tokyo, 4-8 August 1986.

Tapp, M.C. and P.N. White, 1976: A non-hydrostatic mesoscale model. Quart. Jour. Roy. Meteor. Soc., 102, 277-296.

White, P.W., 1978: Mesoscale modelling. The interpretation and use of large-scale numerical forecast products. ECMWF seminars, 1978. 17-55.

WMO, 1987: Development of mesoscale models for weather elements prediction. (Prepared by V.Z. Kiselnikova et al.), PSMP Report Series, 23, 241 pp.

Zhou, X. et al., 1987: A mesoscale numerical model for heavy rainfall forecasting in China's Yangtze River valley. Proc. Int. Symp. on Mesoscale Analysis and Forecasting, Vancouver, Canada, 17-19 August, 517-520.

LES APPLICATIONS DE LA PREVISION NUMERIQUE A ECHELLE MOYENNE

par M. JARRAUD

Direction de la Météorologie nationale - France

I. JUSTIFICATIONS

Il semble pertinent de s'interroger sur l'utilité des modèles à échelle moyenne sur des zones limitées dans la mesure où la résolution horizontale des meilleurs modèles hémisphériques ou globaux est désormais de l'ordre de 150 à 300 km et compte tenu de l'évolution prévisible des supercalculateurs, atteindra sans doute 70 à 100 km d'ici une dizaine d'années. La résolution actuelle semble d'ores et déjà suffisante pour la prévision de la plupart des phénomènes de taille synoptique, comme les dépressions extratropicales. On obtient même des résultats prometteurs pour les fronts et les cyclones tropicaux, du moins lorsque ces derniers sont déjà présents dans l'état initial (figure 1).

Par ailleurs la qualité du système mondial d'observation est, dans de nombreuses régions (en particulier au-dessus des océans), insuffisante pour répondre aux besoins des modèles actuels, et contribue pour une part importante aux erreurs de prévision à courte et moyenne échéances.

Néanmoins, et pour plusieurs raisons, il peut être avantageux d'utiliser une résolution plus fine. La première, et la plus importante, concerne la représentation des montagnes. La figure 2 montre une représentation des montagnes en Europe avec une résolution d'environ 15 km (fichier US-NAVY).L'importance d'un traitement fin de ces reliefs a été clairement démontrée par de nombreux auteurs, par exemple pour des cas de cyclogénèses rapides sur la Méditerranée. Par ailleurs les phénomènes de blocages de basses couches sont souvent sous-estimés, même avec les meilleures résolutions horizontales utilisées dans les modèles globaux (figure 3). Pour y remédier, plusieurs techniques ont été proposées (par exemple l'utilisation de montagnes "enveloppe"), mais avec certains effets secondaires négatifs parfois importants (figure 3).

L'avantage que présente une résolution plus fine apparaît sur la figure 4, qui présente les reliefs utilisés par les deux modèles opérationnels de la DMN : le modèle EMERAUDE à grande échelle (spectrale avec troncature triangulaire T 79) et le modèle PERIDOT à moyenne échelle (point de grille avec une maille de 35 km environ). Les détails du relief dans le modèle PERIDOT correspondent à des phénomènes météorologiques parfois importants. Le Mistral, vent soufflant du nord dans la vallée du Rhône (à l'ouest des Alpes), en est un exemple.

Une deuxième raison d'utiliser des modèles à résolution plus fine que celle des modèles globaux est que celle-ci permet une meilleure simulation de certains processus physiques ou dynamiques, comme les cyclogénèses rapides, même non liées à la présence de montagnes (figure 5). La plupart des études en ont démontré l'intérêt tant pour la phase de creusement (intensité et localisation) que pour la trajectoire. Cela permet en outre, de représenter des structures complexes (par exemple frontales, comme dans la figure 6) souvent associées à des situations délicates pour les prévisionnistes et où l'aspect sécurité peut être essentiel.

Une troisième raison concerne enfin la définition de l'etat initial des modèles; une résolution plus fine permet de mieux prendre en compte les observations synoptiques par exemple dans les zones côtières ou montagneuses mais également les observations à haute densité spatiale ou temporelle, comme les données satellitaires. La figure 7 illustre cet exemple; il s'agit d'une situation où une ligne de grains précédant l'arrivée d'un front froid a provoqué d'importants dégâts dans le sud-ouest de la France. Une étude approfondie avec le modèle PERIDOT (avec une maille de 35 km) a montré l'intérêt d'une analyse fine et d'une utilisation des radiances satellitaires.

II. APPLICATIONS

2.1 Applications à la recherche

Il est important pour les chercheurs de disposer d'outils leur permettant de tester l'impact éventuel d'options trop coûteuses pour être utilisées en configuration opérationnelle compte tenu des ressources en calcul de pointe disponibles. Dans ce domaine, les modèles d'échelle moyenne représentent un outil privilégié permettant de tester les résolutions qu'il sera possible d'utiliser 5 à 10 ans plus tard dans les modèles globaux. Ils permettent également de tester l'impact de résolutions encore plus fines (de l'ordre de 5 à 10 km et d'identifier d'éventuels problèmes : comportement des paramétrisations physiques à ces échelles, limite de l'approximation hydrostatique, etc.). Ils présentent enfin un intérêt pédagogique important pour certains centres nationaux grâce à la possibilité de les utiliser même avec des ressources informatiques limitées.

2.2 Applications à la prévision

Outre leur apport déjà mentionné pour la prévision des phénomènes extrêmes, les modèles à échelle moyenne fournissent une aide croissante aux prévisionnistes pour la prévision des éléments concrets du temps. Dans ce domaine, trois paramètres sont plus particulièrement importants : les précipitations, le vent à 10 m et les températures près du sol (T à 2 m).

Précipitations

Les améliorations considérables des prévisions synoptiques au cours des dernières années se sont accompagnées d'une amélioration des prévisions de précipitations, mais dans une mesure sensiblement moindre; il y a plusieurs raisons à cela mais il convient de citer en premier lieu la médiocrité des observations du champ d'humidité atmosphérique (tant en quantité qu'en qualité). Par ailleurs les précipitations sont associées à des structures d'échelles très fines (fronts, relief) pour lesquelles l'impact d'un modèle d'échelle fine peut se révéler important, la figure 6 illustre cet exemple. La figure 8 montre que certaines différences peuvent être quasi systématiques. Elle présente les cumuls trimestriels pour la période janvier-mars 1988 observés pour 170 stations françaises et prévus entre les échéances 06 et 30 H par les modèles opérationnels français EMERAUDE et PERIDOT. Il convient de signaler que la répartition réelle des stations entraîne une sous-estimation parfois importante des pluies sur les zones montagneuses. Ceci étant, on voit que PERIDOT simule de manière beaucoup plus réaliste qu'EMERAUDE la répartition des précipitations. On observe en particulier des pluies plus abondantes sur l'est de la France et sur le sud du massif montagneux du centre du pays, ainsi qu'une zone plus sèche entre les deux s'étendant le long

de la vallée du Rhône. Les précipitations prévues par EMERAUDE présentent une structure beaucoup plus simple, en liaison sans aucun doute avec la représentation plus grossière du relief (figure 4).

Vent à 10 m

La figure 9 présente des vérifications objectives des prévisions de vent à 10 m issues des modèles PERIDOT et EMERAUDE pour le 4ème trimestre 1987, par rapport aux observations du réseau synoptique. L'apport de PERIDOT est significatif à toutes les échéances tant pour la vitesse que pour la direction du vent, à la fois en terme d'erreur absolue et d'écart type. Comme pour les précipitations une part importante de l'amélioration peut être reliée à une meilleure adaptation (dynamique) au relief plus fin de PERIDOT. De manière générale, l'apport du modèle à l'échelle moyenne est spectaculaire pour les vents locaux tels que le Mistral, l'Autan, le Foehn et les prévisions PERIDOT sont particulièrement appréciées des prévisionnistes marins sur les zones où les effets orographiques sont importants, comme la région méditerranéenne.

Enfin parmi les autres applications qui peuvent tirer profit des prévisions de vent plus fines, il ne faut pas oublier les modèles de trajectoire et de transport de polluant. Un exemple d'une trajectoire complexe avec rebroussement sur la Corse est présenté en figure 10.

Température à 2 m

En Europe, c'est l'un des paramètres les plus importants pour de nombreux usagers et une amélioration même mineure peut se traduire par des économies considérables, par exemple dans le domaine agricole ou celui de l'énergie. En France par exemple, une différence de 1°C en hiver se traduit par une différence de consommation électrique de 1000 MW. Cela aide à mieux interpréter des différences telles que celles de la figure 11.

Outre les améliorations dues à la meilleure prise en compte du relief, l'apport des modèles à échelle moyenne pour les prévisions de température près du sol peut passer aussi par la meilleure description du contraste terre/eau, des échanges d'énergie près du sol.

III. LE FUTUR

Les progrès enregistrés en prévision numérique ces dernières années, tant pour les modèles globaux que pour les modèles régionaux à échelle plus fine font que les sorties de modèles sont de plus en plus utilisées par les prévisionnistes et que devant l'abondance de tels produits, de nouveaux moyens de traitement et de visualisation doivent être développés.

Dans une quinzaine d'années, les modèles globaux auront des résolutions voisines de celle des modèles régionaux actuels, et en parallèle il est probable que ces derniers pourront avec des mailles encore plus fines (de l'ordre de 15 à 30 km) et une résolution verticale accrue, apporter un support plus précis aux prévisionnistes, en particulier dans les situations extrêmes.

Devant l'importance croissante de la prévision des éléments du temps concret, un effort tout particulier devra porter sur l'analyse du champ d'humidité et la modélisation du cycle de l'eau ainsi que sur les problèmes

d'équilibres initiaux entre les divers champs afin d'éviter les périodes d'adaptation ("spin up") qui hypothèquent l'utilisation des modèles dans les toutes premières heures de prévision.

Un effort important devra être consacré à l'exploitation de nouvelles données avec une meilleure fréquence spatiale et temporelle (données satellitaires, données des profileurs de vent, etc.). Leur utilisation optimale conditionne le succès des futurs modèles d'échelle moyenne et passera sans doute par le développement de nouvelles techniques d'assimilation, par exemple de type variationnel.

C'est dans cet esprit que la France, comme plusieurs autres pays, oriente ses efforts en matière de prévision numérique à échelle moyenne. En outre, et afin de minimiser les inconvénients liés aux conditions aux limites latérales inhérentes aux modèles sur domaine limité, l'approche retenue pour la prochaine génération est celle d'un modèle unique global, spectral à maille variable, tel celui suggéré par F. SCHMIDT. Les premiers essais ont confirmé la faisabilité et la souplesse d'une telle approche; la résolution maximale peut être placée en n'importe quel point de la sphère et elle décroît ensuite de manière continue jusqu'au point antipodique où elle est minimale. La figure 12 illustre l'importance relative prise par l'Europe avec un accroissement de résolution de facteur 3 (c'est-à-dire neuf fois plus fine qu'au point opposé). Cette approche permet en outre de résoudre les inconsistences de physique ou de représentation des montagnes qui peuvent se poser avec des modèles couplés.

En conclusion, il est important de souligner que malgré les progrès considérables accomplis en prévision numérique à grande et moyenne échelle, de gros efforts restent à faire pour continuer à améliorer ces modèles, ainsi que la quantité et la qualité des observations nécessaires et pour généraliser le développement et l'utilisation des modèles d'échelle moyenne ou fine dans certaines régions où leur apport peut se révéler essentiel.

Cependant tous ces progrès ne devront pas faire sous estimer le rôle des prévisionnistes. Ils devront certes s'adapter à l'évolution des modèles, mais leur rôle restera essentiel, comme l'exemple récent de la tempête exceptionnelle qui a ravagé l'ouest de la France et le sud de l'Angleterre l'a démontré. Enfin, il est important de prendre conscience que l'amélioration des prévisions continuera à s'accompagner d'une exigeance croissante des usagers. Certaines prévisions qui auraient été classées comme bonnes il y a quelques années sont désormais considérées comme mauvaises. C'est le prix inévitable du succès.

*

* *

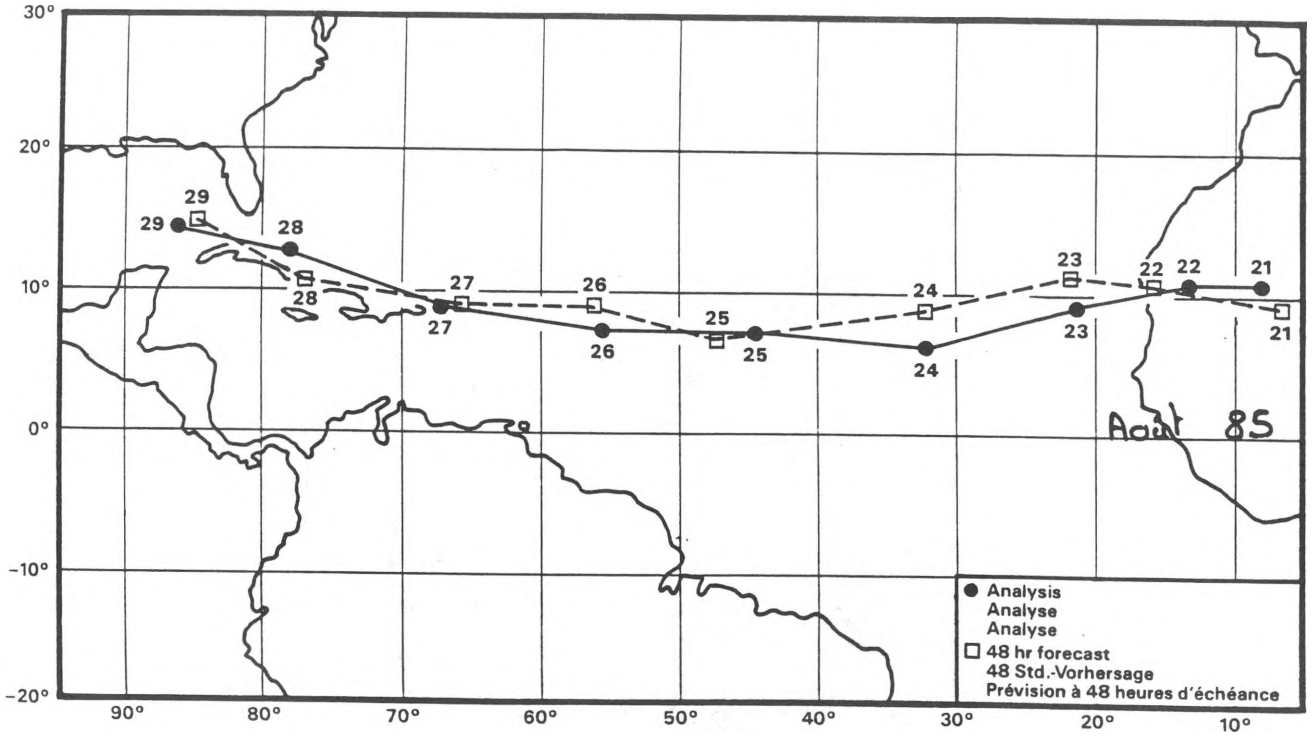

Figure 1 : <u>En haut</u> : trajectoire analysée du 21 au 29 août 1985 du cyclone ELENA (trait plein) et prévisions correspondantes à 48 h du modèle du CEPMMT (trait tireté) (<u>document : CEPMMT</u>)
<u>En bas</u> : image visible METEOSAT du 24 août 1985 à 12 UTC

EUROPE 1/6DEG

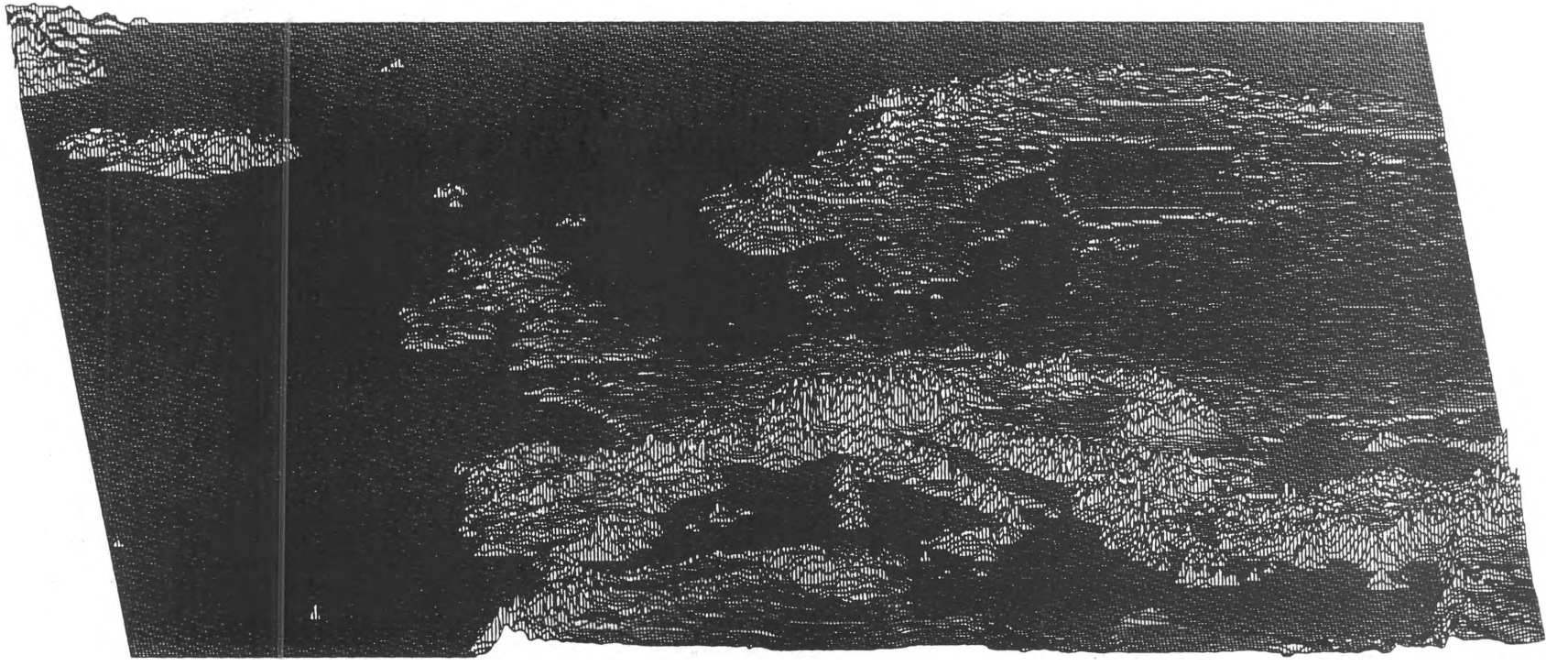

Figure 2 : Représentation à 3 dimensions des montagnes sur l'Europe à partir du fichier US NAVY (résolution 1/6 degré)

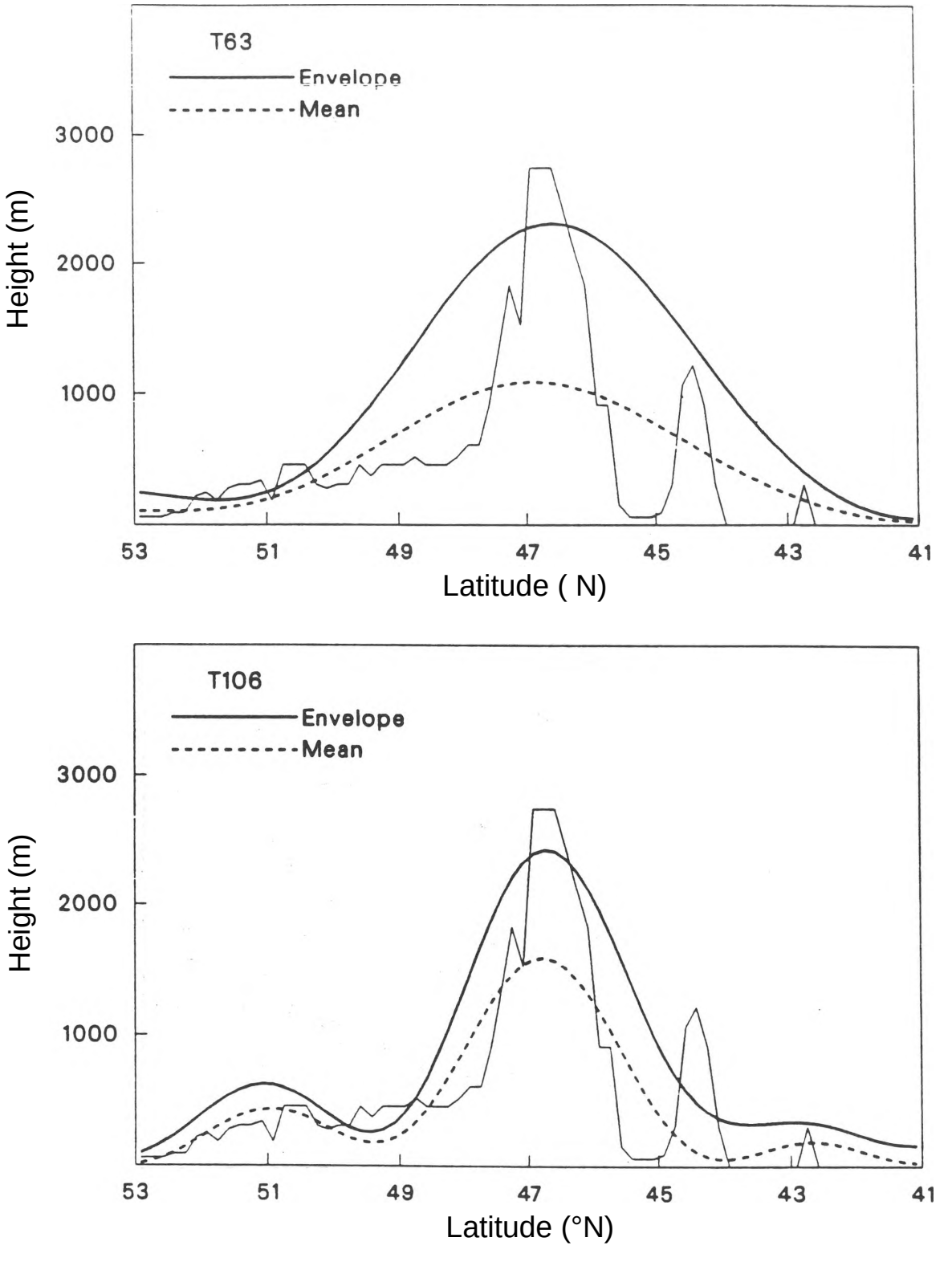

Figure 3 : Coupe nord-sud du relief (en m) de 53°N à 41°N de la latitude, à la longitude 10°5 E
Traits pleins fins : relief moyen sur une grille 10' x 10'
Traits épais : relief enveloppe à résolution spectrale T 63 (en haut) et T 106 (en bas)
(document : CEPMMT)

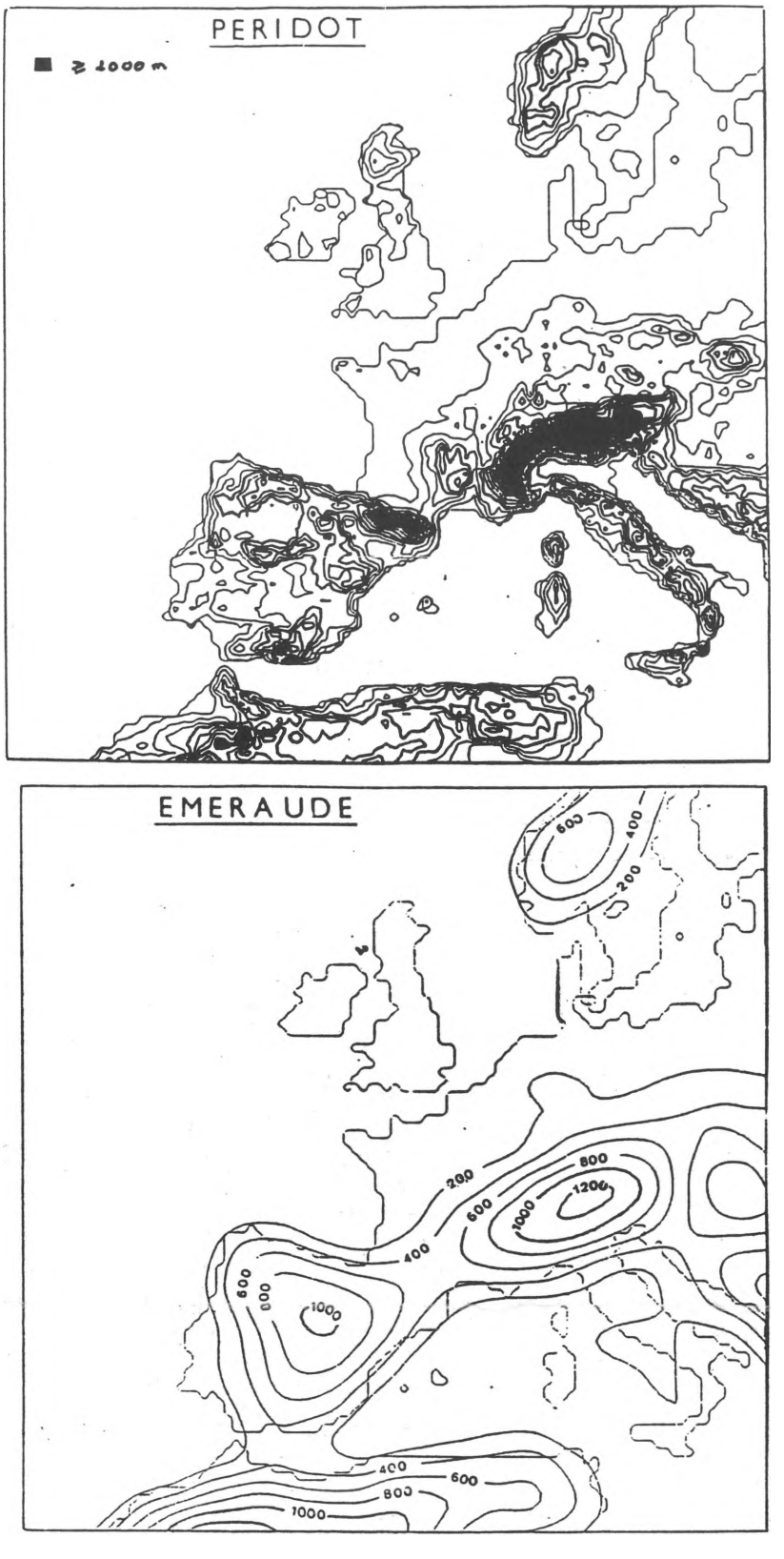

Figure 4 : Représentation des reliefs sur l'Europe utilisée par les modèles PERIDOT (en haut) et EMERAUDE (en bas). L'intervalle entre isolignes est de 200 m.

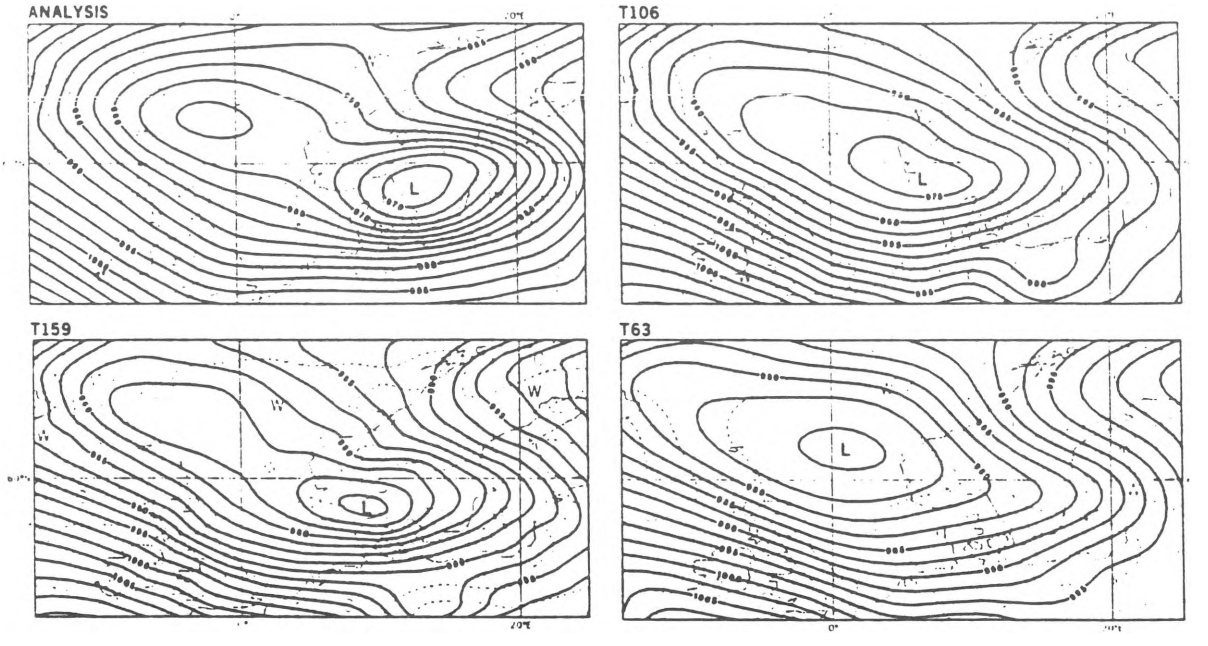

Figure 5 : Champs analysés pour le 25 mars 1986 à 12 UTC (en haut à gauche) et prévisions à 5 jours valables pour la même date réalisées avec le modèle du CEPMMT avec diverses résolutions spectrales horizontales : T 106 (en haut à droite), T 159 (en bas à gauche) et T 63 (en bas à droite) (document : CEPMMT)

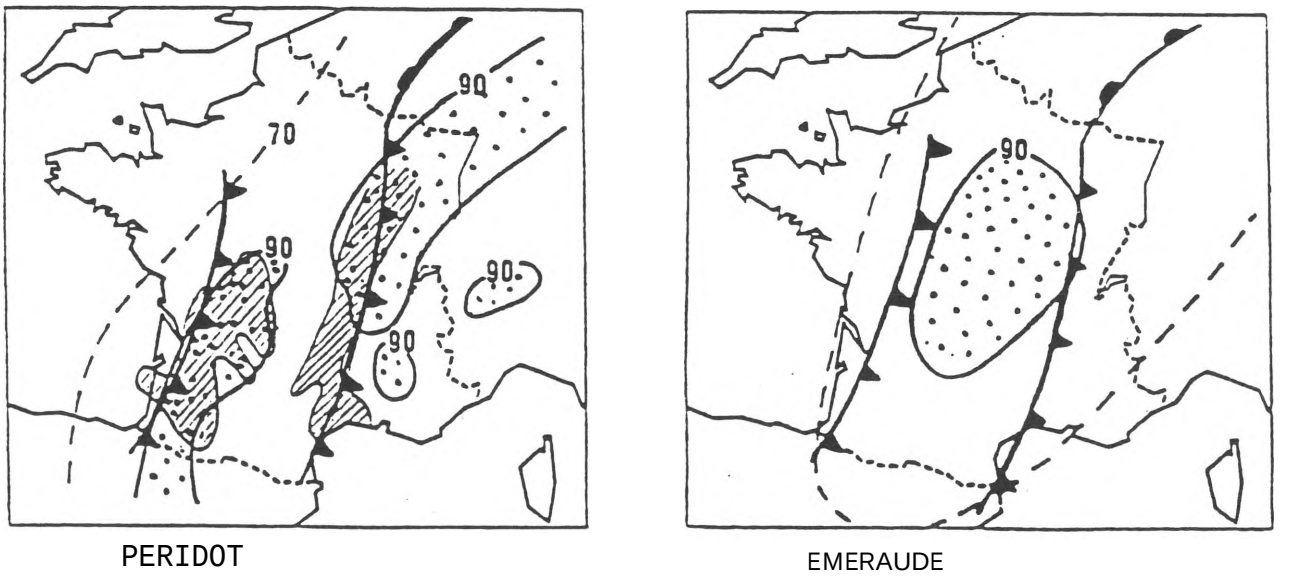

PERIDOT EMERAUDE

Figure 6 : 5 octobre 1985 : prévision PERIDOT et EMERAUDE à 24 h d'échéance de l'humidité relative à 700 hPa. Les parties en pointillés correspondent à des humidités relatives supérieures à 90%. Les fronts correspondent à l'analyse manuelle faite par le prévisionniste et les parties hachurées (sur la prévision PERIDOT) aux observations radar de précipitations.

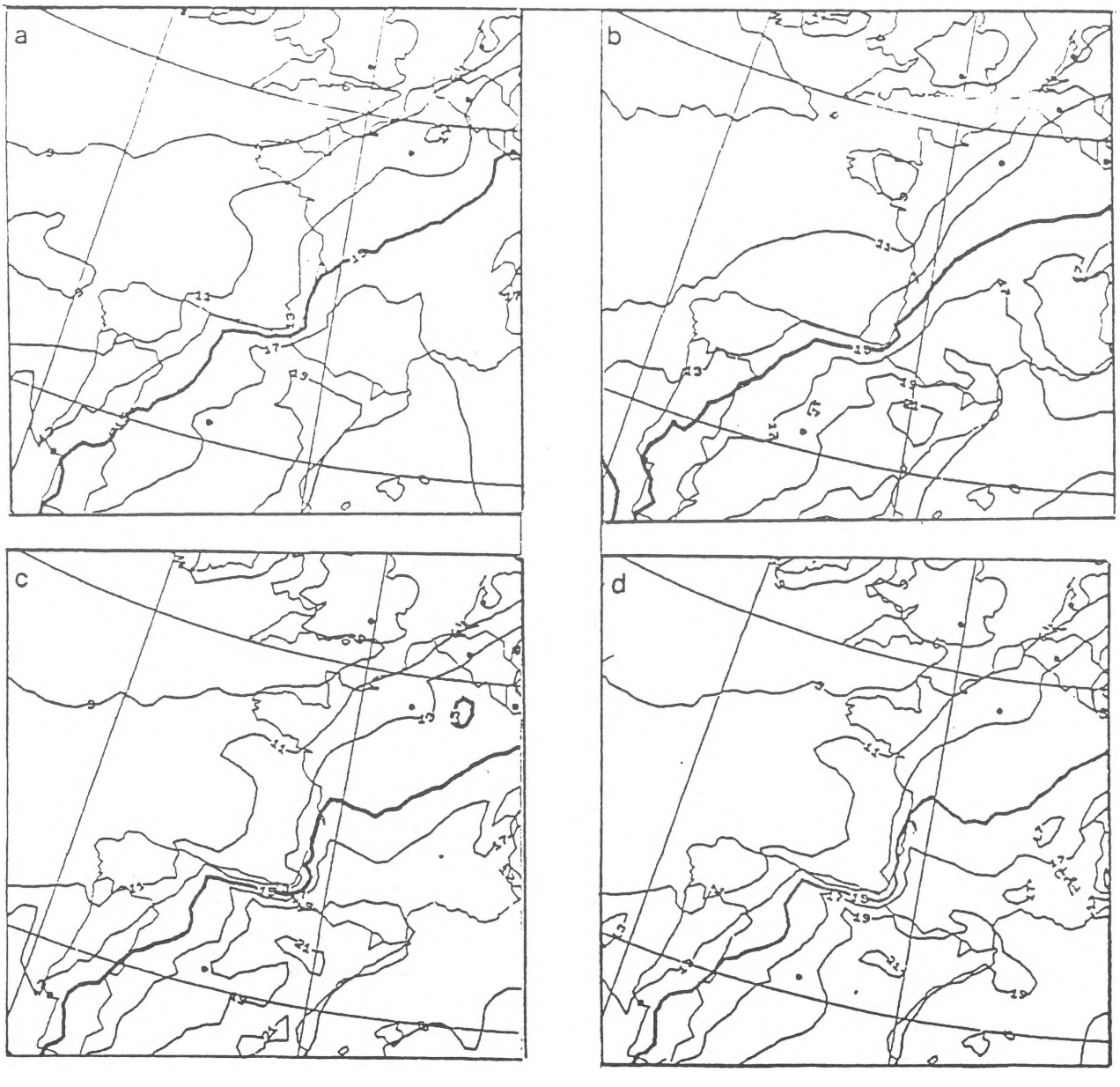

Figure 7 : Cartes de prévision à 6 h de theta prime W pour le 7 juin 1987 à 18 UTC. Les prévisions diffèrent seulement par leur état initial :

a) interpolé à partir de l'analyse EMERAUDE (à grande échelle)
b) analyse PERIDOT (maille fine) avec ébauche EMERAUDE
c) analyse PERIDOT avec ébauche PERIDOT, mais sans utilisation des radiances satellitaires
d) comme c) avec utilisation des radiances satellitaires. Intervalle entre isolignes : 2°

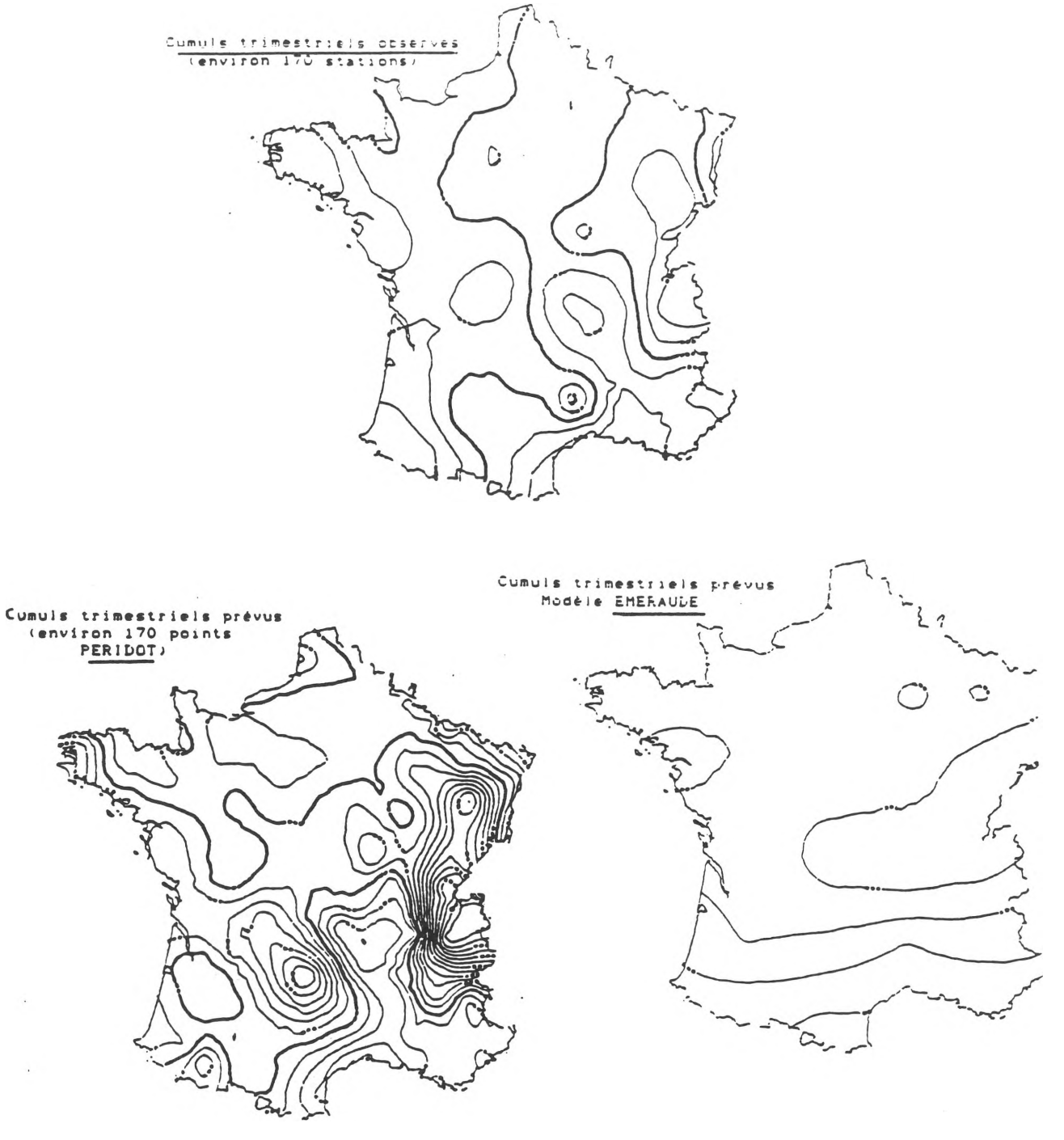

Figure 8 : Précipitations journalières cumulées sur les mois de janvier à mars 1988
En haut : pour 170 stations du réseau français
En bas à gauche : pour les prévisions du modèle PERIDOT, (cumulées entre les échéances 06 et 30 h)
En bas à droite : même chose pour les prévisions du modèle EMERAUDE

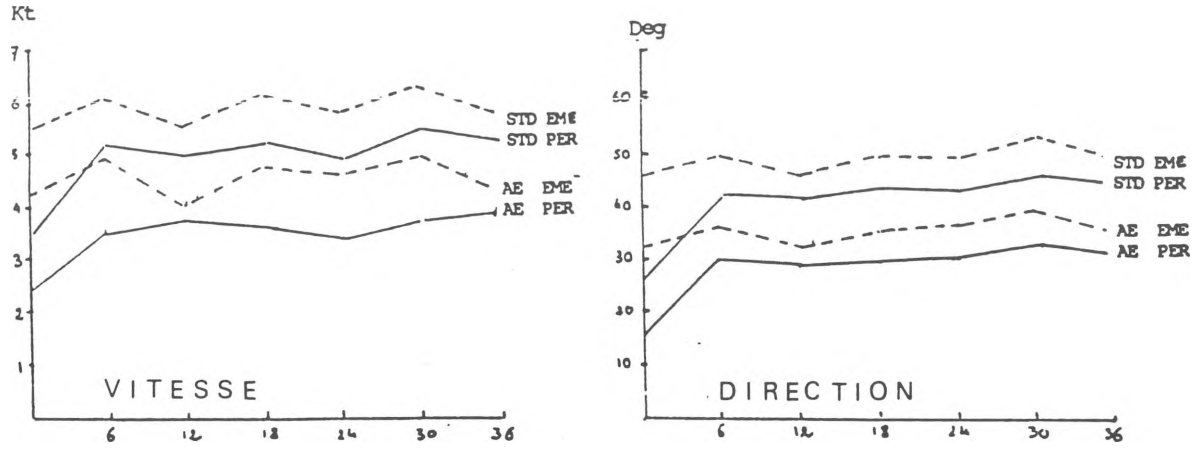

Figure 9 : Erreur absolue (AE) et écart type (STD) pour les prévisions EMERAUDE (traits pointillés) et PERIDOT (traits pleins) de vent à 10 m pour les mois d'octobre à décembre 1987.
Vitesse à gauche et direction à droite.

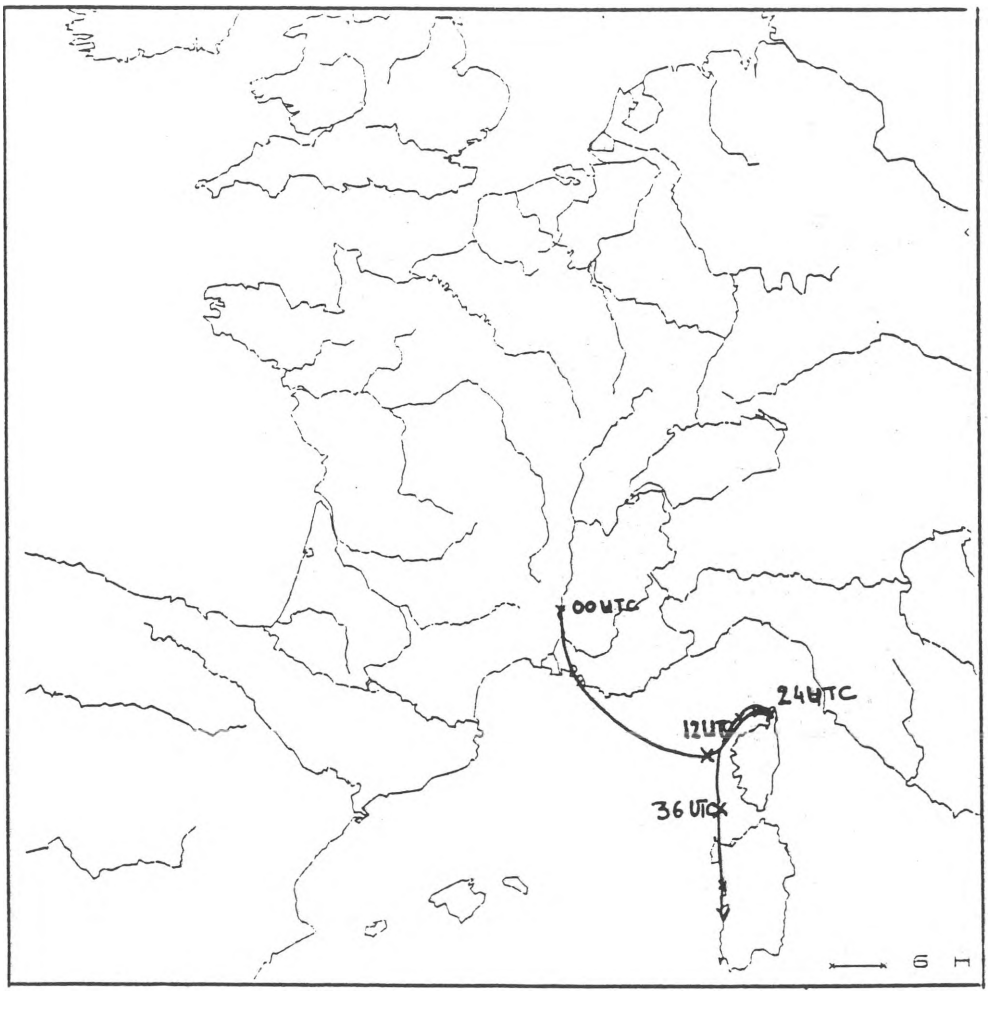

Figure 10 : Exemple de trajectoire à 48 h à partir des prévisions du modèle à maille fine PERIDOT

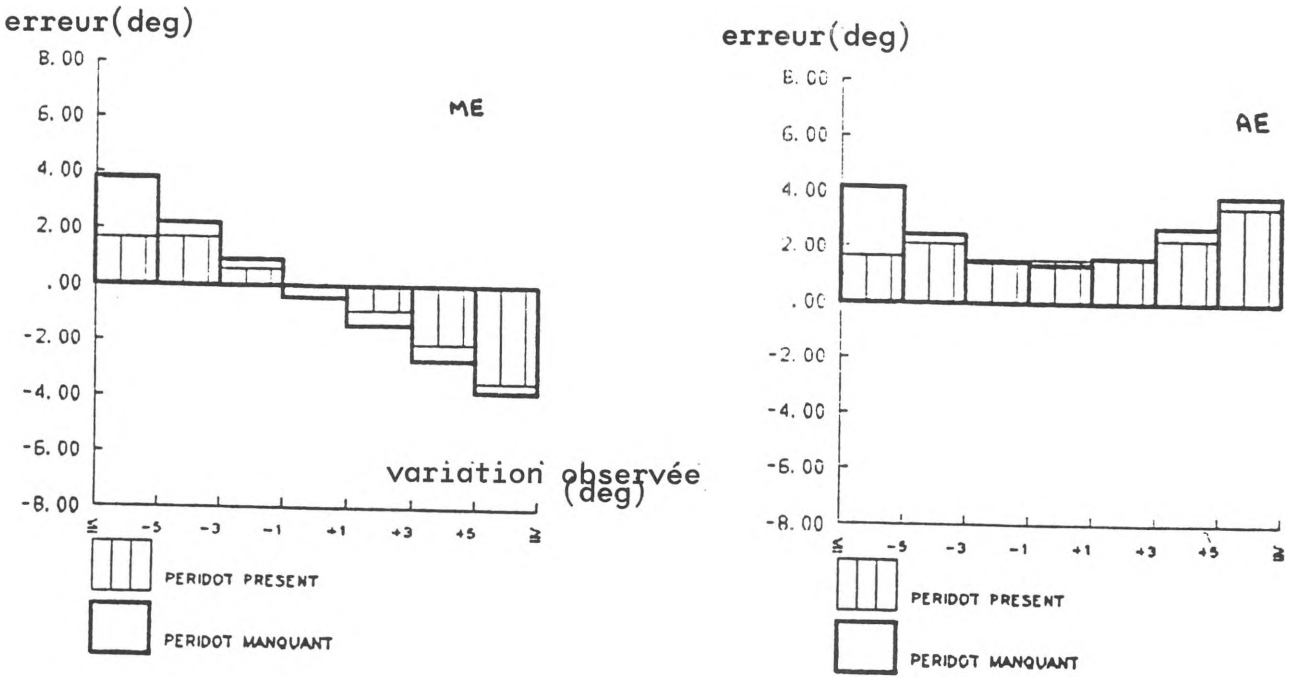

Figure 11 : Evaluation de l'impact de PERIDOT dans la prévision des températures minimales du lendemain pour 6 villes françaises pour 36 jours en 1987.
Les graphiques montrent l'erreur moyenne (ME, à gauche) et l'erreur absolue (AE à droite), sur les températures minimales du lendemain pour les prévisions finales du prévisionniste lorsqu'il n'a pas dispose de PERIDOT (zone sans hachures verticales) tout en ayant des prévisions de modèles à grande échelle (EMERAUDE et/ou CEPMMT) et les erreurs correspondantes sur les situations voisines où il a disposé de PERIDOT.

Les erreurs sont calculées par classes de variation observée entre J et J + 1. A noter qu'il y a peu de cas dans les classes de variations extrêmes.

Figure 12 : Importance relative prise par l'Europe dans le futur modèle ARPEGE à maille variable de la DMN (résolution 9 fois plus fine sur la France que sur le point oppose).